AD-A139 502   MILLIMETER WAVE ATTENUATION IN MOIST AIR: LABORATORY   1/1
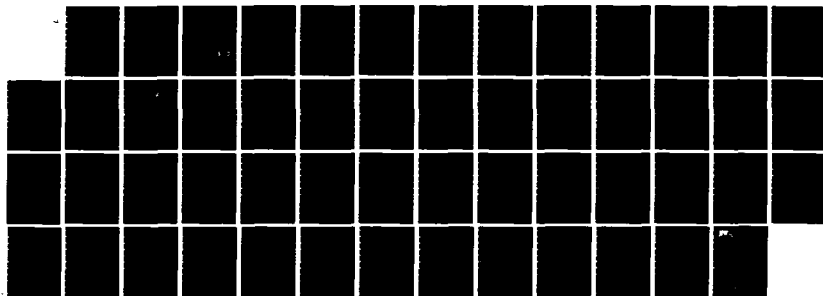   MEASUREMENTS AND ANA.. (U) NATIONAL
              TELECOMMUNICATIONS/INFORMATION ADMINISTRATION BOULDE..
UNCLASSIFIED H J LIEBE MAR 84 ARO-16638.23-GS   F/G 4/1   NL
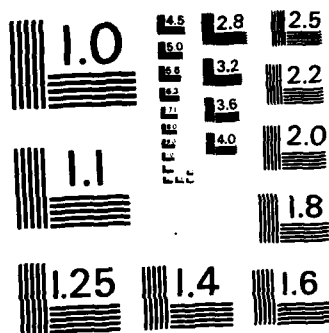
MICROCOPY RESOLUTION TEST CHART

NATIONAL BUREAU OF STANDARDS-1963-A

NATIONAL TELECOMMUNICATIONS AND
INFORMATION ADMINISTRATION

AD A189502

MILLIMETER WAVE ATTENUATION IN MOIST AIR:
LABORATORY MEASUREMENTS AND ANALYSIS

- Final Report -

Hans J. Liebe

1 March 1984

U.S. Army Research Office Contract No. 101-83

DTIC
S ELECTE D
MAR 3 0 1984
B

Institute for Telecommunication Sciences
Boulder, Colorado 80303

MILLIMETER WAVE ATTENUATION IN MOIST AIR:
LABORATORY MEASUREMENTS AND ANALYSIS

- Final Report -

Hans J. Liebe

1 March 1984

U.S. Army Research Office   Contract No. 101-83

DTIC
SELECTED
MAR 30 1984

B

APPROVED FOR PUBLIC RELEASE;
DISTRIBUTION UNLIMITED.

THE VIEW, OPINIONS, AND/OR FINDINGS CONTAINED IN THIS REPORT ARE
THOSE OF THE AUTHOR(S) AND SHOULD NOT BE CONSTRUED AS AN OFFICIAL
DEPARTMENT OF THE ARMY POSITION, POLICY, OR DICISION, UNLESS SO
DESIGNATED BY OTHER DOCUMENTATION.

REPORT DOCUMENTATION PAGE	READ INSTRUCTIONS BEFORE COMPLETING FORM	
1. REPORT NUMBER	2. GOVT ACCESSION NO. AD-A139502	3. RECIPIENT'S CATALOG NUMBER
4. TITLE *(and Subtitle)* MILLIMETER WAVE ATTENUATION IN MOIST AIR: LABORATORY MEASUREMENTS AND ANALYSIS	5. TYPE OF REPORT & PERIOD COVERED Final Report for period 1 Aug 79 - 31 Dec 83	
	6. PERFORMING ORG. REPORT NUMBER	
7. AUTHOR(*s*) Hans J. Liebe	8. CONTRACT OR GRANT NUMBER(*s*) MIPR-ARO-30-79, 42-80, 51-81, 6-82, 64-82, 101-83	
9. PERFORMING ORGANIZATION NAME AND ADDRESS National Telecommunications and Information Admin. Institute for Telecommunication Sciences 325 Broadway Boulder, Colorado 80303	10. PROGRAM ELEMENT, PROJECT, TASK AREA & WORK UNIT NUMBERS	
11. CONTROLLING OFFICE NAME AND ADDRESS U. S. Army Research Office Post Office Box 12211 Research Triangle Park, NC 27709	12. REPORT DATE March 1984	
	13. NUMBER OF PAGES 46	
14. MONITORING AGENCY NAME & ADDRESS*(If different from Controlling Office)* N/A	15. SECURITY CLASS. *(of this report)* UNCLASSIFIED	
	15a. DECLASSIFICATION/DOWNGRADING SCHEDULE N/A	

16. DISTRIBUTION STATEMENT *(of this Report)*

Approved for public release; distribution unlimited.

17. DISTRIBUTION STATEMENT *(of the abstract entered in Block 20, if different from Report)*

N/A

18. SUPPLEMENTARY NOTES

THE VIEW, OPINIONS, AND/OR FINDINGS CONTAINED IN THIS REPORT ARE THOSE OF THE AUTHOR(S) AND SHOULD NOT BE CONSTRUED AS AN OFFICIAL DEPARTMENT OF THE ARMY POSITION, POLICY, OR DE-CISION, UNLESS SO DESIGNATED BY OTHER DOCUMENTATION.

19. KEY WORDS *(Continue on reverse side if necessary and identify by block number)*

Atmospheric propagation model; high-humidity resonance spectrometer; millimeter and submillimeter wavelength range; moist air absorption.

20. ABSTRACT *(Continue on reverse side if necessary and identify by block number)*

Experiments were performed with a millimeter wave resonance-spectrometer capable of measuring absolute attenuation rates α (dB/km) by water vapor up to saturation pressures. Vapor (e) and air (p) pressures were varied at constant temperature and set frequency. Anomalous absorption behavior (i.e., high rates α, extreme temperature dependences, hystereses in pressure and temperature cycles) could be identified as being caused largely by instrumental condensation effects. Uncorrupted data at 138 GHz display, in

DD $_{1\ JAN\ 73}^{FORM}$ 1473   EDITION OF 1 NOV 65 IS OBSOLETE

addition to air-broadening ($\propto ep$), a strong self-broadening component ($\propto e^2$). Based upon these results, a practical atmospheric millimeter wave propagation model (MPM) was formulated that predicts attenuation, delay and noise properties of moist air over the frequency range of 1 to 1000 GHz and a height range of 0 to 100 km. The main spectroscopic data base consists of 48 O_2 and 30 H_2O local absorption lines complemented by continuum spectra for dry air and water vapor. Model input relies upon distributions of meteorological variables along an anticipated radio path. These variables are pressure, temperature, and relative humidity for moist air; suspended droplet concentration for haze, fog, cloud conditions; and a rain rate. In special cases, trace gas concentrations for ozone and carbon monoxide and the geomagnetic field strength can be added.

The research leading to an MPM was reported in 17 publications and is summarized in this report. Theoretical foundations, experimental verifications, and typical radio path behaviors have been addressed. Good agreement was obtained between predicted and measured data (20 to 337 GHz) from both laboratory and field experiments. Implications of the MPM with respect to older modeling codes and needed future work are discussed briefly.

TABLE OF CONTENTS

LIST OF FIGURES AND TABLE

MILLIMETER WAVE ATTENUATION IN MOIST AIR:
LABORATORY MEASUREMENTS AND ANALYSIS

Hans J. Liebe

ABSTRACT

Experiments were performed with a millimeter wave resonance-spectrometer capable of measuring absolute attenuation rates α (dB/km) by water vapor up to saturation pressures. Vapor (e) and air (p) pressures were varied at constant temperature and set frequency. Anomalous absorption behavior (i.e., high rates α, extreme temperature dependences, hystereses in pressure and temperature cycles) could be identified as being caused largely by instrumental condensation effects. Uncorrupted data at 138 GHz display, in addition to air-broadening ($\propto ep$), a strong self-broadening component ($\propto e^2$). Based upon these results, a practical atmospheric millimeter wave propagation model (MPM) was formulated that predicts attenuation, delay and noise properties of moist air over a frequency range of 1 to 1000 GHz and a height range of 0 to 100 km. The main spectroscopic data base consists of 48 O_2 and 30 H_2O local absorption lines complemented by continuum spectra for dry air and water vapor. Model input relies upon distributions of meteorological variables along an anticipated radio path. These variables are pressure, temperature, and relative humidity for moist air; suspended droplet concentration for haze, fog, cloud conditions; and a rain rate. In special cases, trace gas concentrations for ozone and carbon monoxide and the geomagnetic field strength can be added.

The research leading to an MPM was reported in 17 publications and is summarized in this report. Theoretical foundations, experimental verifications, and typical radio path behaviors have been addressed. Good agreement was obtained between predicted and measured data (20 to 337 GHz) from both laboratory and field experiments. Implications of the MPM with respect to older modeling codes and needed future work are discussed briefly.

1. THE EXCESS WATER VAPOR ABSORPTION PROBLEM

Communication systems and sensing devices operating in the millimeter wave (MMW) range are attractive to military planners since weapon deployment has to be assured during periods of adverse weather and in disturbed environments. An optimum trade-off between atmospheric obscurations and angular resolution can be achieved in the frequency range between $f \simeq 90$ and 350 GHz, where propagation is restricted by:

- molecular absorption due to oxygen and water vapor;
- mass concentrations of suspended particles (haze, fog, dust, etc.);
- precipitation effects (rain, wet snow).

The main problem studied during this research effort was predicting correct attenuation rates by moist air,

$$\alpha = \alpha_d + \alpha_v \qquad dB/km \quad .$$

Dry air attenuation α_d, mainly due to oxygen, always makes a contribution which is calculated with the model detailed in [5]. The line-by-line summation in the model includes overlap effects of the 60 GHz absorption band and nonresonant O_2 plus pressure-induced N_2 absorption.

Water vapor attenuation α_v depends on absolute humidity $v(g/m^3)$ which, in turn, is limited by relative humidity RH (%) [3]. Its origin lies in the absorption lines of H_2O vapor which number in the thousands. In principle, α_v can be evaluated from a line-by-line summation of all line features, each contributing at a given frequency as prescribed by a line shape function [9]. In practice, the problem is reduced to an evaluation of local line contributions α_ℓ to which a continuum α_c is added, accounting for excess absorption not covered by the limited line data base; that is,

$$\alpha_v = \alpha_\ell + \alpha_c \qquad dB/km \quad .$$

The MMW frequency range has four atmospheric windows [11] where contributions by α_c can be as high as 90 percent of α_v. The excess has been a major source of uncertainty in the correct modeling of moist air attenuation α.

Basic physical principles underlying the attenuation rate α are difficult to deduce from measurements in the actual atmosphere. Reliability, precision, and scale of supporting meteorological data compromise the quality of most field observations. Controlled experiments simulate atmospheric conditions, thus providing test cases for studying specific loss contributions in isolation. Results

-2-

from such laboratory experiments led to the formulation of a water vapor continuum spectrum α_c. The continuum together with 30 local H_2O absorption lines forms the basis for an atmospheric millimeter wave propagation model. The contribution α_c has been tentatively identified to be a far wing response of the H_2O spectrum above 1 THz [16].

2. MILLIMETER WAVE ATTENUATION BY MOIST AIR

The most important result of this research is a practical atmospheric milli- meter wave propagation model (MPM) based upon meteorological input variables [14]. The MPM predicts attenuation α (dB/km) and dispersive delay β (ns/km) up to 1000 GHz. Interrelations between radio wave propagation and geophysical properties of water vapor are a complex problem as outlined in a comprehensive overview [3] (see Appendix). As the work progressed, various theoretical, analytical and experimental efforts followed, addressing separate topics within the framework set by this review. Overall, a total of 17 publications [1]-[17], 8 internal reports [18]-[25], work by the P.I. on 4 related problems [26]-[29], and 15 presentations have been produced in order to come to grips with moist air as a propagation medium for millimeter waves.

2.1 Theory

Theoretical consultant for the project was the well-known molecular physicist, Professor M. Mizushima of the University of Colorado. He recalculated the rota- tional spectrum of H_2O for quantum numbers $J \leq 16$ in the vibrational ground state ($\nu = 0$) and the rotational spectrum of O_2 including vibrationally excited states ($\nu = 0,1,2$), and applied the results to predict atmospheric transparency up to frequencies of 1000 GHz [9], [10] (see Appendix). A detailed computer code is available in FORTRAN IV. Some new ideas with regard to collision-broadened line shapes were outlined [19], and contributions to excess absorption were estimated by possible, though very weak, electric dipole transitions in isotopic species of N_2 and O_2 [20].

2.2 Modeling

Modeling reduces the theoretical complications of describing interactions between MMW's and atmospheric molecules to a parametric presentation of engineering utility. It runs the gamut from meteorological observables assessing the absorber population within a radio path, through specific attenuations, to experimental and

theoretical aspects. Intricate "molecule-by-molecule," "line-by-line," and "layer-by-layer" calculation procedures have been converted into a simple computer code. The outcome of observations can be predicted provided the geophysical variables are available. In general, agreement with experimental data at frequencies between 20 and 337 GHz is within limits of their stated uncertainty (typically better than ± 10 percent).

The following provides guidance to the output of the modeling effort:

millimeter wave propagation model MPM, latest version -   [14];
program descriptions of the MPM -   [18], [14], [12]
local line model (30 H_2O and 48 O_2 lines) -   [4], [5
water vapor continuum absorption (see Appendix A4) - [11], [13], [15], [16
simplifications of the MPM -   [12], [1.
applications of the MPM - [7], [8], [11], [13], [14], [23], [24], [27]-[29].

A typical graphical output of the MPM is shown in Figure 1. When examining the attenuation rates α, as listed in Table 1 for "window" and "line" (185 GHz) frequencies, on a per g/m^3 concentration (v) basis, one notices in Figure 2 striking differences between the old, Gaut-Reifenstein-based model [11] and MPM predictions. Discrepancies at warmer temperatures T are caused mainly by a v^2-dependence of the continuum α_c (see Eq. 29 - p. A27) which are amplified by the strong temperature ($\approx T^{17}$) dependence of v_s(100% RH).

2.3 Experiment

The experiment consists of a millimeter wave resonance spectrometer and an integrated humidity simulator. The instrument is capable of measuring absolute electromagnetic properties (attenuation, dispersion, refraction) of moist air for relative humidities between 0 and 100% RH [16] (Appendix). An insulated box contains a high-vacuum stainless steel vessel, which houses a temperature-controlled mini-lake (10 cm across) and the radio test path. MMW signals around 35 and 140 GHz have been employed over equivalent free-space path lengths between 350 and 150 m; temperatures are controlled to better than 1/100 of a degree Celsius; pressure ranges over seven orders of magnitude (10^3 to 10^{-4} mb); and relative humidity is varied between 0 and 100 percent. Data acquisition is computerized, with a choice of operational modes covering time scales from 10 seconds to many days. The resonance signal that carries the absorption information is detected with a digital waveform analyzer.

Mechanical design details are given in [21] and results of tests on temperature-vs-humidity performance are presented in [22]. The millimeter wave

-4-
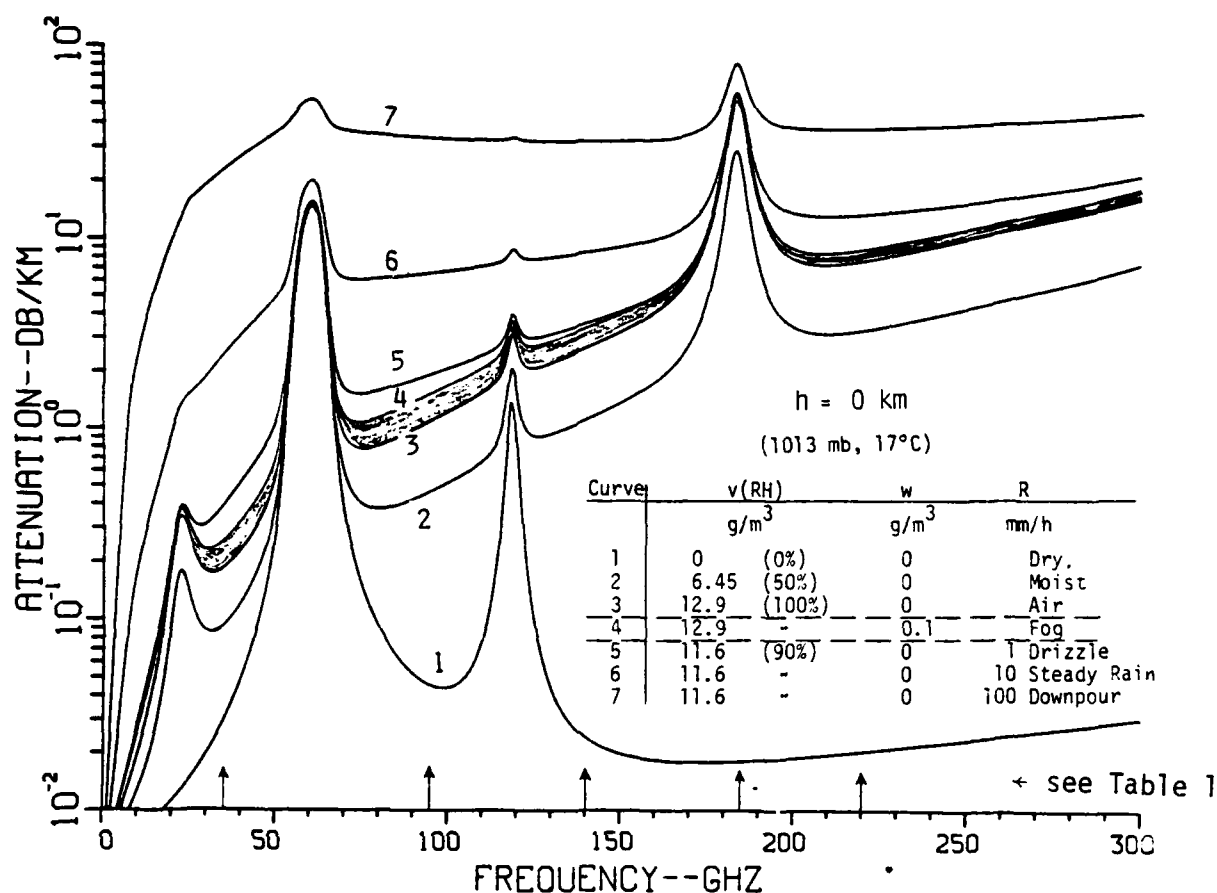
Figure 1. MPM predictions of specific attenuation α (dB/km) for dry and moist air, including fog (about 300 m visibility) and rain events [14].

sources [that is; klystrons centered at 35 GHz (OKI 35V11), at 73 GHz (OKI 70V11A), and at 139 GHz(VARIAN VC 715S), and a Gunn oscillator centered at 92 GHz (MYCRON)] operated CW in a phase-locked mode with 10 kHz resolution, or frequency-stepped under program control. In addition, a free running swept-frequency mode was provided. A tripler (MYCRON, 6P2 diode) generated 73 x 3 ≃ 220 GHz power in amounts between 0.5 and 2 mW. Performance curves are given in Figure 3. The tripler varactor diode failed repeatedly (6 times, so far). Consequently, we have not yet been able to perform moist air attenuation measurements at 220 GHz. Some circuit details of the phase-lock loops are shown in Figure 4.

Table 1.

Predicted specific attenuation α (dB/km) of sea level air (p = 1013 mb) at various relative humidities RH (%) and temperatures T(K) for five millimeter wave frequencies f (GHz) [14].

f	T	v_s	Specific Attenuation α				
			100% RH	75% RH	50% RH	25% RH	0% RH
35 GHz	K	g/m³			dB/km		
	300	25.49	0.399	0.275	0.172	0.090	0.028
	290	14.31	0.207	0.153	0.105	0.065	0.031
	280	7.65	0.119	0.095	0.073	0.052	0.034
	270	3.87	0.079	0.068	0.057	0.047	0.038
95 GHz							
	300		2.239	1.475	0.853	0.375	0.040
	290		1.052	0.729	0.453	0.225	0.044
	280		0.521	0.381	0.242	0.142	0.048
	270		0.277	0.216	0.157	0.103	0.053
140 GHz							
	300		5.027	3.303	1.894	0.800	0.021
	290		2.346	1.608	0.975	0.447	0.023
	280		1.126	0.804	0.513	0.253	0.025
	270		0.556	0.411	0.275	0.147	0.027
185 GHz							
	300		77.27	58.24	39.04	19.63	0.016
	290		45.98	34.59	23.14	11.61	0.017
	280		26.00	19.54	13.05	6.55	0.018
	270		13.90	10.44	6.97	3.50	0.019
220 GHz							
	300		13.08	8.63	4.97	2.10	0.018
	290		6.16	4.23	2.56	1.16	0.019
	280		2.97	2.11	1.34	0.64	0.021
	270		1.45	1.06	0.70	0.35	0.022
Curve ID (Figure 2)			1	2	3	4	Dry Air
(Figure 1)			3	-	2	-	1
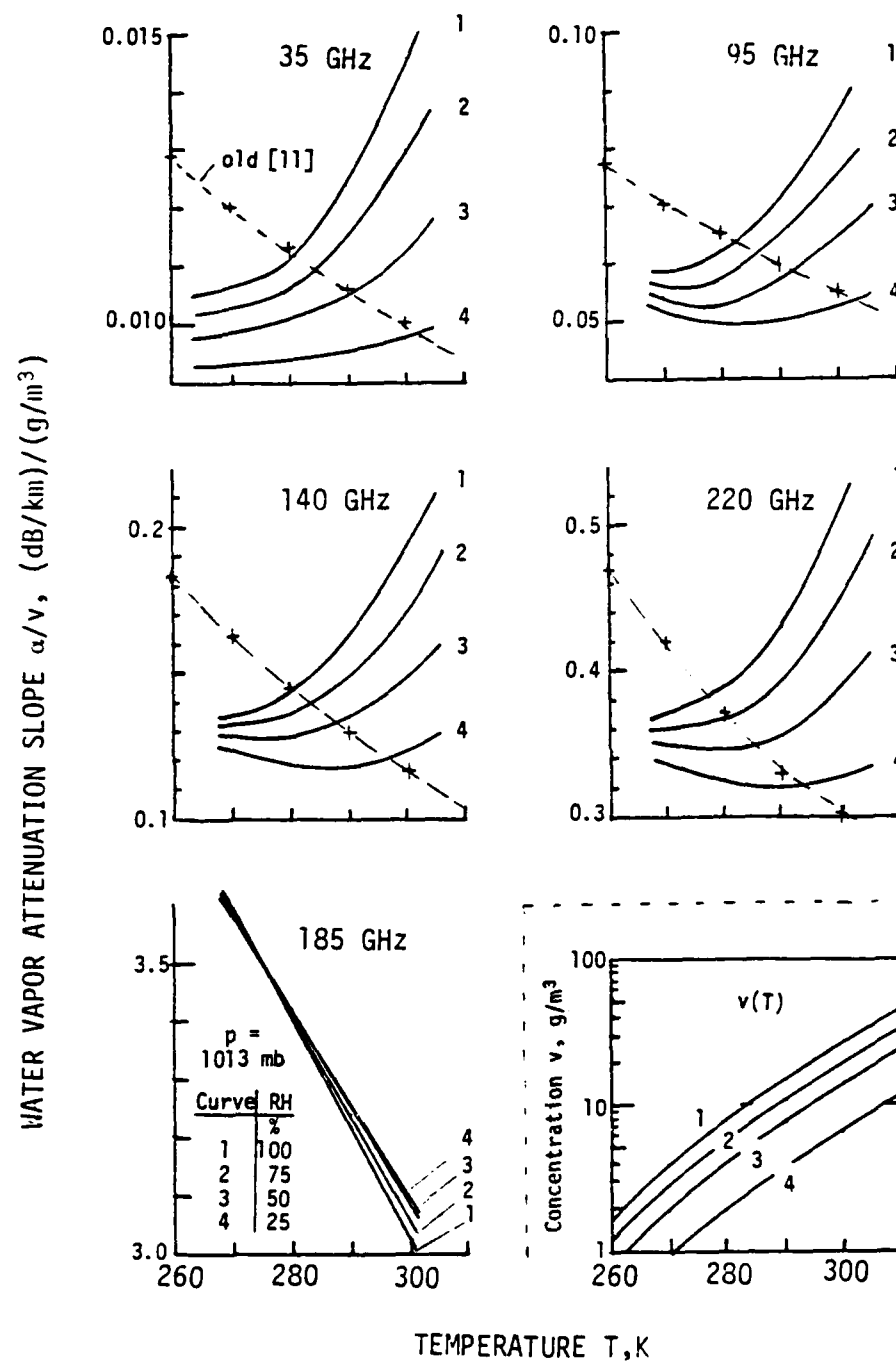
Figure 2. Specific water vapor attenuation α_v per unit concentration $v(g/m^3)$ for the conditions listed in Table 1.

-7-
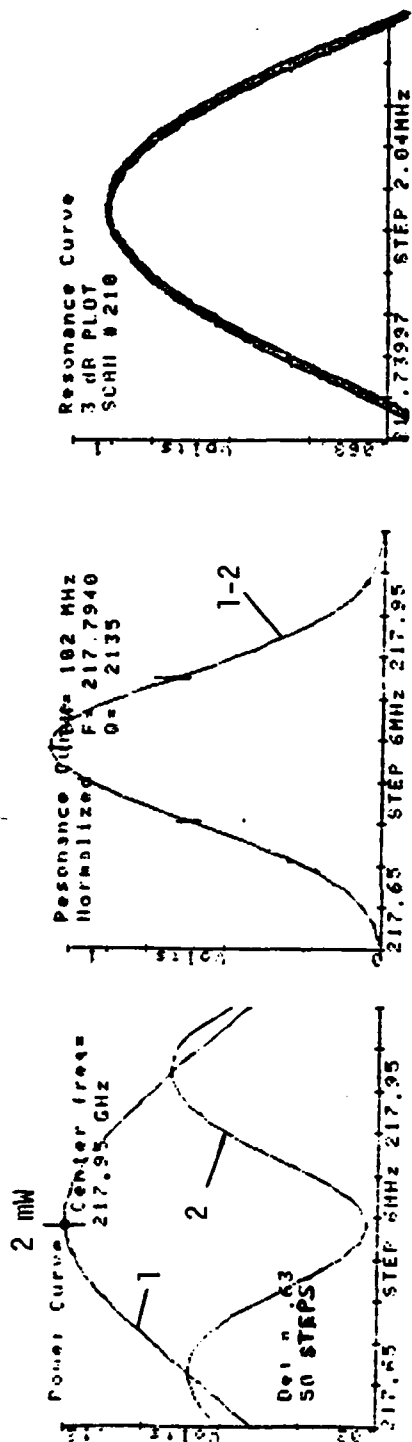
MENU:

```
Set Klystron for
  PEAK of Power curve
  DE-TUNE CAVITY
  and Press CONT

Power Curve
Center frequency  72.602
Multiplier= 3
Amplitude= .025164
Span set at +/-   500 MHz
Y axis (VOLTS)
  MIN- .07 MAX .03
Number of samples= 50
Detector 3 dB factor= .63
CHANGE (Y/N)?
```

Tune cavity to
RESONANCE
and Press CONT
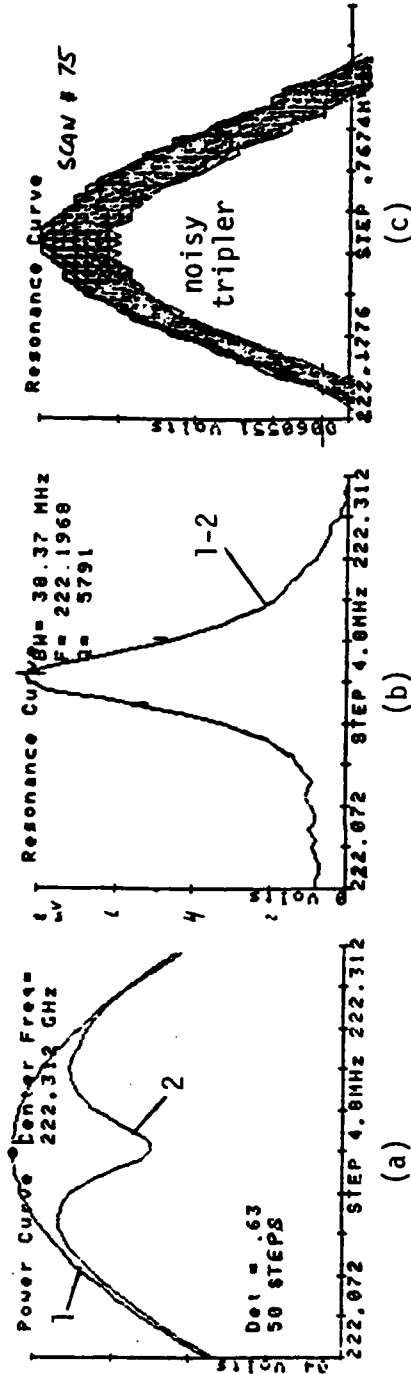
Figure 3.   Power curves of the 220 GHz synthesizer: (a) stepped-frequency mode under program control through resonances of two wavemeters centered at 217.95 and 222.2 GHz; (b) reduced resonance curves; and (c) retraces of the resonance center for 210 (= 3.5 hrs) and 75 (= 1.25 hrs) scans each in 50 steps.

-8-

Parametric studies of the attenuation rate α were performed. Experimental variables are frequency f, total pressure P, temperature T, and humidity v(RH). Absolute attenuation due to water vapor and moist gas mixtures has been measured up to saturation pressures (RH = 100%) and void of the instrumental (condensation) errors plaguing earlier measurements. Hysteresis effects in cycles of relative humidity (Fig. 11, p. A13) indicated condensation on the spectrometer mirrors and resulted in highly erroneous attenuation values.[*] A large body of earlier data had to be disqualified because of this. Slight, localized heating (+ 1°C) of the mirrors and a double-sealed coupling iris cured the problem.

Laboratory results in support of the MPM are reported in [1], [6], [13], [15], [16], [17], [21], [22], [24], and [26]. Measurements at 35 GHz [26] proved to be inconclusive since moist air attenuation α is relatively weak (Table 1). Measurements at 96 GHz were performed with a well calibrated horizontal radio path, 27 km long and operated in Boulder, CO (h = 1.5 km) [14], [24d]. Most of the data in support of the new continuum α_c were taken at 138 GHz [16].

2.4 Needed Future Work

Two shortcomings of the propagation model MPM lie in

- the missing confirmation of the physical origin for the water continuum α_c and

- an oversimplified treatment of opaque atmospheric conditions caused by haze, fog, clouds, dust, smoke, etc.

Additional parametric studies of the water vapor continuum absorption for self- and air-broadening should be performed at high relative humidities (RH = 80 to 100%), different temperatures (T = 270 to 320 K), and total pressures (P = 100 to 1500 mb) at the two window frequencies, f = 140 and 220 GHz (see Table 1). Artificial aerosol populations of known chemical composition and concentration can be added to study their growth/evaporation behavior as a function of humidity.

The pressure-broadened water vapor absorption line centered at 183.3 GHz might be included in the parametric laboratory studies to obtain accurate strength, width, shift, shape data, which are particularly important to remote sensing applications.

---

[*] We suspect that this source of instrumental error also affected results reported by other workers, thus contributing to the many inconsistencies of reported water vapor excess absorption [3].
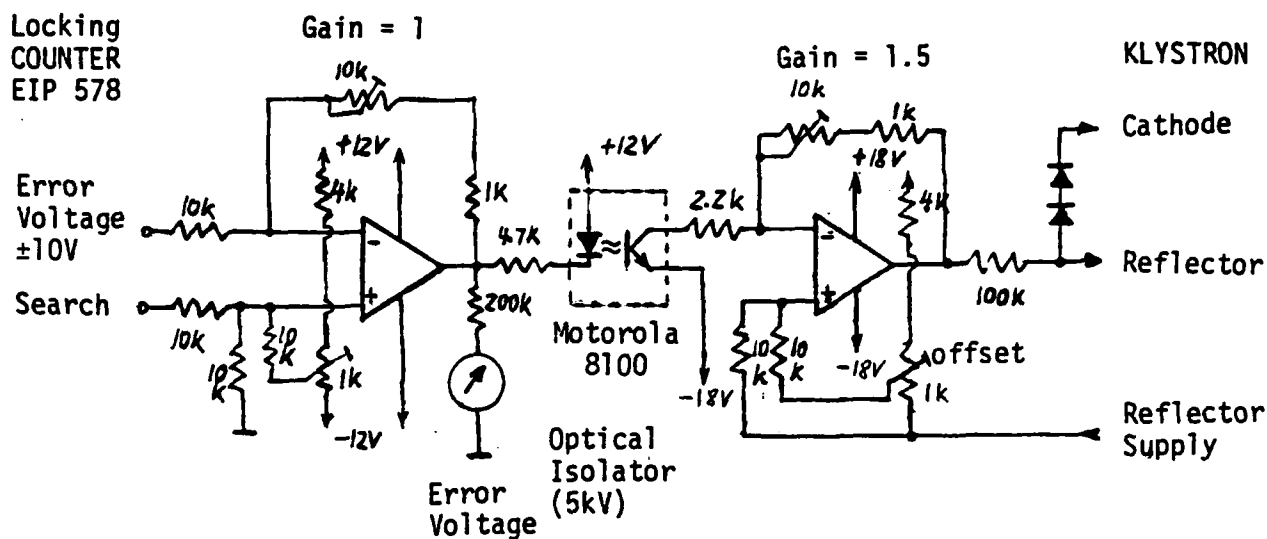
(a) Klystron Phase-lock High-voltage Isolation
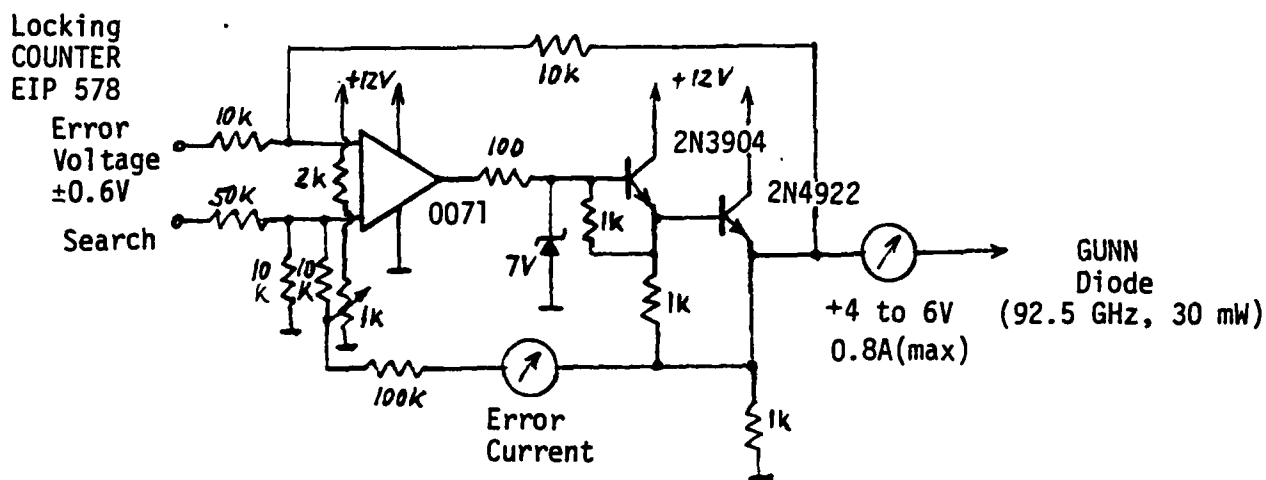
(b) Gunn Phase-lock Current Driver

Figure 4. Diagrams of circuits used to control (a) a klystron and (b) a Gunn
oscillator by means of a phase-locking counter.

3. LIST OF PUBLICATIONS/REFERENCES*

A. Manuscripts Published Under ARO Sponsorship

(25 copies each have been forwarded to ARO Information Processing)

	Acknowledgment
[1] H. Liebe, Quantitative line and band shape studies with a pressure-scanning mm-wave dispersion spectrometer, Proc. 4th Int'l. Conf. IR & MM Waves, IEEE Cat. No. 79 CH 1384-7, W 4.4, December 1979.	ARO 30-79
[2] H. Liebe, Millimeter wave attenuation in moist air: a review, in Proc. Workshop MM & SubMM Atm. Propagation, U.S. Army Missile Command, Technical Report RR-80-3, (D. Essenwanger and D. Stewart, editors), pp. 118128, February 1980.	ARO 30-79
[3] H. Liebe, Atmospheric water vapor: a nemesis for millimeter wave propagation, in "Atmospheric Water Vapor," (A. Deepak et al., editors), Academic Press, pp. 143-201, December 1980 (see APPENDIX).	ARO 30-79
[4] R. Burke, P. DeLogne, H. Gebbie, H. Liebe, and G. Richards, URSI Working Party report: Attenuation by oxygen and water vapor in the atmosphere at millimetric wavelengths, Radio Sci. 16(5), 825-829, 1981.	N/A
[5] H. Liebe, Modeling attenuation and phase of radio waves in air at frequencies below 1000 GHz, Radio Sci. 16(6), 1183-1199, 1981 (ITS Outstanding Paper Award).	ARO 42-80
[6] H. Liebe, Laboratory studies of water vapor absorption in atmospheric EHF windows, Proc. 6th Int'l. Conf. IR & MM Waves, IEEE Cat. No. 81 CH 1645-1, T 4.7, December 1981.	ARO 42-80/ 51-81
[7] H. Liebe, Attenuation of radio waves in air below 1000 GHz for heights 0 to 100 km, Poster Paper at DoD-NASA Meeting on Near MM Waves, Goddard Space Flight Center, and at XXth URSI General Assembly, both Washington, DC, 1-11, August 1981.	ARO 42-80
[8] H. Liebe, The atmospheric propagation medium between 45 and 75 GHz, AGARD Conf. Proc. CP-331, pp. 4/1-12, 1982.	ARO 6-8
[9] M. Mizushima, Absorption of millimeter to submillimeter waves by atmospheric water molecules, Int'l. J. IR & MM Waves 3(3), 379-384, 1982 (see APPENDIX).	H. Liebe

---

* AVAILABILITY OF PUBLICATIONS -
Requests for copies of journal articles should be addressed to the journal.
NTIA Reports are available via the accession number from the National
Technical Information Service, 5285 Port Royal Road, Springfield, VA 22161.
Technical Memoranda and Internal Reports are not generally available, but
additional information may be secured by contacting the author.

Reference	Acknowledgment

[10] M. Mizushima, Transparency of earth's atmosphere in the ITS
frequency region below 1 THz, Int'l. J. IR & MM
Waves 3(6), 889-895, 1982 (see APPENDIX).

[11] H. Liebe, Atmospheric window transparencies near 35, 90,   ARO 51-81/
140, and 220 GHz, IEEE Trans. Ant. & Prop. AP-31(1),   6-82
127-135, 1983 (invited by the IEEE Wave Propagation
Standards Committee).

[12] K. Allen and H. Liebe, Tropospheric absorption and   ARO 6-82
dispersion of millimeter and submillimeter waves,
IEEE Trans. Ant. & Prop. AP-31(1), 221-223 and
AP-31(6), 1004.

[13] H. Liebe and D. Layton, Experimental and analytical aspects   ARO 101-83
of the atmospheric EHF water vapor continuum, Proc.
URSI Com. F Symp., Belgium, June 1983 (ESA Report
SP-194, pp. 477-486).

[14] H. Liebe, An atmospheric millimeter wave propagation model,   ARO 101-83/
NTIA Report 83-137, December 1983 (NTIS Acces. No. PB   6-82/51-81/42-80
84-143494).

[15] H. Liebe, The atmospheric water vapor continuum below 300 GHz,   ARO 101-83
Proc. 8th Int'l. Conf. IR & MM Waves, IEEE Cat. No. 83
CH 1917-4, Th 6.3, December 1983.

[16] H. Liebe, The atmospheric water vapor continuum below 300 GHz,   ARO 101-83
Int'l. J. IR & MM Waves 5(2), 207-227, 1984 (see APPENDIX).

[17] H. Liebe, V. Wolfe, D. Howe, Test of wall coatings for a moist   ARO 101-83
air spectrometer cell, Rev. Sci. Instr. (submitted).

B. Internal Reports and Related Reports

(1 copy each has been forwarded to ARO)

[18] H. Liebe and R. Rosich, Computer program description for EHF properties of
clear air, NTIA-ITS Internal Report, August 1979.

[19] M. Mizushima, Radiation process as an adiabatic process, Dept. Phys., CU,
1979.

[20] M. Mizushima, Importance of $N^{14}N^{15}$ and $O^{16}O^{18}$ in the atmospheric absorption of
mm to submm waves, Dept. of Phys., CU, 1980.

[21] D. Kraft and H. Liebe, Interferometer design, IDL-Report, 12 pp.,
CU, December 1980.

[22] I. Mahoobi, Moist Air Spectrometer Performance, IDL-Report, 37 pp.,
CU, August 1981.

[23] J. Hopponen and H. Liebe, Simulation of millimeter wave propagation through
the atmosphere, NTIA-ITS Internal Report, August 1983.

[24] Excerpts from ITS Annual Technical Progress Report--
       a) 1980: pp. 1, 75-76, 79-81, 159;
       b) 1981: pp. 57-65, 71-72, 130;
       c) 1982: pp. 35-36, 45-52, 127;
       d) 1983: pp. 33, 50-55, 146-147.

[25] H. Liebe, Gaseous extinction, absorption and dispersion, review for Progress in Radio Science 1980-1983, Chapter 4 (Propagation in the Clear Atmosphere), to be published by URSI.

[26] H. Liebe, Molecular absorption test at 35 GHz, NTIA Report 82-96 (sponsored by USABMDSC and DNA), February 1982 (NTIS Acces. No. PB82-193426).

[27] K. Allen, H. Liebe, C. Rush, Estimates of millimeter wave attenuation for 18 United States cities, NTIA Report 83-119, May 1983 (NTIS Acces. No. PB83-240630).

[28] H. Liebe, Calculations with the ITS millimeter wave propagation model, NTIA-ITS Internal Report for CCIR, Study Group 5, IWP 5/3, July 1983 (33 pp.).

[29] H. Liebe, K. Allen, E. Violette, E. Dutton, System performance model for terrestrial millimeter wave communications: a development plan for Army applications, NTIA Technical Memorandum TM-83-92 (sponsored by USACEEIA), August 1983.

C. Abstracts of Presentations

(1 copy each has been forwarded to ARO)

H. Liebe, Atmospheric water vapor - A calamity for EHF propagation, URSI Comm. F, International Symposium, Lennoxville, Canada, May 1980 (hand-out, 18 pp.).

H. Liebe, New results for the atmospheric O_2 microwave spectrum, 3rd Ann. Rev. Conf. Atm. Transm. Models, AFGL, Hanscom AFB, Bedford, MA, May 1980.

H. Liebe, EHF refractivity of moist air, International Symposium on Electromagnetic Waves, URSI-C, Munich, W-Germany, August 1980 (hand-out, 12 pp.).

H. Liebe and V. Wolfe, Design problems associated with a millimeter wave spectrometer cell used in high humidity studies, National Radio Science Meeting, URSI-A, Boulder, CO, January 1981.

H. Liebe and B. Shaw, A model for 1 to 1000 GHz propagation in moist air, National Radio Science Meeting, URSI-F, Boulder, CO, January 1981.

H. Liebe, Attenuation and phase of radio waves in air below 1000 GHz, 4th Ann. Rev. Conf. Atm. Transm. Models, AFGL, Hanscom AFB, Bedford, MA, June 1981.

H. Liebe, Millimeter waves in the atmosphere, Colorado School of Mines, Physics Colloqu., Golden, CO, November 1981.

H. Liebe, Strategy for MMW systems, ERADCOM-NVEOL Workshop on 94 GHz/220 GHz/10μm Systems, Ft. Belvoir, VA, November 1981.

H. Liebe, EHF attenuation and delay properties of model atmospheres, National Radio Science Meeting, URSI-F, Boulder, CO, January 1982.

H. Liebe, Relative humidity performance of millimeter wave spectrometer, IFAORS Workshop on Hygroscopic Aerosols, Vail, CO, April 1982.

H. Liebe, Atmospheric window transparencies near 35, 90, 140, 220 GHz and higher, National Radio Science Meeting, URSI-F/J, Boulder, CO, January 1983.

H. Liebe, Experimental and analytical aspects of the atmospheric EHF water vapor continuum, 6th Ann. Rev. Conf. Atm. Transm. Models, AFGL, Hanscom AFB, Bedford, MA, May 1983.

H. Liebe, Atmospheric water vapor continuum absorption below 300 GHz, NOAA-ERL-WPL Seminar, Boulder, CO, March 1984.

H. Liebe, Millimeter wave propagation model for moist air based on local lines, 7th Ann. Rev. Conf. Atm. Transm. Models, AFGL, Hanscom AFB, Bedford, MA, May 1984.

H. Liebe, Millimeter wave attenuation by atmospheric water vapor, invited for Highlights Session F2 at XXIst URSI General Assembly, Florence, Italy, August 1984.

Publications Summary

	ARO-sponsored	Related
Journal Papers	9	-
Reports	1	2
Conference Proceedings	7	-
Internal Reports	8	2
Presentations	12	3

4. SCIENTIFIC PERSONNEL

Principal Investigator	Period
Dr. Hans J. Liebe	9/79 to 2/84

Theory

Prof. Masataka Mizushima[*]	1/80 to 12/82

Spectrometer Construction

David Kraft[+]	1/80 to 2/81
Karl Gebert[+]	6/81 to 12/82
Issa Mahoobi[+]	3/81 to 8/81

Electronic Design

Forrest E. Marler	7/80 to 12/81
Donald H. Layton	1/82 to 12/83

Programming

Duane C. Hyovalti	10/79 to 12/79
Benjamin Shaw	1/80 to 12/81
Kenneth C. Allen	7/81 to 6/83

Student Assistants

Vincent Wolfe[*]	10/79 to 2/84
Margy Kemp	4/81 to 6/81

[*]Department of Physics, University of Colorado, Boulder, CO 80309.
[+]Instrument Development Laboratory, University of Colorado, Boulder, CO 80309.

5. CONTRACT NUMBERS

ARO Proposal Number: 16638-GS

Contract Number	Period
ARO 30-79	8/79 to 4/80
ARO 42-80	5/80 to 4/81
ARO 51-81	5/81 to 9/81
ARO 6-82	10/81 to 7/82
ARO 64-82	8/82 to 9/82
ARO 101-83	10/82 to 2/84

APPENDIX

FOUR SELECTED REPRINTS

---

[1]Corrected Version

ATMOSPHERIC WATER VAPOR

Edited by

Adarsh Deepak

Institute for Atmospheric Optics and Remote Sensing
Hampton, Virginia

Thomas D. Wilkerson

Institute for Physical Sciences and Technology
University of Maryland
College Park, Maryland

Lothar H. Ruhnke

Atmospheric Physics Branch
Naval Research Laboratory
Washington, DC

ACADEMIC PRESS   1980
A Subsidiary of Harcourt Brace Jovanovich, Publishers

New York   London   Toronto   Sydney   San Francisco

PREFACE

This volume contains the technical proceedings of the International Workshop on Atmospheric Water Vapor held in Vail, Colorado, September 11-13, 1979.

The workshop was organized to bring together researchers in various related fields to assess the present state-of-the-art in measurement, modeling, and application of atmospheric water vapor properties and to identify those important problems in which further effort, in the near future, is needed for better understanding of the atmosphere itself, and of electromagnetic propagation through the atmosphere. One hundred and eleven scientists from universities, government agencies, research laboratories, and industry in the United States, England, France, Germany, and India attended the Workshop in which forty five papers were presented. Complete texts of thirty nine of these papers and some selected discussions are included in this volume.

Atmospheric water vapor plays an important role in many atmospheric processes, such as those related to weather, climate, atmospheric chemistry, radiative transfer, electrooptic imaging, and remote sensing. Knowledge of the global distribution of water vapor and its transport, optical properties (absorption and emission) in the infrared and microwave regions, and influence on electromagnetic propagation, are of particular interest to a wide range of scientific disciplines.

The workshop program was divided into seven paper presentation sessions, one open discussion and one panel session. Thirty invited and fifteen contributed papers covering the various aspects of atmospheric water vapor were presented in the seven sessions under the excellent guidance of the session chairmen, as indicated: S. A. Clough, Optics and Spectroscopy of Water Vapor; H. J. Liebe, Microwave and Millimeter Wave Phenomena; G. M. Resch, Geoastrophysical Applications; P. M. Kuhn, *In Situ* Measurements of Water Vapor; V. E. Derr, Remote Sensing of Water Vapor; F. Baer, Meteorology of Water Vapor; V. Mohnen, Atmospheric Chemistry and Microphysics of Water Vapor. The papers discussed the current state of knowledge, as well as the results of the latest investigations in specific areas of research. The moderators for the open and panel discussion sessions were A. Gebbie and V. Mohnen, respectively. Ample time was allowed for discussions following each paper and in the discussion sessions. Discussions were recorded and the transcripts post-edited.

To ensure proper representation of major disciplines involved, a Technical Program Committee, composed of the following individuals, was set up: A. Deepak, Institute for Atmospheric Optics and Remote Sensing (IFAORS), Associate Chairman; L. H. Ruhnke, Naval Research Laboratory (NRL), Cochairman; T. D. Wilkerson, University of Maryland, Cochairman; K. Jayaweera, National Science Foundation (NSF); P. M. Kuhn, National Oceanic and Atmospheric Administration (NOAA); G. M. Resch, Jet Propulsion Laboratory (JPL); J. Rogers, Federal Aviation Administration (FAA); and S. Tilford, National Aeronautics and Space Administration (NASA) Headquarters.

The workshop was cosponsored by Naval Research Laboratory, Naval Air Systems Command, Office of Naval Research (ONR), National Aeronautics and Space Administration, National Oceanic and Atmospheric Administration, Federal Aviation Administration, National Science Foundation, University of Maryland, and the Institute for Atmospheric Optics and Remote Sensing.

The editors wish to acknowledge the enthusiastic support and cooperation of the members of the Technical Program Committee, session chairmen, speakers, and participants for making this a very stimulating and highly beneficial workshop for everyone. Special thanks are due the authors for their cooperation in enabling a prompt publication of the workshop proceedings. It is a pleasure to acknowledge the valuable assistance of IFAORS staff, especially, Sherry Allen, Sue Crotts, and June Ewing, in the smooth organization of the workshop, and H. Mulcahy and M. Goodwin in preparing and typing of the manuscripts.

The editors hope this volume will be a useful contribution to the field of atmospheric water vapor and serve as a reference volume for many years to come.

Adarsh Deepak
Thomas D. Wilkerson
Lothar H. Ruhnke

Atmospheric Water Vapor:
A Nemesis for Millimeter Wave Propagation [1]

Hans J. Liebe

U.S. Department of Commerce
National Telecommunications and Information Administration
Institute for Telecommunication Sciences
Boulder, Colorado

Millimeter waves offer an attractive way of solving unique system problems because of their ability to penetrate clouds, smog, dust or fog. This makes them a logical choice over electro-optical devices for adverse weather applications. Spectral lines of oxygen and water vapor ultimately limit the atmospheric transparency; hence, most applications operate between the absorption lines in four window regions (that is, 24 to 48, 77 to 110, 120 to 160, and 200 to 260 GHz). Observations have established the existence of excess water vapor absorption (EWA), which is most evident in these windows. Excess implies that the effect is not related to the known spectral properties of the water molecule. EWA is found to increase in nontrivial manner with humidity and the discrepancies can be as large as a factor of 10. Several groups (most notably at the Appleton Laboratory, UK), have gathered evidence of EWA from laboratory and field observations and brought forward hypotheses to account for the data. Qualitative explanations are based on the assumption that water molecules in moist air form larger molecules with a dimer being the first step in a series of stable species. Hydrogen bonding, ion attraction and attachment of the polar H_2O to foreign particles (aerosol growth) are the ordering forces considered in the clustering process. An assessment of the current EWA picture will be given and avenues of research attacks are discussed to solve the enigma in the quantitative description of the interaction between millimeter waves and moist air.

I. INTRODUCTION

Atmospheric water in both vapor and liquid states is the major deterrent to an unrestricted exploitation of propagation of millimeter and, more so, of infrared wavelengths. For most applications, the operation of ground-based systems is limited to seven window regions W1 to W7, these being the gaps between molecular absorption lines and bands:

Absorption Feature	Region	Window Range
22 GHz H_2O line	W1	24 to 48 GHz
60 GHz O_2 line complex	W2	70 to 115 GHz
119 GHz O_2 line	W3	120 to 165 GHz
183 GHz H_2O line	W4	200 to 310 GHz
325 GHz H_2O line	W5	340 to 365 GHz
380 GHz H_2O line and 1823 more (H_2O rotational band)	W6	20 to 38 THz
6.3 μm H_2O band	W7	60 to 100 THz
2.7 μm H_2O band		

The main attraction of millimeter wave systems is their ability to penetrate the somewhat opaque atmosphere (haze, fog, clouds, dust, smoke, light rain) under circumstances in which electro-optical and infrared systems normally fail. Accurate and detailed knowledge of atmospheric transmission is essential to an evaluation of the advantages of millimeter waves over the shorter wavelengths.

One objective of this paper is to focus attention on unsolved problems in the construction of a valid model for atmospheric millimeter wave transmission, subject to the following conditions: Frequency, $v = 10$ to 1000 GHz, with special emphasis on the EHF range, $v = 30$ to 300 GHz; altitude, $h = 0$ to 30 km; and relative humidity, RH = 0 to ≤ 100%. The radio engineer uses the optical term "clear" for moist, but unsaturated air (RH < 100%), and ignores haze conditions. Although many constituents contribute to the total atmospheric attenuation rate, α (dB/km), absorption in the window is dominated by water vapor and is of greatest concern for practical situations. At present, describing water vapor absorption mechanisms and relating them to measurable quantities is partly an empirical matter and lacks credibility in a general sense.

The following interaction effects between millimeter waves and air are well documented:

Case		References
(a)	Absorption line theory	1, 4, 13, 31
(b)	Moist air refraction	2, 5, 7, 47-50
(c)	Water vapor absorption	1, 3, 4, 7, 14, 16, 17, 24, 25
(d)	Water vapor dispersion	2, 4, 5, 7, 17, 62, 67
(e)	Water vapor continuum absorption	11, 12, 18, 21, 22, 24, 26, 31
(f)	Oxygen absorption	15, 17, 19, 65
(g)	Complete line parameter compilation for all atmospheric molecules known as the AFCL Tape,	110
	HITRAN Model and FASCODE	10, 14, 25, 29
(h)	Scattering loss by particles	33, 32, 35-37
(i)	Dielectric loss of water	25, 27, 32, 102-106

Other physical effects, which have been taken into account in infrared transmission models (9), (20), and (23) are:

(k)	Submicron aerosol particles	38, 41, 42
(l)	Growth of submicron particles in moist air	34-37

Of a more speculative nature are considerations of

(m)	Water dimer $(H_2O)_2$ spectra	6, 8, 21, 43, 58, 64, 66, 69, 81, 86, 89, 109
(n)	Water cluster $(H_2O)_n$, n>2	21, 22, 44
(o)	Water ion activity	28, 45

The water polymer hypotheses have the inherent weakness that except for the dimer (43), neither definite structural observations have been made nor millimeter wave spectra calculated. In the cases (m) to (o), production and growth mechanisms (for example, ion-induced) as well as size and number density distributions have not been identified for the natural atmospheric environment.

Measured absorption in the windows W1 to W7 could provide clues for the understanding of which basic physical mechanisms are missing in current models. New instrumentation, such as the dispersion spectrometer (63,65) and the saturation hygrometer (107), might prove helpful in future investigations. Available experimental results on absolute attenuation rates, path transmittances, and thermal emission from laboratory (46-71) and field (73-101) observations in cloudless moist air are generally higher than values predicted on the basis of molecular absorption alone. It is a fact, even after allowing for difficulties in measuring the highly variable water content quantitatively, that the absorption by water vapor in the atmospheric transmission windows W1 to W7 is not completely understood.

Section II of this paper presents the framework for a radio path modeling scheme of which details, such as measurements and validation, have been published (15,17,19). The model serves as a basis for the definition and discussion, in Section IV, of the problem of excess water vapor absorption (EWA) in the light of experimental data. Section III is devoted to a brief presentation of relevant physical properties of atmospheric water vapor.

II. EHF RADIO PATH MODELING

Millimeter waves traveling through the cloudless (RH ≤ 100%) atmosphere suffer both deterministic and random variations in amplitude and phase. Radiation is absorbed and refracted by gases and submicron particles. This interaction is modeled with the intent to predict the following frequency-dependent propagation effects: (a) absorptive loss of coherent radiation, (b) time of propagation between two points, (c) refractive ray-bending and ducting, (d) generation of incoherent noise, and (e) scintillations due to random fluctuations of the medium in space and time. The array of mathematical and empirical expressions used to compute these various effects is called the Propagation Model. Such a parameterization scheme depends foremost on spectroscopic information about kind and number density of absorber species and on their distribution within the path volume.

A. The Propagation Model

Complex refractivity N(ppm) is a convenient macroscopic measure of the interaction between millimeter wave radiation and the individual absorbers in moist air. A value of N accounts for the effectiveness and number density of a particular absorber population. Later these dependences are formulated in terms of measurable quantities. At this point, N is assumed to be known

and the basic relations that determine the electromagnetic behavior of a radio path are written down. The complex refractivity of a gaseous medium in ppm

$$N = N_0 + D(\nu) + j\, N''(\nu) \qquad (1)$$

consists of three components; namely, the frequency independent refractivity N_0 plus various spectra of refractive dispersion $D(\nu)$ and absorption $N''(\nu)$. The atmosphere is characterized as a linear network with both passive and active properties. The amplitude and phase response of a plane radio wave traveling the distance $L(km)$ and having an initial field strength E_0 is described by

$$E = E_0 \exp\,(\Gamma L) \qquad (2)$$

where

$$\Gamma = j(2\pi\nu/c)(1 + N \cdot 10^{-6}) \qquad (3)$$

is the propagation constant of the intervening medium, c being the speed of light. Usually, real and imaginary parts of N are separated and expressed as the power attenuation rate in dB/km

$$\alpha = 0.1820\nu\,IM(N) \qquad (4)$$

and the phase delay rate in radian/km

$$\varphi = 0.0209\nu\,RE(N) \qquad (5)$$

The frequency ν is in gigahertz (GHz) throughout the paper.

The attenuation rate α is the more familiar quantity in atmospheric wave propagation. The phase rate φ must be considered when it varies spatially (for example, radar pointing accuracy, long-baseline interferometry, maximum dish size for reflector antennas, etc.) or with frequency (for example, bandwidth limitations of a communication channel). Characteristics of short, horizontal radio paths may be approximated by an average value of N. More general path geometries, such as a ground-to-satellite link, are treated by dividing the path into segments having quasi-constant N-values and summing. The cumulative behavior between the ray points s_1 and s_2 is expressed in dB by the total attenuation

$$A = \int_{s_1}^{s_2} \alpha(s)\, ds \qquad (6)$$

or by the transmittance (multiply by $1/10 \log e = 0.23026$ to convert dB to Np)

$$\tau = \exp(-0.230A) \qquad (7)$$

The medium becomes transparent when τ approaches one and, on the other hand, opaque for $\tau \geq 0$.

The total phase change for the same path is given in radians by

$$\phi = \int_{s_1}^{s_2} \varphi(s)\, ds \qquad (8)$$

which translates into the travel-time in ns of the wave by

$$\eta = \phi/2\pi\nu \qquad (9)$$

The path differential ds is, in practice, an increment Δs over which N is quasi-constant, and depends upon the altitude, h; the starting angle, θ, from the zenith in the case of a slant path; and refractive bending of the ray (Snell's law) due to gradients $\delta\varphi/\delta s$ (19).

Absorption by the atmosphere causes emission spectra. Each unit of volume maintains thermal equilibrium with its environment via collisions; hence, the path element ds radiates an equivalent blackbody emission $T(s)\,\alpha(s)\,ds$, which is reduced by the transmittance $\tau(s)$ along the path of observation. The resulting brightness temperature in K

$$T_B = 0.230 \int_0^\infty T(s)\,\alpha(s)\,\tau(s)\, ds \qquad (10)$$

is either less than or equal to the ambient temperature T. Equations (6), (8), and (10) constitute the key by which performance limitations of EHF systems operating over clear-air propagation paths may be evaluated. A transfer function exhibiting constant amplitue (A = constant), frequency-linear phase delay [D(ν) = 0], and no noise (T_B = 0) implies ideal channel behavior. A broadband signal occupying a frequency interval $\Delta\nu$ is distorted by the deterministic spectra of D(ν) and N''(ν); in addition, T_B imposes detection limitations. As a bonus, the emission spectra $T_B(\nu)$ afford opportunities to sense remotely the state of the atmosphere by passive radiometric means (for example, Ref. 39 and 40).

B. The EHF Refractivity of Moist Air

The physical state of moist air is described by

$$\left.\begin{array}{ll} \text{dry air pressure (1 kPa = 10 mb)} & P\,,\ kPa \\ \text{relative inverse temperature (T in K)} & t = 300/T \\ \text{water vapor partial pressure} & e\,,\ kPa \end{array}\right\} \quad (11)$$

Calculation of the frequency-independent refractivity in ppm in Eq. (1) is straightforward (47-50)

$$N_0 = 2.589\ p\,t + (41.6\,t + 2.39)\ et \qquad (12)$$

Water vapor refractivity is about 16 times more effective, on a per molecule basis, than dry air in generating propagation phenomena such as delay, ray bending, ducting, scintillations, etc.

The dispersion contribution in ppm

$$D(\nu) = \sum_i (S\,F')_i - 41.6\ et^2 \qquad (13)$$

and the absorption spectrum in ppm

$$N''(\nu) = \sum_i (S\,F'')_i + N_\nu'' + N_x'' \qquad (14)$$

require further elaboration. Frequency-dependent molecular spectra are of two types:

1. Line spectra of absorption SF'' and of dispersive refraction SF', having strength S in units of kHz and shape factors F' and F'' in units of GHz^{-1}; the sums over i consider millimeter wave lines (see Tables 1 and 2) of O_2 (i = 2 to 45)[2] and H_2O (i = 46 to 74). Spectra of the trace gases O_3, CO, N_2O, SO_2, NH_3, etc., are neglected (10,17,29,31,110).

2. Continuum water vapor spectrum N_ν'' due to far-wing contributions of very strong infrared lines. A third term, N_x'', which is not fully understood, was added to the absorption to account for contributions other than those of the rotational water vapor line spectrum (see Section IV).

Common to each spectroscopic feature is an intensity-against-frequency distribution function, the shapes F'(ν) and F''(ν). For h < 20 km, the shape functions are (17),(67)

$$F' = \left[\frac{(\nu_0 - \nu) + \gamma I}{(\nu_0 - \nu)^2 + \gamma^2} + \frac{(\nu_0 + \nu) + \gamma I}{(\nu_T + \nu)^2 + \gamma^2}\right] \qquad (15)$$

and

.

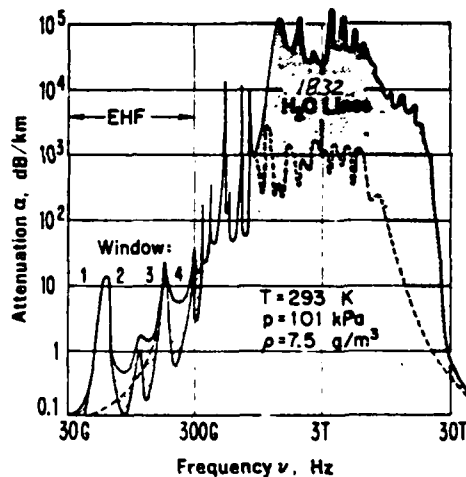[2] The nonresonant oxygen spectrum, i = 1 is discussed in Ref. 17.

FIGURE 1. Attenuation rate α at sea level (h = 0 km, e = 1.015 kPa) over the frequency range, ν = 30 GHz to 30 THz displaying the envelope for maximum/minimum values of the rotational water vapor spectrum. Calculated by using the AFGL Tape (10).

$$F'' = \left(\frac{\nu}{\nu_o}\right)\left[\frac{\gamma - (\nu_o - \nu)\,I}{(\nu_o - \nu)^2 + \gamma^2} + \frac{\gamma - (\nu_o + \nu)\,I}{(\nu_o + \nu)^2 + \gamma^2}\right] \qquad (16)$$

introducing the spectroscopic parameters of center frequency ν_o, width γ, and overlap interference I. F' and F'' are in units of $1/GHz$.

For $h > 20$ km, only isolated resonant lines are present, spread over a megahertz frequency scale. Equations (15) and (16) are replaced by Lorentzian shapes

$$F'_L = (\nu_o - \nu)/[(\nu_o - \nu)^2 + \gamma^2] \qquad (17)$$

and

$$F''_L = \gamma/[(\nu_o - \nu)^2 + \gamma^2] \qquad (18)$$

where F'_L and F''_L are in units of $1/GHz$. Peak dispersion at $\nu = \nu_o \mp \gamma$ and maximum absorption at $\nu = \nu_o$ are given in ppm by

$$\pm D_m = S/2\gamma$$
$$N''_m = S/\gamma \qquad (19)$$

For $h > 40$ km, a further decrease in pressure converts the pressure-broadened Lorentzian into a Doppler-broadened Gaussian shape with a different width in kHz of

$$\gamma_D = 6.20\ \nu_o/\sqrt{mt} \qquad (20)$$

where m is the molecular weight (e.g., O_2, $m = 32$, $t = 1$, $\nu_o = 60$ GHz: $\gamma_D = 65.8$ kHz).

The convolution of Lorentzian and Gaussian shape functions is called the Voigt profile, which is governed by the parameter γ/γ_D. The Voigt profile is appropriate when this ratio falls in the range between ≈ 10 and 0.1. Numerical evaluation of the height-dependent complex Voigt function requires considerable computational effort (19).

1. *Microwave Spectrum of Oxygen (O_2-MS)*. The O_2 molecule has electronic, vibrational, and rotational energy levels with transitions causing spectral lines from the optical to the EHF range. The EHF lines are fine structure transitions between rotational triplet energy levels. All pertinent information on the O_2-MS is tabulated; that is, the line parameters have been reduced to five coefficients a_1 to a_5, which are listed in Table I together with the center frequencies ν_o (17,19). Dependence on atmospheric properties is expressed by

$$S = a_1\ p\ t^3\ \exp[a_2(1 - t)] \qquad (21)$$

$$\gamma = a_3\ (p + 1.3e)\ t^{0.9} \qquad (22)$$

$$I = a_4\ p\ t^{a_5} \qquad (23)$$

where S and γ are in kHz and GHz, respectively. Water vapor influences the O_2-MS through Eq. (22).

2. *Microwave Spectrum of Water Vapor*. From the AFGL line parameter compilation (10), 1838 H_2O lines were read up to 31 THz when a maximum intensity ($\nu = \nu_o$) cutoff of 2×10^{-3} dB/km (300 K) is applied. For the EHF range, 29 lines (see Table 2) must be considered explicitly and the remaining ones are lumped into a continuum far-wing contribution. An individual line is described by

$$S_\nu = b_1\ e\ t^{3.5}\ \exp[b_2(1 - t)] \qquad (24)$$

$$\gamma_\nu = b_3(p + 4.80\ e)t^{0.6} \qquad (25)$$

$$I_\nu = 0$$

where S_ν and γ_ν are in kHz and GHz, respectively.

3. *Continuum Water Vapor Spectrum*. The remaining 1809 (that is, 1838 - 29) H_2O lines make far-wing contributions; they are fitted by (17)

$$N''_{\nu,i} \approx 1.9 \times 10^{-5}\ p\ e\ t^4\ (\nu/30) \qquad (26)$$

The continuum absorption N''_ν in ppm is of a magnitude and functional form that is similar to the empirical Gaut-Reifenstein expression (11)

$$N''_\nu = 5.6 \times 10^{-5}\ p\ e\ t^{3.1}\ (\nu/30) \qquad (27)$$

which was introduced by Waters (31) and has proven useful to other workers (32,108). The far-wing contributions to refractivity of all rotational H_2O lines yield with Eq. (12) in Eq. (13) the term $41.6\ et^2$ (3,4,5). The contribution of the local lines, $i = 46$ to 74 to this value is in ppm

$$\sum_i[SF'(\nu \to 0)]_i = 4.75\ et^3 \qquad (28)$$

Very accurately measured refractivity can serve as a test for the low frequency response of theoretical line shapes applied to the rotational H_2O spectrum if one is sure of the spectroscopic data base. A more detailed discussion of Eqs. (26) and (27) follows in Section IV.

4. *Temperature Behavior*. A closer look at the spectral line response aids in understanding the temperature dependence of EHF attenuation and phase dispersion rates in moist air. Line intensities are sensitive to temperature variations at various rates. The peak line intensities in ppm [Eq. (19)] are described by

	$S\gamma$
O_2	$(a_1/a_3)\,[p/(p + 1.3e)]\ t^{2.1}\exp[a_2(1 - t)]$
H_2O	$(b_1/b_3)\,[e/(p + 4.8e)]\ t^{2.9}\exp[b_2(1 - t)]$

$$(29)$$

The line intensities are independent of temperature when

		$t = 1.1$	1.3	1.5	2
O_2	$a_2 = 2.1\ln t/(t - 1)$	2.00	1.87 (see Table 1)	1.70	1.46
H_2O	$b_2 = 2.9\ln t/(t - 1)$	2.76	2.54 (see Table 2)	2.35	2.02

$$(30)$$

Lines with values lower than those prescribed by Eq. (30) increase in intensity when the temperature drops ($t > 1$) and vice versa. A useful approximation at a fixed frequency is given by

$$\alpha(t) = \alpha(300\ k)\ t^\gamma \qquad (31)$$

where the exponent γ is obtained by fitting model data.

C. The Radio-Path Model

The path is assumed to be in a spherically stratified atmosphere in which each layer is homogeneous. The integral expressions (Eqs. (6), (8) and (10)) are evaluated by the *layer-by-layer* method (19,29) by using numerical integration techniques since closed-form solutions are lacking because of the complicated temperature height profile.

Mean conditions are modeled by the U.S. Standard Atmosphere 1976, and in situ data from radiosonde ascents can be programmed in directly. Whatever description of the atmosphere is employed, model or data, it is converted in the computer into n-layers each having an assigned set of values of $p(h)$, $e(h) \leq e_s$, $t(h)$. Values for α are calculated by using Eqs. (4), (14), (16) and (21) to (25) and for φ by applying Eqs. (5), (12), (13,) (15) and (21) to (25), by the standard *line-by-line* superposition (29) and adding the continuum b_ν (27).

The radio path is assumed to be a ray (that is, plane wave case), and the general procedure is to calculate the local $N(h)$ (1) for the programmed altitude grid reporting p, e, t and to store N_o, $D(\nu)$, and $N''(\nu)$ separately on file. The ray starts at a surface height h_o with an elevation angle θ and is guided through the inhomogeneous medium until it reaches the intended final height h_1. Refraction is most pronounced at the lowest heights and causes substantial ray bending when θ is close to 0° (tangential path); thus, many fine steps are required initially.

Modeling is introduced for the purpose of predicting the mean of EHF propagation effects and the limits of their variability from readily available climatological data bases. In order to apply such a tool in an optimum manner, it is important to consider the uncertainties in the spectroscopic data and the limitations imposed by the numerical calculation procedure.

D. Typical Examples

The examples presented in Figs. 1 to 7 almost speak for themselves. Figure 1 is a presentation of the complete rotational water vapor spectrum for a typical sea-level condition. It was calculated by using the AFGL Data Tape (10) rather than the EHF model given in sections B and C, and serves to demonstrate the very strong (over 6 orders of magnitude) absorption due to water vapor in the far-infrared that allows on the low frequency end just a few window ranges for transmission.

A more refined modeling result is depicted in Fig. 2. It displays at higher altitudes ($h = 16$ km) spectral signatures of the trace gases O_3, CO, N_2O, which are not included in the described model. At tropospheric heights ($h = 0$ and 4 km), only lines of H_2O and O_2 (see markings at bottom of figure) are important. The figure gives, in essence, a picture of atmospheric molecular absorption in the millimeter and submillimeter wavelength range. These computations by Burch and Clough (24) agree well with reported data and the presented model (Eqs. (27) and (4)) of the water vapor continuum spectrum labeled α_x. The attenuation rate spans seven orders of magnitude over the frequency range $\nu = 100$ to 1000 GHz and altitudes $h = 0$ to 16 km where > 99.5% of the atmospheric water vapor is contained. The transparency in the window ranges W2 to W5, which are valleys between the absorption line peaks, is dominated by the water vapor continuum α_x. Figure 2 affirms the dominant role that

TABLE 1. Data Base for O_2^{16} Spectral Lines in Air up to 1000 GHz

i	Center frequency ν_0 GHz	Strength a_1 kHz/kPa	Temperature exponent a_2	Width a_3 GHz/kPa	Interference a_4 1/kPa	Temperature exponent a_5	ID	
1	0	3.070ᵃ E-4	--	5.6 E-3	--	--	Nonresonant	
	50.47360	0.940 E-6	9.6900	8.60 E-3	5.200 E-6	1.79		37⁻
	50.98730	2.440 E-4	8.6900	8.70 E-3	5.500 E-6	1.69		35⁻
	51.50302	6.040 E-5	7.7400	8.90 E-3	5.600 E-6	1.77		33⁻
5	52.02117	1.410 E-5	6.8400	9.20 E-3	5.500 E-6	1.81		31⁻
	52.54223	1.080 E-5	6.0000	9.40 E-3	5.690 E-6	1.79		29⁻
	53.06680	6.370 E-5	5.2200	9.70 E-3	5.280 E-6	1.89		27⁻
	53.59572	1.240 E-4	4.4800	10.00 E-3	5.440 E-6	1.83		25⁻
	54.12997	2.265 E-4	3.8100	10.20 E-3	4.800 E-6	1.99		23⁻
10	54.67116	3.893 E-4	3.1900	10.50 E-3	4.840 E-6	1.90		21⁻
	55.22136	6.274 E-4	2.6200	10.79 E-3	4.170 E-6	2.07		19⁻
	55.78380	9.471 E-4	2.1150	11.10 E-3	3.750 E-6	2.07		17⁻
	56.26478	5.453 E-4	0.0109	16.46 E-3	7.740 E-6	0.89	D1ᵇ	1⁺
	56.36339	1.335 E-3	1.6550	11.44 E-3	2.970 E-6	2.29		15⁻
15	56.96818	1.752 E-3	1.2550	11.81 E-3	2.120 E-6	2.53		13⁻
	57.61249	2.125 E-3	0.9100	12.21 E-3	0.940 E-6	3.76		11⁻
	58.32389	2.369 E-3	0.6210	12.66 E-3	-0.550 E-6	-11.10	D2	9⁻
	58.44660	1.447 E-3	0.0827	14.49 E-3	5.970 E-6	0.79		3⁺
	59.16422	2.387 E-3	0.3860	13.19 E-3	-2.440 E-6	0.07		7⁻
20	59.59098	2.097 E-3	0.2070	13.60 E-3	3.440 E-6	0.49		5⁺
	60.30604	2.109 E-3	0.2070	13.82 E-3	-4.350 E-6	0.68	D3	5⁻
	60.43478	2.444 E-3	0.3860	12.97 E-3	1.320 E-6	-1.20		7⁺
	61.15057	2.486 E-3	0.6210	12.48 E-3	-0.360 E-6	5.84		9⁺
	61.80017	2.281 E-3	0.9100	12.07 E-3	-1.590 E-6	2.86		11⁺
25	62.41122	1.919 E-3	1.2550	11.71 E-3	-2.660 E-6	2.26	D4	13⁺
	62.48626	1.507 E-3	0.0827	14.68 E-3	-5.030 E06	0.85		3⁻
	62.99800	1.492 E-3	1.6550	11.39 E-3	-3.340 E-6	2.18		15⁺
	63.56854	1.079 E-3	2.1150	11.08 E-3	-4.170 E-6	1.96		17⁺
	64.12778	7.281 E-4	2.6200	20.78 E-3	-4.480 E-6	2.00		19⁺
30	64.67892	4.601 E-4	3.1900	10.50 E-3	-5.150 E-6	1.84		21⁺
	65.22408	2.727 E-4	3.8100	10.20 E-3	-5.070 E-6	1.92		23⁺
	65.76474	1.520 E-4	4.4800	10.00 E-3	-5.670 E-6	1.78		25⁺
	66.30206	7.940 E-5	5.2200	9.70 E-3	-5.490 E-6	1.84		27⁺
	66.83677	3.910 E-5	6.0000	9.40 E-3	-5.880 E-6	1.74		29⁺
35	67.36951	1.810 E-5	6.8400	9.20 E-3	-5.600 E-6	1.77		31⁺
	67.90073	7.950 E-6	7.7400	8.90 E-3	-5.800 E-6	1.73		33⁺
	68.43080	3.280 E-6	8.6900	8.70 E-3	-5.700 E-6	1.65		35⁺
	68.96010	1.280 E-6	9.6900	8.60 E-3	-5.300 E-6	1.74		37⁺
39	118.75034	9.341 E-4	0.0000	15.92 E-3	-0.441 E-6	0.89		1⁻
40	368.49835	6.790 E-5	0.0200	15.60 E-3	0	--	---	1,3⁻
	424.76312	6.380 E-4	0.0112	14.70 E-3	0	--	---	1,3
	487.24937	2.350 E-4	0.0112	14.70 E-3	0	--	---	1,3⁺
	715.39315	9.960 E-5	0.0891	14.40 E-3	0	--	---	3,5⁻
	773.83873	5.710 E-4	0.0798	14.00 E-3	0	--	---	3,5
45	834.14533	1.800 E-4	0.0798	14.00 E-3	0	--	---	3,5⁺

ᵃUnits: ppm/kPa

ᵇD denotes doublet

TABLE 2. Data Base for H_2O^{16} Spectral Lines in Air up to 1000 GHz

i[a]	Center frequency v_0 GHz	Strength b_1 kHz/kPa	Temperature exponent b_2	Width b_3 GHz/kPa		ID (lower quant. no.) (10)			References
46	22.235080	0.105	2.143	28.1	E-3	5	2	3	(7,56,57)
	68.052000	0.002	8.750	28.0	E-3	4	1(1)[b]	4	(10)
•	183.310091	2.380	0.653	28.2	E-3	2	2	0	(51,55,13)
	321.225644	0.046	6.160	22.0	E-3	9	3	6	(10,13)
50 •	325.152919	1.550	1.520	29.0	E-3	4	2	2	(10,13)
•	380.197372	12.300	1.020	28.5	E-3	3	2	1	(10,13)
	386.778000	0.004	7.330	16.0	E-3	11	2	10	(10,110)
	437.346670	0.063	5.020	15.0	E-3	6	6	0	(10,13)
	439.150812	0.921	3.560	17.5	E-3	5	5	0	(10,13)
55	443.018295	0.191	5.020	14.8	E-3	6	6	1	(10,13)
•	448.001075	10.700	1.370	24.6	E-3	3	3	0	(10,13)
	470.888947	0.328	3.570	18.1	E-3	5	5	1	(10,13)
	474.689127	1.240	2.340	21.0	E-3	4	4	0	(10,13)
	488.491133	0.256	2.810	22.2	E-3	7	1	7	(10,13)
60	504.219000	0.038	6.690	12.7	E-3	7	7	0	(10,110)
	505.126000	0.012	6.690	13.0	E-3	7	7	1	(10,110)
•	556.936002	526.000	0.114	31.7	E-3	1	0	1	(10,13)
•	620.700807	5.210	2.340	21.6	E-3	4	4	1	(10,13)
	658.340000	0.460	7.760	32.8	E-3	1	0(1)	1	(10)
65 •	752.033227	259.000	0.336	30.2	E-3	2	0	2	(10,13)
	836.836000	0.012	8.110	17.0	E-3	11	2	9	(10,110)
	859.810000	0.015	7.990	27.0	E-3	2	0(1)	2	(10)
	899.380000	0.091	7.840	30.0	E-3	1	1(1)	1	(10)
	903.280000	0.064	8.350	28.0	E-3	2	2(1)	1	(10)
70	907.773000	0.179	5.040	20.4	E-3	8	3	5	(10,110)
•	916.169000	8.900	1.370	24.9	E-3	3	3	1	(10,110)
•	970.320000	9.400	1.840	24.6	E-3	4	3	1	(10,110)
•	987.940000	145.000	0.180	29.9	E-3	1	1	1	(10)
74 •	1097.368000	840.000	0.656	33.5	E-3	3	0	3	(10,110)

Plus 1809 additional lines up to 31 THz, of which 361 lines have strengths, $b_1 > 1000$. The strongest lines are at:

•	2774.100000	2023.000	0.208	29.5	E-3	1	1	0	Max. strength
•	6076.500000	2500.000	1.370	20.4	E-3	3	3	0	Max. attenuation

[a] Continued from Table 1.

[b] (1) denotes 1. vibrationally excited state.

• Stronger lines.
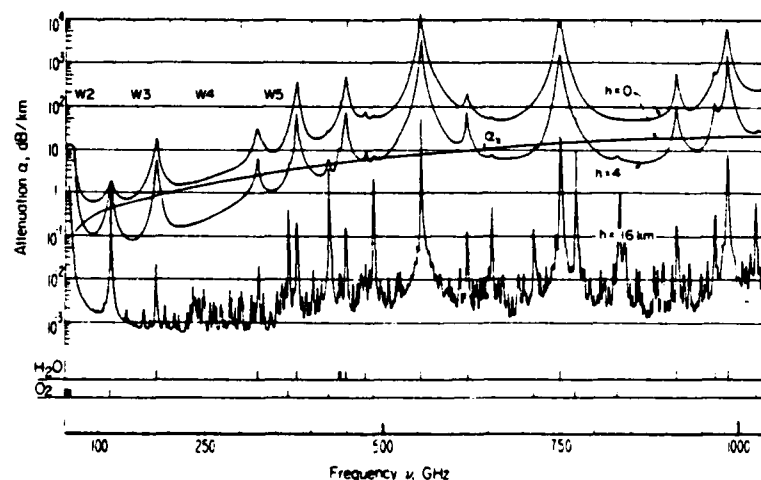
FIGURE 2. Attenuation rate α at the altitudes, h = 0, 4, and 16 km over the frequency range, v = 100 GHz to 1000 GHz. The following atmospheric conditions and trace molecular number densities $N(m^{-3})$ were used in the calculation (24):

h, km	p, kPa	t	e, Pa	$N(O_3)$	$N(CO)$	$N(H_2O)$
0	101.0	1.041	786.000	6.79E17	1.91E18	7.12E18
4	61.6	1.144	133.000	5.77E17	1.28E18	4.76E18
16	10.4	1.385	0.061	3.01E18	2.59E17	9.67E17

FIGURE 5. Zenith attenuation A through the first 30 km of the U.S. Standard Atmosphere 1976 for dry (RH = 5%), moderate (50%), and humid (100%) air over the frequency range, ν = 30 GHz to 300 GHz (EHF). The relative humidity RH was assumed to be constant for h = 0 km to 8 km (19). The experimental data are from Ref. 80 and Table 5.
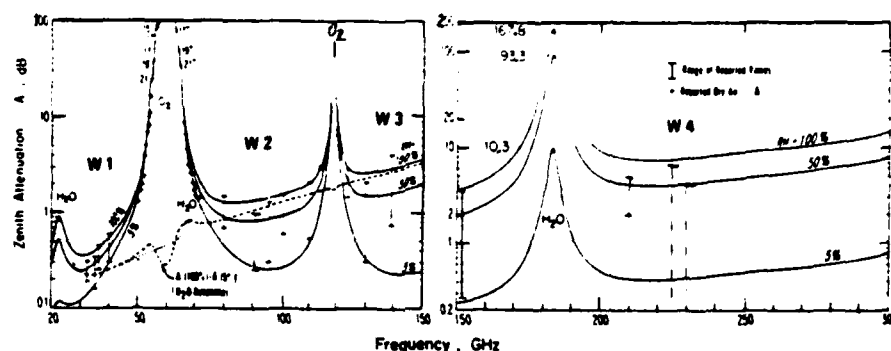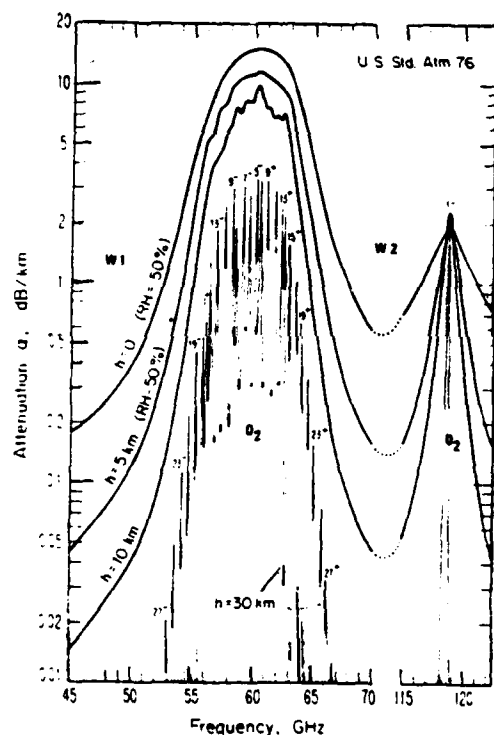

FIGURE 3. Attenuation rate α at the altitudes, h = 0, 5, 10, 30 km over the frequency range, ν = 45 GHz to 125 GHz displaying band and line structure of the oxygen microwave spectrum.
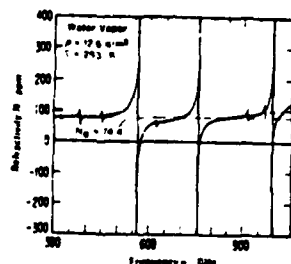
FIGURE 4. Pure water vapor refractivity N_o + D(ν) for e = 1.705 kPa over the frequency range, ν = 300 GHz to 1000 GHz from measurements and calculation (67).
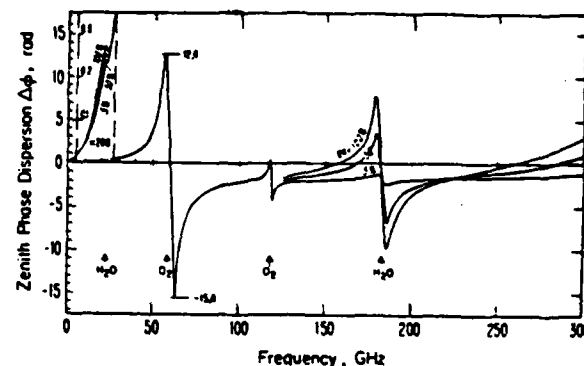
FIGURE 6. Zenith phase dispersion $\Delta\phi = \phi - \phi_o$ (Eq. (18)) for the same conditions specified in Fig. 5. The frequency-independent delay time due to $\phi_o\{N_o(h)\}$ is (Eq. (9)):

RH,%	5.000	50.000	100.000
τ,ns	7.666	7.977	8.266

water vapor absorption plays in atmospheric millimeter wave propagation, even at modest humidities (RH = 46% for h = 0).

A more detailed picture of molecular attenuation appears in Fig. 3. The oxygen microwave spectrum dominates in the ranges 50 to 70 GHz and 115 to 123 GHz. At levels close to the surface, the 60-GHz lines are merged into an unstructured band shape, the maximum intensity of which is pressure-proportional, until the lines separate (h > 15 km). Above 15 km, the shielding effect breaks down and radio channels with up to 400 MHz bandwidth can be accommodated between the lines. If there is a line close to the frequency of interest, isolated line behavior takes over. In the frequency-agile applications, it is possible to tune to a more or less constant shielding factor (for example, 0.5 dB/km) over the height range h = 0 to = 30 km. Above h > 30 km, Zeeman splitting has to be considered in the frequency intervals $\nu_o \pm 5$ MHz until the O_2 lines vanish above h > 100 km (19).

It is encouraging to the author to see experimentally verified results on millimeter wave water vapor refractivity expressed by N_o + D(ν), an example of which is presented in Fig. 4. After many careful measurements of microwave refractivity in the fifties and sixties (2,3,5,47-50,56), this marks a new start in a heretofore inaccessible frequency range. In comparison with conventional absorption spectroscopy, refractive dispersion measurements are superior for absolute intensity studies (15,57,65). An important result of Fig. 4 is the fact that the much stronger lines beyond
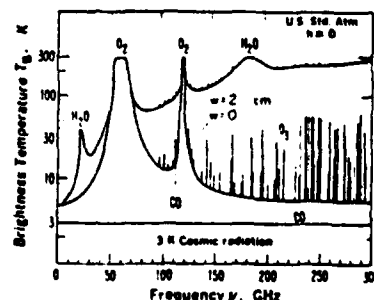
FIGURE 7. Zenith brightness temperature (atmospheric noise) T_B downwelling to ground from a dry (w = 0) and a moist (w = 2 cm, Eq. (33)) air mass (31).

1000 GHz determine, by means of their far-wing intensity, most of the microwave refractivity N_0 (see Eq. (28)).

E. Cumulative Behavior

A standard example for an inhomogeneous medium is the one-way zenith response through the U.S. Standard Atmosphere 1976 (19). Figures 5 and 6 display the cumulative attenuation A and cumulative phase dispersion $\Delta\phi$, for which 48 height levels up to h = 30 km are summed. Except for the vicinity ($\nu_0 \pm 10$ MHz) of the O_2-MS lines, these curves represent the one-way zenith path behavior. Three humidity profiles $\rho(h)$ were used to model RH = 5, 50, and 100% in each of 26 height layers between h = 0 and 8 km. The RH drops rapidly below 1% above h = 8 km. The frequency range 55 to 65 GHz is opaque (A > 30 dB) for any system attempting to look through. The transmittance, Eq. (7) is measurable when the atmosphere is somewhat transparent (A < 30 dB), and it can be determined either by the absorption of a signal coming from the outside (sun emission, satellite beacon) or by the thermal emission originating predominately in 8 km thick layers. Frequencies around 57 and 63 GHz yield the maximum and minimum phase dispersion for the 60-GHz band, which is almost independent of the water vapor content. Actually, the foreign-gas broadening of the O_2-MS by water vapor (see Eq. (22)) reduces the attenuation slightly with increasing vapor pressure (see fig. 5: A(100%) – A(5%)). Comparison of the total attenuation A with measurements (see Table 5) yields reasonably good agreement when the empirical assumptions formulated by Eq. (27) are used in the calculation. The amount of water vapor absorption for a given atmospheric condition can be estimated, to some extent, if the surface vapor concentration ρ_0 is known.

The EHF thermal emission by H_2O, O_2, O_3 and CO was calculated by Waters by using Eqs. (10), (7) and (4) and the absorption coefficients given in Eq. (31). Calculations are shown in Fig. 7 both for no water vapor and for a total precipitable water vapor of 2 cm. The integral is evaluated for h = 0 to 60 km. Clear-sky emission varies primarily with the amount of water vapor. The calculations are for observations in the zenith direction from ground level. Cosmic radiation of 3 K, which is incident on the atmosphere from the top, has been added to Eq. (10).

III. PHYSICAL PROPERTIES OF ATMOSPHERIC WATER VAPOR

The clear atmosphere appears in the EHF radio path modeling scheme only as a p-t-e (Section II, B) parameter system. The real atmosphere is an enormous theater of diverse but related and incessant activities (33). Water, endlessly changing its phases, is the main actor on this stage. On a global scale, each year about 1 m of the ocean depth is evaporated, whereas the average water content of the atmosphere represents a depth of roughly 2 cm. Water vapor is rapidly exchanged causing it to be a patchy, capricious medium with parcels (scale sizes, 10 to 100 m), blobs (< 0.5 m) and strata (≈ 1 m) of moisture that probably account for a fair share of the scatter and inconsistencies in millimeter-wave propagation data taken from field observations. The total integrated water vapor and liquid water in a vertical column can be detected with high time resolution (≥ 10 s) by ground-based radiometry in the microwave range (40). In relating millimeter-wave propagation and atmospheric water vapor, one has to be generally content to make predictions with no more than statistical certainty.

The fact that the three phases of water contribute to the weather cycle at the prevailing conditions (p-t-e) is most fundamentally a consequence of the molecular structure of H_2O. Water molecules tend to associate through hydrogen bonds[J] having about one-tenth the strength of a molecular bond. Very specifically, in the solid phase four H-bonds form a rigid lattice; in the liquid phase, on the average, two H-bonds amalgamate chainlike links; and in the gaseous phase, a chance exists to associate singly H-bonded molecules to dimers (21,43, 44) or aggregate into clusters of preferred sizes (that is, 10 to 50 molecules) (22,28) under the influence of ion-activity (45). If further notice is taken that atmospheric air is never free from invisible particles having a variety of origins, chemical compositions, sizes, and affections for water vapor, then the radio engineer will almost despair at the prospects of ever putting order in the atmospheric pandemonium. The value of the interdisciplinary Workshop on Atmospheric Water Vapor for providing guidance with this task must be stressed.

A. Absolute Humidity

The amount of water vapor (that is, absolute humidity ρ), present in the atmosphere depends upon: (a) evaporation from surfaces; (b) transport by motions on various scales, mainly through the troposphere; (c) condensation-forming clouds and fog that causes precipitation fallout. The radio propagation engineer measures the amount of water vapor by means of an average concentration $\bar{\rho}$, which varies at sea level between the extremes of 0.1 (dry, winter, polar) and 60 g/m³ (wet, summer, tropical). The height distribution is approximated from a known ground level ρ_0 by

---

[J]The electron-rich end of O in the polar molecule H_2O attracts an electron-poor H end of a neighbor H_2O.

$$\rho(h) = \rho_0 \exp(-h/2 \text{ km}) \tag{32}$$

and the most realistic measure for predictions is the total precipitable water vapor in cm (10 g/m³/km = 1 cm).

$$w = \int_{s_1}^{s_2} \rho(s) \, ds \approx 0.2 \, \rho_0 \tag{33}$$

The quantity w is measured, for example for a zenith path, with a microwave radiometer (39,40). The variations of the dry air parameter p(h) and t(h) are described by standard height profiles and attention is called to the model of the U.S. Standard Atmosphere (for example, (33)). The number density for the atmospheric gases with constant volume mixing ratio (O_2, N_2, CO_2, noble gases; or referred to as dry air) follows directly from the p-t combinations. Over the height range h = 0 to 16 km, the changes are for p from 101 to 10 kPa (1 kPa = 10 mb) and for t from 0.9 (333 K) to 1.5 (200 K). Ozone (O_3), besides water vapor, has a variable mixing ratio which is modeled separately. Examples of O_3 millimeter wave spectra are shown in Figs. 2 and 7 as reported by others.

Fractional fluctuations due to water vapor paths and turbulence are typically in the ranges

$$\left. \begin{array}{l} \delta\rho = \pm 80\% \\ \delta t = \pm 1\% \\ \delta p = \pm 0.1\% \end{array} \right\} \tag{34}$$

Variability of humidity for a midlatitude location with a medium of 7.4 g/m³ is diurnally $\pm$ 1.0, seasonally $\pm$ 6.3, and locally $\pm$ 1.2 g/m³.

1. Molecular Quantities. The molecular world of sea level air is very empty. The molecular radius $r \approx 1.8 \times 10^{-4}$ cm, average spacing d, and average distance l between collisions are in the radios r : d : l = 1 : 18 : 320 (33). Most of the time, a molecule is unperturbed by neighboring molecules. The number of dry air molecules per unit volume (m⁻³) is

$$N_d = 2.415 \times 10^{23} \, pt \tag{35}$$

(e.g., p = 101, t = 1 : N_d = 2.44 × 10²⁵).

Water vapor is an imperfect gas. From thermodynamic measurements, it is known that there are slightly more H_2O molecules per unit volume than predicted by the ideal gas law. The correction is made by introducing the second virial coefficient B(t). The molecular number density of H_2O for a given vapor concentration (in g/m³)

$$\rho = 7.219 \, e \, t \tag{36}$$

follows from the relationship in m⁻³

$$N_v = [(2.989/\rho) \, 10^{-23} + B(t)]^{-1} \approx 3.346 \times 10^{22} \rho \tag{37}$$

(e.g., ρ = 10 : N_v = 3.35 × 10²³).

Very few values for B(t) have been reported (44,69):

t	0.9	1	1.2
T, K	333	300	250
B, 10⁻²⁷ m³	-2.8	-1.9	-0.9

The deviations from ideal behavior

$$\epsilon = [N_v/N_v^0 \, (B = 0)] - 1 \tag{38}$$

are small, even at saturation (see Eq. (43)):

t	0.9	1	1.2
$\rho = \rho_s$, g/m³	130	25.5	0.82
ϵ, 10⁻³	12.3	1.6	0.03

The deviation ϵ led to the postulation of a dimer molecule $(H_2O)_2$. The molecular structure (43) and the millimeter wave spectrum of the dimer (6,8,69) are well established; however, its number density under tropospheric conditions is not known.

The dimer number density is expected to depend strongly on temperature since the hydrogen bond strength is rather weak. Data which are suspected to be caused by a dimeric effect can be analyzed for their percent change-per-degree or for their power law (tY) dependence to allow a positive identification:

Data % Change/K	y	eV/molecule	kcal/mole	
-1.56	3.8	0.1	2.31	
-2.54	7.7	0.2	4.60	*H-bond
-3.78	11.6	0.3	6.90	
-6.22	19.3	0.5	11.60	
-12.10	39.0	1.0	23.10	*Conden- sation

Bond strength is expressed in units of eV/molecule or kcal/mole and the value expected for a hydrogen bond lies between 3 and 5 kcal/mole. The dimer number density in m^{-3} was proposed to follow an expression (6)

$$M_D = M_v^2 \cdot k(t) \tag{39}$$

An approximate equation in m^3 for $k(t)$ was derived from expressions given by Bohlander (69)

$$k = 1.8 \times 10^{-27} t^{5.6} \tag{40}$$

which when combined with Eqs. (37) and (39), yields in m^{-3}

$$M_D = 2.0 \times 10^{18} \rho^2 t^{5.6} \tag{41}$$

and for the fractional dimer concentration

$$M_D/M_v = 6.1 \times 10^{-5} \rho t^{5.6} \tag{42}$$

(for example, $\rho = 20$, $t = 1$: $M_D/M_v = 1.2 \times 10^{-3}$).

Other estimates on the fractional dimer concentration M_D/M_v are reported in Ref. (21): 0.4×10^{-3} for $\rho = 20$ assuming 5.4 kcal/mole; and in Ref. (44): 1.9×10^{-3} at $t = 1$ and 0.95×10^{-3} at $t = 1.11$, when extrapolated from saturated water vapor data taken over the range $t = 0.77$ to 0.84. These ratios M_D/M_v are close to values of c defined in Eq. (38).

B. Relative Humidity

The examples of atmospheric millimeter wave propagation (Figs. 1 to 7) showed clearly the dominant influence of water vapor. Some difficulties in predicting this influence obviously are related to the fact that water vapor is a vapor and not a gas. The first consequence of the vapor state is that a maximum concentration ρ_s cannot be exceeded. A balance exists between two states called the saturation point. At saturation, the rate at which molecules evaporate from a plane surface (liquid or solid) equals the rate of incoming condensing molecules. The saturation concentration over water for atmospheric conditions is fitted by

$$\rho \le \rho_s = 17.39 \, t^6 \, 10^{(10-9.834t)} \tag{43}$$

in g/m^3 and is in a very rough approximation simply in g/m^3

$$\rho_s = 25 \, t^{-17} \tag{44}$$

Equation (43) is programmed into the radio path model (Section II), which uses RH(h) information to calculate with t(h) the values e or ρ.

The saturation concentration defines relative humidity

$$f = \rho/\rho_s = 0.04 \rho t^{17} = 0.28 \, et^{18} \le 1 \tag{45}$$

or, in the more familiar percent notation, RH = 100f ≤ 100%. The maximum vapor concentration varies over a wide range as a function of temperature:

T, K	t	t^{-17}	ρ_s (true)[a]	ρ_s, Eq. 43	ρ_s, Eq. 44
333.30	0.900	6.000	130.350	130.400	150
300.00	1.000	1.000	25.500	25.500	25
273.16[b]	1.098	0.203	4.850	4.840	5
250.00	1.200	0.045	0.822	0.822	1

[a] Smithsonian Hydrometric Table (see (33)).

[b] Triple Point

The interdependences between RH, ρ, w, and T are shown in Fig. 8. The humidity condition RH = 100% is a delicate balance point for phase changes. A drop in temperature by 1 K decreases the water vapor density of saturated air by about 6%. Energy is released during condensation which was stored in the random motion of H_2O molecules. One cubic meter of a forming cloud that converts 1 g of vapor into the liquid phase releases 2.5 kJ.

The latent heat release can generate electric fields. Depending upon the suddenness, the amount of cooling, and the water vapor supply, more or less violent updrafts (such as cumulonimbus clouds in thunderstorms) feed a turbulent air motion. Small aerosols are lofted into the upper region of a
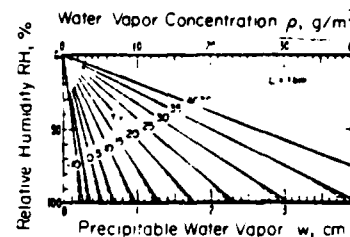
FIGURE 8. The amount of precipitable water vapor w in a radio path of length, L = 1 km and the corresponding homogeneous water vapor concentration ρ, both as a function of relative humidity RH for various temperatures T. The temperature dependence of saturation water vapor pressure e_s and maximum vapor concentration ρ_s (RH = 100%) (33) is:

T, C	e_s, kPa	ρ_s, g/m³
-30	0.051	0.453
-20	0.125	1.070
-10	0.286	2.360
0	0.611	4.840
10	1.227	9.390
20	2.337	17.270
30	4.243	30.310
40	7.378	51.020

The broken lines indicate schematically the range where water uptake by aerosol takes place (Fig. 9).

forming cloud while the larger, heavier ones remain suspended at lower levels. The small aerosols carry a positive charge, the lower levels take on a negative charge. The charge separation generates high electric field strengths and lightning discharges occur when a value of about 30 MV/m is reached. Even before, additional ions must be produced, which are suspected to have catalytic influence on the formation of homomolecular cluster $(H_2O)_n$ with n = 10 to 50 (28).

C. Submicron Hydrometeors

Atmospheric air is never free from invisible particles (aerosols) having a wide variety of origins, sizes, and chemical composition, and most importantly, having the ability to convert water vapor into submicron hydrometeors. To account for aerosol activity, one must follow the evolution of particle size spectra
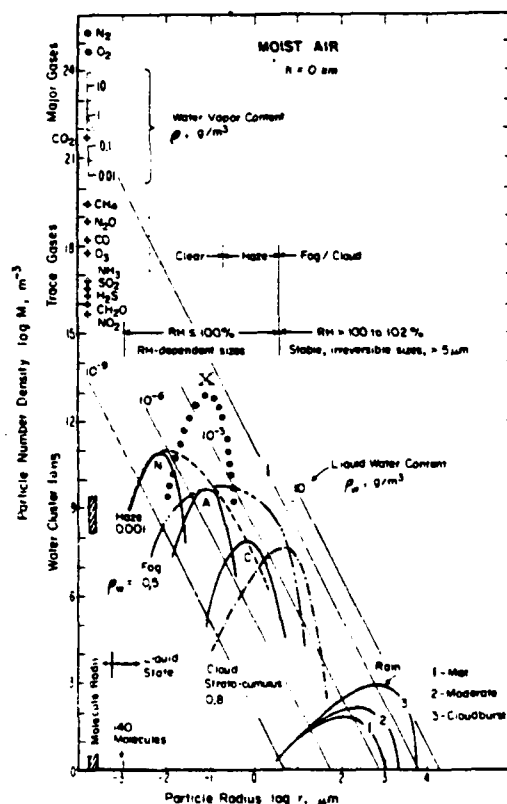
FIGURE 9. Schematic size distribution of number density M for equivalent spherical atmospheric particles from molecular to rain drop sizes, $r = 10^{-4}$ to 10^4 µm (32,33,41).

and the attendant microphysical processes of mass transfer over many orders of magnitude in size ($r = 2 \times 10^{-8}$ to 1 cm) and number density ($N = 10^{23}$ to 1 m^{-3}). This problem of scale is sketched in Fig. 9 to illustrate the extent of the difficulties. The amount of relevant literature dealing with aerosols is over-whelming and the referenced material (33-45) is probably an incomplete selection in the search for nonmolecular millimeter wave absorbers in moist air.

Aerosol models start from dry particles, distributed over three distinct size ranges (Fig. 9) (35-38): N, nucleation mode; A, accumulation mode; C, coarse particle mode; and X, hypotheti-cal submicron distribution required to explain EWA (see Section IV). Each mode is described by representative values of a

log-normal distribution (23,43). A major process for the forma-tion of the N-mode is the trace gas-to-particle conversion. Sulphur dioxide, for example, nucleates with water vapor to form sulfuric acid primary particles in large numbers (as high as 10^{15} m^{-3}), which are rapidly (within ms) coagulated by Brownian motion into the N-mode (34). This mode may contain sizable mass concentrations, $\rho_A(N) \lesssim 20$ $\mu g/m^3$ (38), but more to the point, it presents an enormous surface area S_A to the vapor phase and enables the aerosol to respond quickly to changes in relative humidity RH. Particle number density N_A and total surface area S_A for 1 mg of water distributed in spherical droplets of radius r within 1 m^3 are related as follows:

r, μm	N_A, molec/m^3	S_A, cm^2	
N	0.01	2.4×10^{14}	3000	
A	0.10	2.4×10^{11}	300	
C.	1.00	2.4×10^{8}	30	(46)

The mixture of gas and suspended particles is called an aerosol.

Solution droplets, such as H_2SO_4, are highly hygroscopic; that is, they adapt their size by taking up water if the RH in the ambient air is larger than the equilibrium RH over the drop-let's surface. In a reverse situation, their size will shrink because of evaporation. Other hygroscopic agents are salt particles found in maritime (NaCl) as well as in urban [for example, $(NH_4)_2SO_4$] environments. These crystals undergo a sudden phase transition to become solution droplets at critical RH values (RH = 76% and 80% for NaCl and $(NH_4)_2SO_4$, respectively). The aqueous particles, or so-called hydrometeors, collect in stable, RH-dependent sizes predominantly in the A-mode. A third type of aerosol particle is relatively passive dust grains in sizes commensurate with the A and C modes. The solid matter accumulates a film of water on its surface. All the particle population is able to aggregate water (CW) but the small, hygroscopic parts of the CW (CCN) play the dominant role.

The total aerosol mass concentration in air with a humidity of $\rho = 1$ g/m^3 can range from $\rho_A = 1$ (clean air) to 400 $\mu g/m^3$ (polluted). At RH = 50%, an average mass loading of about 0.1 mg/m^3 has been deduced from data collected at 291 locations in the U.S. (38). Values between 0.5 (clean air) and 3 mg/m^3 (polluted) are reported for ρ_A in cloud free aerosol (42).

Water vapor-to-liquid conversion becomes effective when RH exceeds 80%. An aerosol population can triple, even quadruple its dry state size, and thus lead to more than a hundred-fold increase in mass concentration. Since the average size stays below 1 μm, a more or less invisible cloud exists, optically categorized in the atmosphere as haze. Optically active sizes (> 0.5 μm) in sufficient number are only produced if the limit RH = 100% is exceeded. In that case, the available amount of water (for example, that due to a sudden cooling of saturated air) is shared either by many (> 10^9) active particles (CCN) and small (r = 8 μm), uniform droplets form as fog or cloud, or by very few (< 10^8) and large (r > 100 μm), destabilizing droplets that pro-duce rain.'

The water uptake of aerosol has a theoretical foundation in the relationship between the ambient RH and the equilibrium radius of a particle. Hänel provided empirical data on the hydrometric activity of aerosol (35). He defined a mass growth factor $g(f = RH)$ with respect to the dry mass concentration ρ_A^0 and measured in the laboratory the equilibrium growth behavior of typical air samples. Two examples are depicted in Fig. 10. The accretion of water to particles is substantial when RH exceeds 80% and gives them almost pure water properties; that is, $\rho_A(f > 0.8) = \rho_w$. Two approximate expressions for $g(f)$ can be formulated (35)

$$g(f) = 4f^2 \quad (f < 0.8) \tag{47}$$

and

$$g(f) = 1/(1-f) \quad (f < 0.95) \tag{48}$$

if differences and hystereses in the growth behavior due to the chemical makeup are disregarded. A detailed discussion of models for growth factors can be found in Refs. 36 and 37.

By referring to radio path modeling, it is possible, at this point, to formulate a path-integrated liquid water content in mm

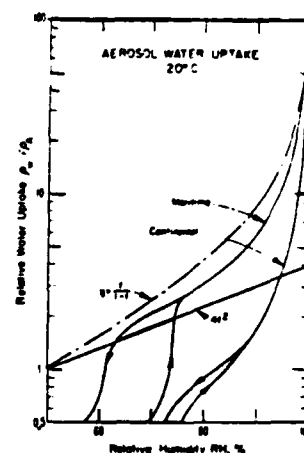$$W = \int \rho_w \, ds = \int \rho_A^0 \, g(f) \, ds \propto \int [\rho_A^0/(1-f)] \, ds \tag{49}$$

FIGURE 10. Water uptake [mass growth factor $g(f = RH)$] of two representative aerosol samples [maritime: NaCl; Continental: $(NH_4)_2SO_4 + SiO_2$] as a function of increasing and decreasing relative humidity RH (35).

The water content W increases at the expense of the precipitable water vapor w defined by Eq. (33); hence, in cm

$$w(f) = w(f=0) - W \tag{50}$$

The amount of liquid water in moist air (RH ≤ 100%) is difficult to measure. Several indirect methods have been developed. Three more promising techniques are

1. The mass concentration C_A^0 of a dried air sample is determined by micro-weighing and available (35) empirical growth factors $g(f)$ are applied. For example, at RH = 99%, the values for g range between 65 and 120 and yield W = 0.013 to 0.024 mm when ρ_A^0 = 0.2 mg/m^3 over a path length L = 1 km.

2. A passive, radiometric microwave method measures at two (or more) different frequencies the sky noise T_B (see Eq. (10) and Refs. 39 and 40). The brightness temperature T_B is converted into zenith attenuation A (dB) by means of the spectroscopic data base. Guiraud et al. (40) perfected the technique, which uses an instrument operating at 20.6 and 31.65 GHz. The retrieval algo-rithms for the simultaneous determination of water vapor and water liquid content are adjusted to take into account a priori statistics (that is, a representative radiosonde profile). For example, the climatology of Oklahoma City yielded (40) in cm

$$w = 6.22 \, A(20) - 2.72 \, A(31) - 0.01$$

and in mm

$$W = 1.30 \, A(31) - 0.53 \, A(20) - 0.001 \tag{51}$$

The frequency 20.6 GHz is close to the 22 GHz vapor line (Table 2) and responds mainly to vapor; the frequency 31.65 GHz is remote from the line and responds to the dielectric loss of water. This instrument provides around-the-clock monitoring of w and W.

A typical record over 7 consecutive days (Oklahoma City, April, h = 360 m, locking at zenith) displayed for each 24-hour period the following extremes (40):

Day	w, cm	W, mm
1	2.5 to 1	0.01 to 0.02
2	1 to 2.6	0.02 to 0.5
3	2.4 to 0.8	0.02 to 2
4	1 to 2	0.03 to 1.5
5	0.5 to 1.2	0.1
6	0.8 to 1.3	0.1
7	2.4 to 4.2	0.1 to 1.5

The point of this example is that the low limits of W usually exceed the values that are obtained when using an average dry aerosol mass concentration and assumed $g(f)$- factors. The high limits of W are most likely due to visible clouds since their size range (r = 7 to 100 μm) contains the bulk of the water. Unfortunately, the data were not accompanied by notes providing information or meteorological or optical conditions. A similar, satellite-borne radiometer yields, over ocean surfaces with well-defined emission temperatures, the same information on w and W on a global scale (39).

3. The measurement of optical transmission gives insight into the average aerosol state. Both the optical ($\lambda = 0.55$ μm) attenuation rate α_{ij} and the visibility V = 20 dB/α_{ij} are related to the liquid water content ρ_w. In general, Mie scattering theory has to be applied in order to predict values of α_{ij} based on available size distributions and the complex refractive index of the particle material (23,33,35).

For the purpose of this paper, it is sufficient to bypass the elaborate, lengthy calculations and discuss the main features with the help of a simple empirical expression (27,37)

$$\alpha_\mu \approx 300 \, \rho_w^{0.6} \qquad \text{or} \qquad V = 0.067/\rho_w^{0.6} \qquad (52)$$

where α_μ is in dB/km and V is in km. The relationships between α_μ, V, and the path-averaged water content δ_w are approximately:

ρ_w , g/m^3 ..	< 0.001	0.01	0.05	0.1	0.5
α_μ , dB/km.	< 5	19	50	75	198
V , km ...	> 4	1.1°[1.5]	0.4 [0.5]	0.27 [0.3]	0.10 [0.08]
	Clear	Haze . RH ≤ 100%		Fog, RH > 100%	

°[ ] = experimental value

Frequently, haze and fog conditions are described merely by stating the measured value of the visibility V° which, however, depends on the definition of the threshold value [20 dB for L = 1 km in Eq. (52)]. Nilsson performed detailed Mie calculations on five different aerosol models with the result that visibility V (16 dB threshold) and relative humidity RH are related directly (23). The range of RH for these models is

V , km	50	15	5	2
RH,	20 to 73	84 to 95	96 to 99	98.7 to 99.7

In summary, the salient points of this section are:

1. The physical foundations for path-averaged water vapor w (Eq. 33) and liquid water content W (Eq. 49) were traced in measurable quantities. Both are expected to be the main source for millimeter wave absorption in moist air.

2. The number density N of the major molecular absorbers was given for O_2 in Eq. (35), for H_2O in Eq. (37), and for $(H_2O)_2$ in Eq. (41).

3. The water-vapor-to-water-droplet conversion in atmospheric aerosol and the associated scale problems were discussed to aid in the comprehension of the stages that a water molecule has to undergo before precipitating out of the atmosphere. The key role of relative humidity RH (Eqs. 43 to 48) in this process was underlined.

4. The interdependence between the optical properties (Eq. 52) of moist air and the liquid water content is not unique; it depends strongly on the aerosol size distribution.

IV.   EXCESS WATER VAPOR ABSORPTION--EWA

Water vapor absorption (Eq. 14) in the millimeter wave windows stems from the fact that the intensity of the local millimeter wave lines $N_l^v = \Sigma S F°$ (Table 2) is insignificant and that two other absorption terms, N_v^c and N_x^c, become dominant. The far-wing response N_v^c of the rotational spectrum of H_2O beyond 1000 GHz (Fig. 1) is estimated by applying the approximation $\gamma << \nu << \nu_0$ to the line shape F° (Eq. 16) and results in

$$F_v^c = 2\gamma\nu/\nu_0^3 \qquad (53)$$

where F_v^c is in units of 1/GHz. The H_2O far-wing continuum of one line in ppm follows with Eqs. (24), (25), (53), and (11) as

$$N_v^c = SF_v^c = C_L(1.50 \, pp \, t^{3.1} + \rho^2 \, t^{2.1})\nu \qquad (54)$$

where

$$C_L = 0.184 \, b_1 \, b_3/\nu_0^3 \qquad (55)$$

For moist air, the ρ^2-term due to self-broadening is always smaller (< 20%) than the foreign gas-broadening term po. The far-wing contribution of the strongest H_2O line (Table 2: $\nu_0 = 2774$ GHz, $C_L = 5.14 \times 10^{-10}$) is for an atmospheric condition described by p = 100 kPa, t = 1.023 (20°C), $\rho_s = 17.27$ g/m^3, at the frequency $\nu = 300$ GHz, $N_v^c = 4.77 \times 10^{-4}$ ppm or $\alpha_v = 0.026$ dB/km, to which the ρ^2-contribution is 11%. The line center attenuation rate, in comparison, is $\alpha_m = 7.40 \times 10^5$ dB/km. Most certainly, line shape theory (Eq. 16) is overtaxed when it is applied to predict relative intensities in the far-wing over seven orders of magnitude.

An unspecified term N_x^c was added to Eq. (14) to account for discrepancies between predictions based on summing N_v^c-terms (54) and measurements. The only certainty in the conflicting evidence for N_x^c is its correlation with atmospheric humidity. The abbreviation EWA (excess water vapor absorption) is used to describe N_x^c. For simplicity's sake, different, mostly exponential temperature functions have been reduced to a power law t^y (Eq. 31). In this section, the exponents of physical (ρ^x, t^y) and frequency (ν^z) dependences are formulated for absorption models and compared with those for experimental data. This procedure appears to be one practical way of identifying a specific absorption mechanism, especially since EWA observations are not overwhelmingly consistent.

Two schools of thought have evolved to explain EWA:

1. A molecular approach searching for water polymers $(H_2O)_n$ and their spectra in the atmosphere. Sizes of n = 2 (dimer)[42] (6,8,21,69,81,86,89) and n > 3 (cluster) (21,28) are possibilities.

2. Liquid water uptake by submicron aerosol particles under conditions of high relative humidity (RH > 85%) (9,20,23,25,30, 35).

Each conjecture is supported by *some as well as contradicted by other bits and pieces of experimental evidence.*

A.   Definition of EWA

Window attenuation, both model and experimental, is fitted to expression in dB/km of the form

$$\alpha = 0.182\nu N'' = C \, \rho^x \, t^y \, (\nu/30)^z p \qquad (56)$$

where x, y, z are the proper exponents of a particular absorption model.

The AFGL compilation lists 38 350 H_2O lines from 20 GHz to 331 THz (10) ordered in seven bands (14), of which 1809 rotational lines up to $\nu = 13$ THz contribute to the millimeter wave continuum (17). A fit to these results yielded Eq. (26), which can be reformulated into Eq. (56). Magnitude and exponents for the line continuum are given in dB/km/g/m^3/kPa by

$$C_v = 8.4 \times 10^{-6}$$

and   (57)

$$x_v = 1.2$$
$$y_v \approx 3$$
$$z_v \approx 2$$

These exponents are based on the molecular number density (Eq. 37) displaying the exponents x = 1 and y = 1. With Eqs. (56) and (57), it follows for the sample conditions above ($\nu = 300$, p = 100, $\rho = 17$, t = 1.023) that $\alpha_v = 2.75$ dB/km.

The dimer spectrum is discussed in detail in Refs. 69 and 109. Absorption should follow dependencies given by Eq. (57), but modified for the dimer number density (Eq. 41). The response predicted in this fashion in dB/km/(g/m^3)^2 is

$$C_D \approx \text{(value of Table 4)}$$

and   (58)

$$x_D = 2$$
$$y_D \approx 8$$
$$z_D = \text{values of Table 4}$$

Aerosol liquid water attenuation is obtained from published dielectric data on bulk water (Fig. 13) yielding in dB/km in the Rayleigh approximation [ε' = $(n_w')^2$ + $(n_w'')^2$, ε" = $2n_w'n_w''$] (25,30, 32).

$$\alpha_A = 0.82\nu\rho_w \, \varepsilon''/[(\varepsilon' + 2)^2 + (\varepsilon'')^2] \qquad (59)$$

Another method of calculating the aerosol liquid water attenuation assumes that the medium has a refractive index $n_A' = 1$, and that the attenuation in bulk water is increased due to wavelength shortening ($\lambda_w = \lambda_0/n_w'$). This allows to formulate

$$\alpha_A = (\alpha_w/n_w') \, (W/L) \qquad (60)$$

Both methods have been applied to the latest dielectric data on water (106) producing somewhat different values (see Table 4). Frequency and temperature dependencies, when approximated using Eq. (60), follow in dB/mm from the rough data fit

$$\alpha_w/n_w' \approx 24 \, (\nu/300)^{0.65} \, t^{-6}$$

Now, if the liquid water content is estimated by Eqs. (49), (47), and (45), W = 6 x 10^{-3} L ρ^2 t^{14} ρ_s^4, one obtains for the expected aerosol response in the form of Eq. (56) that

$$x_A \gtrsim 2$$
$$y_A = 28$$
$$z_A = 0.65 \qquad (61)$$

In summary, millimeter wave window attenuation α might very well be a combination of up to five different contributions:

$$\alpha = \alpha_L(\text{local lines}) + \underbrace{\alpha_v(\text{far-wings}) + \alpha_A + \alpha_D + \alpha_x(\text{cluster?})}_{\text{EWA}} \qquad (62)$$

A parametric study of water vapor concentration (ρ) and temperature (t) dependencies could, in principle, reveal the following behavior in the attenuation rate:

[4]*Jone already in 1919 had considered a water dimer to explain anomalous dielectric water vapor results (72).*

T °C	ρ_s, g/m³	ρ_s^2 (g/m³)²	t	t^3 Eq. (57)	t^8 Eq. (58)	t^{28} Eq. (61)
				Multiplication factor with respect to 300 K data		
-20	1.07	1.15	1.185	1.664	3.890	116.00
-10	2.36	5.57	1.140	1.482	2.850	39.00
0	4.84	23.34	1.098	1.324	2.110	14.00
10	9.39	88.20	1.060	1.191	1.590	5.10
20	17.27	298.30	1.023	1.071	1.200	1.90
30	30.31	918.70	0.990	0.970	0.923	0.76

Data obeying $x = 1$ and $y = 3$ but displaying magnitudes different from C_W (Eq. 57) can be interpreted as failure of the line shape function (Eq. 16) to predict far-wing intensities. Discrepancies of this nature will be most pronounced for dispersion intensities (Eq. 15). Wing data of $D(\nu)$ drop more gradually ($\propto 1/\nu$) with decreasing frequency, and actually blend into the well-known refractivity N_0 (Eq. 12) for $\nu < 100$ GHz, as seen in Fig. 4.

B. Excess Water Vapor (EWA): Evidence from Laboratory Data

Laboratory measurements play an important role in verifying modeling schemes for EHF properties of moist air. Generally, all the spectroscopic parameters (> 200) entering into Eq. (1) should be deduced from absolute intensity measurements under well controlled ν-p-t-ρ conditions. By a judicious choice of the experimental variables, it is possible to investigate most parameters separately.

Numerous millimeter wave and infrared studies of water vapor and moist air have been reported. References 46 to 72 are selected for their bearing on the EWA problem. Evidence for EWA from these efforts is summarized in Table 3. It is not limited to absorption, but also shows up in dispersion spectra $D(\nu)$ (63) and in refractivity N_0-studies (48,49,52,56,63). The experiments are performed by various techniques. The radio path is simulated in an enclosure either for a single-transit or a multiple-reflection (resonator) passage. Detection sensitivity increases with path length. The transmitted energy can be a single frequency, a frequency pair for differential measurements, or a broadband (Fourier transform) signal. Main variables for an experiment are either frequency or pressure, the latter being

preferable for EWA studies. Gas mixture control and vacuum reference are laboratory advantages for absolute intensity studies.

Water vapor is recognized to be a medium that is difficult to control, even in the laboratory, due to its attractive force toward surfaces. The surface area of the laboratory enclosure -eplaces, in a way, the micro-surface of an atmospheric aerosol population. Water molecules do not ordinarily aggregate spontaneously, but water vapor becomes liquid water when wettable surfaces are present to retain the impinging molecules. A threshold of $> 2 \times 10^{-5}$ cm^{-1} in the surface-to-volume ratio is sufficient to form a continuous interface between vapor and liquid (38). This value is always exceeded in atmospheric air (see Eq. 46) as well as in a laboratory test chamber. An experimenter can select surface materials that, to a certain extent, passivate the attraction for water vapor. A systematic study was made of various surface coatings applied to an electro-polished stainless steel (SS 304) cavity (3440 cm³ and 1265 cm², S/V = 0.37 cm^{-1}) evacuated for > 24 hours to 10^{-4} torr and subjected to pure water vapor, $e_0 = 2.40$ kPa at 23.0°C. Results on the relative amount e/e_0 of water-uptake by the walls and the time response of the adsorption (τ_{Ad}) and desorption (τ_{De}) process are as follows:

Coating	e/e_0 %	No.[b]	τ_{Ad} s	τ_{De} s
Teflon FEP120 (DuPont), 1 coat	-1.00	20	180	500
SS 304, electropolished	-1.50	30	150	400
HMDS[a] silanizing	-1.15	27	190	750
Parylene C (Union Carbide)	-1.60	32	140	580
Silicone SR240 (GE)	-2.10	42	200	550
Teflon FEP120, 2 coats	-2.90	58	230	5500
Clear lacquer	-4.00	80	300	7200
60 GHz spectrometer cell, untreated (63)	-19.5(1) (S/V = 1.28 cm^{-1})	102	2 hrs	5 hrs

[a] Hexamethylidisilazane $[(CH_3)_3Si]_2NH$
[b] Number of molecular layers

The need for minimum S/V-ratios and judicious material selection for laboratory enclosures is clearly evident upon comparing the performance of one of the typical spectrometer cells with the preceding test. Water vapor surface effects have been recognized (52); yet, in many cases (46,49,56), they were excused as a possible source of error for the reported data. Work close to saturation requires a circulating gas-handling system with controlled mixing and continuously monitored RH levels (107). Additional sources of error are disturbances in thermodynamic

TABLE 3. Summary of Laboratory Studies of Continuum H_2O Absorption

Frequency ν, GHz	Continuum H_2O absorption				Experimental Conditions				Ref.
	x (D)	y (T)	z (V)	Foreign gas	H_2O density ρ, g/m³	Tempera-ture T, K	Path length or L, m	Resonator Q, x 10³	
18-31	1,2			Air	0-40	318		800 (Q-box)	46
22	2			N_2	0-50	312		45	56
22.24	1,2				0-20	297	(30)	16	63
31.62	1,2	2.10	2		0-35	280-325	(>100)	>200	63
117-120	>1				0-25	295	150		74
170-300	2				0-20	295		100	53
213	2	4.26		N_2	0-60	270-320	(40)	Q-box	66
210-300	2	>10			3-6	273-333	28		58
450-960					1	295	2		59
890.965	1,2				0-35	293.323	10-60		58
300-1500	2		0.5			290-355	5-103	and Q-box	69
9-18THz						283.329	133		69
12-36T	1,2								12
14-27T	1,2	>10			2-20	293-313	500		60
21-38T	1	5.5			14	296-388	1185		54
28-33T	1,2	2.16	2	N_2,O_2	0-20	289-301			70
75-86T	1,2				14	298	21		68

equilibrium: (a) the vapor heats up when injected into an
evacuated cavity, (b) the adsorption process releases heat and
vice versa, (c) the ambient gas temperature is lowered during
pump-down. All laboratory results on spectroscopic data
(N_0, D, N'') of water vapor should be seen in light of these
comments. Some selected examples displaying EWA behavior are
discussed in the following.

1. Moist Air Studies. Llewellyn-Jones et al. (66)
investigated the temperature dependence of the frequency
$v = 213$ GHz by studying moist nitrogen (p = 93 kPa) over the
range $T = 270 - 320$ K. The attenuation (Eq. 62) for these
conditions can be described by the empirical expression in dB/km

$$\alpha = 0.22\rho t^2 + 0.01\rho^2 t^4 + 0.03\rho^2 t^{26} \qquad (63)$$

Close to saturation, the following values result from Eq. (63):

T, K	t	ρ, g/m^3	α, dB/km
250	1.20	1	0.32 + 0.02 + 3.43 = 3.8
273	1.10	5	1.33 + 0.37 + 8.94 = 10.6
38?	1.05	10	2.43 + 1.22 + 10.67 = 14.3
300	1.00	20	4.40 + 4.00 + 12.00 = 20.4

2. Pure Water Vapor Studies. In the case of self-broadening
an exponent $x = 2$ (Eq. 54) is expected. Mrowinski (56) observed
$\alpha_x \approx 3 \times 10^{-4} \rho^2$ dB/km at $v_0 = 22.235$ GHz and $T = 39°C$, in
addition to the line absorption α_ℓ. Measurements by Liebe (63)
at 30.6 GHz and 61.2 GHz, $T = 300$ and 325 K yielded in dB/km

$$\alpha = 4 \times 10^{-3}\rho t^2 (v/60)^2 + 8 \times 10^{-4}\rho^2 t^{10}(v/60)^{2.5} \qquad (64)$$

The same experiment gave for the refractive dispersion (ppm),
$D = N'(61.2) - N'(30.6)$, the result

$$D = 2 \times 10^{-3}\rho t^8 + 1.2 \times 10^{-3}\rho^2 t^{16} \qquad (65)$$

wh... is an average of the type of result exhibited in Fig. 11.
The dispersion response resembles the water uptake curves (see
Fig. 10) published by Hänel (35) and provided the impetus for
the discussion presented in Section III.C.

Bohlander experimented extensively in the 100 GHz to 1000 GHz
range and deduced from attenuation data, including results from
other investigators, the component α_x/ρ^2 shown in Fig. 12 and
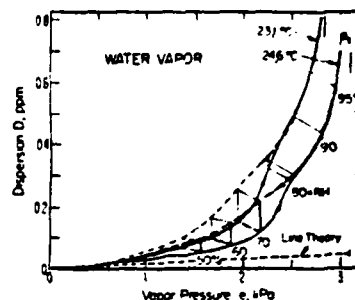listed in Table 4 (69, 109). He also calculated (by theoretical

*FIGURE 11. Dispersion D of pure water vapor measured with a
spectrometer cell between the frequencies 61.2 and 30.6 GHz
(63). A strong anomalous component is displayed exhibiting a
condensation/evaporation hysteresis typical for water uptake
activity (see Fig. 10).*

means) the envelope of a rotational dimer spectrum, a fractional
dimer concentration (Eq. 42) of 10^{-3} being assumed. The data
fit between EWA and the dimer attenuation (c/x in Table 4) is
poor; the spectral shapes do not match. The fit is much improved
if the aerosol attenuation rate (Eqs. 59 and 49) in dB/km

$$\alpha_A = (\alpha_w/n_w')\rho_w \qquad (66)$$

is used in the comparison (a/x in Table 4). Equation (66)
assumes pure liquid water droplets of submicron size. Actually,
based on this fit, it is possible to predict a liquid water con-
centration ρ_w that is needed to reproduce the EWA data of Table
4; that is, in g/m^3

$$\rho_w = 1.1 \times 10^{-3} \rho^2 \qquad (67)$$

At this point, the reader might recollect the arguments that have
been brought forward to formulate Eqs. (47), (49), (59) –
(61). Millimeter wave attenuation by submicron hydrometeors is
derived from Mie's scattering equations in the Rayleigh approxi-
mation (33). The refractive index and attenuation rate of bulk
water are presented in Fig. 13 (102-106). The bulk water attenua-
tion α_w is higher because of refractive wavelength shortening in
the medium; hence, the division by n_w' is applied for the gaseous
aerosol medium ($n' = 1$).

*TABLE 4. The EWA Component α_x/ρ^2 Reported in Refs. 69 and 109 Compared with the Water Dimer
Spectrum α_D/ρ^2 Calculated by Bohlander (69) and with the Aerosol Liquid Water Attenuation (a,b).*

Atten- uation	Code	Frequency v, GHz										T, °C	Ref.	Fig.
		100	200	300	400	500	600	700	800	900	1000			
α_x/ρ^2	x	+)	19	26	32	37	42	46	50	52	55	23	69	12
α_D/ρ^2	c	4	10	18	45	50	40	25	15	11	7	23	69	12
α_A/ρ_w (Eq. 59) b		*) 4	9	16	21	26	31	36	40	43	46	25	25, 32, 106	
(Eq. 60) a		7	16	23	28	33	38	42	45	48	51	25	106	
		H_2O—Attenuation Rate												
Data	a/x		0.84	0.88	0.88	0.89	0.90	0.91	0.90	0.92	0.92			
	b/x		0.47	0.62	0.66	0.70	0.74	0.78	0.80	0.83	0.84			
Fit:	c/x		0.53	0.69	1.41	1.35	0.95	0.54	0.30	0.21	0.13			

+) Units: [dB/km/(g/m^3)^2] $\times 10^{-3}$
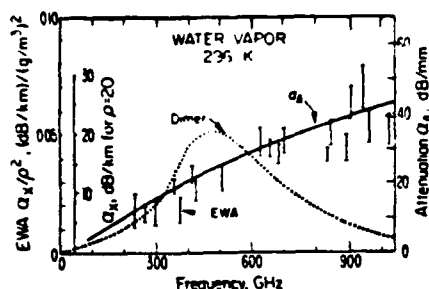
*) Units: dB/km/g/m^3

FIGURE 12. *Summary of reported frequency dependence for excess water vapor absorption, compared with a rotational dimer band spectrum ($N_D/N_v = 10^{-3}$) (69) and the absorption spectrum α_A of liquid water in submicron hydrometeors (see Table 4).*
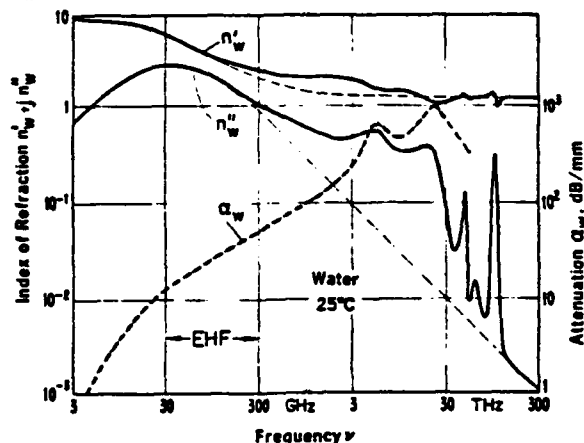

FIGURE 13. *Complex refractive index n_w and bulk attenuation rate α_w of water as a function of frequency, $\nu = 3$ GHz to 300 THz (composite from Refs. 102 to 106).*

The refractivity $N_0 = 40.4\rho + \delta N_0$, when measured at 40°C and 21.4 GHz and 23.6 GHz (49,56,63) exhibited also the anomalies δN_0:

RH,%	≤ 85	91.0	94.0	97.0	98.0	99.0
δN_0, ppm	0	0.3	0.8	1.5	1.8	2.5

C. EWA Evidence from Field Measurements

Millimeter wave field measurements are carried out in three ways (37-101):

1. attenuation rate α (dB/km) for horizontal, line-of-sight paths;

2. total zenith attenuation A(dB); and

3. sky noise T_B(K), often employed to infer the A value.

Most of the measurements are performed at single frequencies; a few were carried out in a broadband mode (Fourier transform technique) (86,90,93,98,101). Several difficulties plague field observations:

1. absolute calibration;

2. large scatter (± 10% to ± 30%) in data due to unspecified weather along the path;

3. scarceness of data at high humidities (RH > 90%);

4. lack of simultaneous recordings of the integrated water vapor w (Eq. 33);

5. absence of data on integrated liquid water W (Eq. 49) and visibility V (Eq. 52) in cloud-free air; and

6. difficulty of fitting data empirically to surface-based meteorological variables.

Horizontal and zenith path data are summarized in Table 5 and compared with model calculations by using the U.S. Standard Atmosphere (19). As expected, the window (W1 to W5) absorption increases with the water vapor concentration ρ or path-integrated water vapor w. It was observed earlier that measurements in the 100 GHz to 117 GHz range revealed considerably higher values of water vapor absorption than were predicted by H_2O line shape theory (73).

Generally, the absorption A is divided into a dry contribution (A_d) and a wet term (A_w). The dry term is caused by oxygen absorption originating from a well-known spectroscopic data base (Section II); hence, in W1 to W3, it can serve as a check value.

The wet term determines the transparency in all window ranges. Transparency is tightly coupled to humidity (that is, ρ, w, and W(RH)) causing various propagation limitations (for example, usable range L or minimum elevation angle θ) with increasing amounts of water vapor in the path volume. A typical case exists when weather conditions change from clear and dry to cloudy and wet. The water vapor absorption problem fades rapidly away above h > 3 km. It has become a standard practice to separate the wet term into two components: one proportional with ρ (monomer), the other with ρ^2 (dimer) dependence. The first field results to support the dimer hypothesis were taken at 220 GHz (76). Comparing these data with other available data in Table 5, one notices that in about half the cases a squared (x = 2) water vapor dependence improves the fit.

A horizontal path that operated at 182.9 GHz, close to the 183 GHz H_2O line (Table 2), exhibited differences in the water vapor proportionality depending upon clear or cloudy sky conditions. The difference, 3.90 compared with 4.20 dB/km, was reconciled when a temperature dependence of t^{10} was assumed, which is about four times the t dependence for the 183 GHz line (Eq. 29; $t^{2.3}$) (77). The same experiment produced at 171 GHz a relationship between attenuation rate ρ and concentration that becomes increasingly nonlinear when $\rho > 10$ g/m³. Measurements in W5 (330 GHz to 360 GHz) required a linear (x = 1, y = 2.3) and squared (x = 2, y = 11) water vapor term to fit the data (89). Condensation effects were evident in recent W4 and W5 data (101). For the first time, the importance of relative humidity RH was recognized. An EWA contribution with x = 2 and y = 16 to 30 can be isolated and an increase of α_x with beginning fog conditions was measured. Predicted attenuation rates in fog are in the range 3 to 15 dB/km for $\nu = 100$ to 300 GHz, $\rho_w = 1$ g/m³ and T = 4°C (25). An independent measurement of water vapor w and liquid W contributions would be desirable.

Cumulative data taken through the total air mantle are more difficult to interpret for their phenomenological origins. In most cases, zenith attenuation A is correlated with the surface water vapor concentration ρ_0. Simultaneous measurements of the integrated vapor w, either by microwave (see Eq. 51) or infrared techniques (93) are rare. The maximum attenuation detectable in the EHF range is A ≤ 30 dB. The dry term A_d of a slanted radio path follows the secant law $A_d(90°)/\sin\theta$, even for low angles ($\theta \leq 10°$); the wet term A_w increases very rapidly below $\theta < 10°$ (91). A tangential path ($\theta = 0$) traverses about 38 times the air mass at zenith but perhaps 100 times the water vapor content.

It seems certain that A_w is a continuum spectrum (79,93,98, 108) and that earlier observations of spectral dimer features (81,86,90,64) were instrumental effects. To quote from Ref. 93: "[EWA] shows no spectral features and scales with w." The frequency dependence of the empirical continuum spectrum (Eqs. 28 and 4) was z = 2. A fit of the A_w term between 15 GHz and 230 GHz (Table 5) yields in dB approximately

$$A_w \approx 0.013\,\rho_o\,(\nu/30)^{1.7} \qquad (68)$$

and the frequency dependence drops to z = 1.22 for window data taken between 140 GHz and 300 GHz (93).

Field data mostly serve the practical purpose of establishing an operational data base. Agreement with model calculations (Section II) is fair, when it is considered that the model makes use of Eq. (27) to describe the water vapor continuum. Either integrated vapor w or surface concentration ρ are useful predictors of millimeter wave window absorption (Table 5).

D. EWA Discussion

A water vapor continuum spectrum dominates the transmission behavior of atmospheric window ranges (W1 to W5: Figs. 1 to 3). Three absorption mechanisms have been parameterized to aid in identifying the respective relative contributions to the continuum. In the course of this paper, the following picture evolved:

	Far- wing Eq. (57)	Dimer Eq. (58)	Aerosol Eq. (61)	Laboratory data	Field data
Relative magnitude C/C_v	1.0	EWA	EWA	2 to 10	> 2
Water vapor x	1.2	2	$\gtrsim 2$	1 + 2	1 + 2
Temperature y	3.0	8	28.0	5.5, 10, > 10, 16, 26	10, 11, 16 to 30
Frequency z	2.0	Fig. 12	0.8	1.5 to 2.5	1.2, 1.7, 2

The empirical expressions (Eqs. 62 to 68) merely organize experimental data; they are not found to be entirely satisfactory to uniquely support even one particular absorption scheme. At present it is difficult to relate EWA contributions quantitatively

TABLE 5.   Summary of Reported EHF Radio Path Attenuation and Comparison with Model Calculations

(a)   Horizontal Path at Sea Level[a]

	Model (19)		Field data[b]			
RH,%	0	100[c]	0	100[c]	Water vapor data fit	Ref.
ν, GHz	α, dB/km		α, dB/km		ρ, g/m³	
80.000	0.010	0.56	—	0.510	$0.04(2)\rho$	81
130.000	0.020	1.28	—	1.540	$0.12(3)\rho$	81
171.000	0.010	4.93	0.200	4.800	$0.375\rho + b\rho^2$	77
250.000	0.000	4.57	—	4.900	0.38ρ	101
304.000	0.000	8.16	0.000	41.000	3.2ρ	75
337.000	0.000	16.89	0.600	18.400	$0.8\rho + 0.05\rho^2$	100
345.000	0.000	13.50	0.000	8.400	$0.45\rho + 0.016\rho^2$	89
350.000	0.000	14.00	—	17.900	1.4ρ	101

(b)   Zenith Path from Sea Level[a]

		Model (19)		Field data			(A_v) or		
	ν, GHz	A_d, dB	A, dB	A_d, dB	A, dB	ρ_o		w, cm	Ref.
	15.000	0.050	0.11	0.055	0.106	0.004ρ			31
	15.000	0.050	0.11	0.046[b(a)]	0.085[b(b)]	0.003ρ			91
	20.600	0.090	0.56	0.11(2)	0.52(2)			$d_{av} + bw^2$	97
W0	22.000	0.065	0.88	0.33(3)	1.150			$0.27(2)w$	88
	22.300	0.066	0.90	0.200	0.900	0.07ρ			85
	22.235	0.066	0.91	0.110	0.720	$0.048(8)\rho$			31
	31.700	0.120	0.35	0.13(2)	0.35(2)			$0.032w^2 - 0.026w$	97
W1	35.000	0.150	0.39	0.16[b(c)]	0.300[b(d)]	0.010ρ			91
	35.000	0.150	0.39	0.170	0.340	$0.013(2)\rho$			31
	35.000	0.150	0.39	0.100	0.250	$d_{a\rho} + b\rho^2$			84
	36.000	0.160	0.41	0.15(2)	0.640	$0.038(6)\rho + b\rho^2$			97
	80.000	0.450	1.37	0.5(2)	1.400				87
	90.000	0.250	1.38	0.170	0.940	$0.06(2)\rho$			31
	91.000	0.240	1.40	0.320	1.510			$0.2w + 0.06w^2$	80
W2	95.000	0.220	1.48	0.41(4)	1.500			$0.35(2)w$	88
	95.000	0.220	1.48	0.250	1.350	$d_{a\rho} + b\rho^2$			84
	110.000	0.450	2.10	0.6(2)	2.180	$0.27(3)\rho$			87
	111.000	0.470	2.20	0.97(17)	2.400			$0.45(14)w$	88
	118.000	14.110	16.45	10.000	12.000				87
W3	123.000	1.110	3.39	1.67(6)	3.400			$0.56(4)w$	88
	150.000	0.100	3.63	0.28(25)	4.000			$1.19(14)w$	88
	210.000	0.070	7.63		9.200	0.72ρ			82
	225.000	0.050	7.64	0.050	6.900	$0.54(30)\rho$			95
W4	230.000	0.050	7.82	1-5					83
	230.000	0.050	7.82	0.000	4.800	$0.37(5)\rho$			94
	240.000	0.040	8.32		7.900	0.62ρ			32
	300.000	0.020	17.40		13.400	1.05ρ			82
W5	345.000	0.010	31.00		23.000	$1.18(8)\rho$			89
	411.000		104.00		50.000	4ρ			32
	667.000				150.000	12ρ			32

[a] Digits in parenthesis give the Standard Deviation from the mean in terms of final listed digits.

[b] Tangential path: (a) x 69, (b) x 173, (c) x 53, and (d) x 142 (Ref. 91).

[c] $\rho_s = 12.8$ g/m³ or $w_s = 3.08$ cm and U.S. Standard Atmosphere 76.

[d] a,b - coefficient not given.

to observed variables. Results vary greatly from one experiment to the next, even under controlled laboratory conditions. EWA is most prevalent when RH > 90%; however, the best type of measurement has not yet been undertaken.

There are objections to both interpretations of EWA. Unclear problems with respect to the dimer are: (a) no direct physical evidence in the atmosphere; (b) no match to the frequency-envelope of a proposed spectrum (Table 4); and (c) no unique match to the temperature dependence. A promising EWA hypothesis is, at present, the vapor-to-liquid conversion of water by aerosol particles under conditions where $RH \leq 100\%$. Here the objections lie in the fact that invisible or haze clouds (see X-distribution in Fig. 9) must exist with liquid water concentrations close to those measured in fogs or clouds (for example, RH = 96%, T = 10°C, ρ = 9, and ρ_w = 0.1 g/m^3, by using Eq. (67)). Delonge raises the point that for the case of an inhomogeneous distribution of liquid aerosol water, the visibility V is improved due to the $\rho^{0.6}$-dependence (Eq. 52) whereas millimeter waves respond just to the total water W (Eq. 49; Ref. 30).

Which explanation for EWA has the most merit can only be answered by additional, completely controlled experiments performed in the laboratory.

V. CONCLUDING REMARKS

The role that atmospheric water vapor plays in millimeter wave propagation was traced by means of data from modeling, laboratory, and field studies. The assumptions and approximations made, the reasoning used, the relative importance of various parameters, the limitations of available data, and the separation of water vapor and liquid water effects have been addressed. Molecular absorption due to oxygen is prominent in the 45 GHz to 125 GHz range (Fig. 3); water vapor dominates at higher frequencies, actually up to 30 THz (Figs. 1 and 2). Considering only molecular absorbers (H_2O and O_2) for a cloudless atmosphere leads invariably to discrepancies between predicted and measured attenuation rates. The problem is most apparent in the EHF window ranges. A horizontal path at sea level can experience, at 220 GHz for example, the following varying attenuation rates (32):

Clear air	1.6 to 11.2 dB/km
Fog	0.4 to 4.7 dB/km
Rain (< 10 mm/hr)	1 to 7 dB/km

These values demonstrate the relative importance of understanding the clear air problem first. Clear air attenuation is related to atmospheric water vapor content; unfortunately, more than two-thirds of this contribution is described only by empirical formulas that lack both physical insight and general applicability.

A reasonably concise model for the molecular absorption was presented in Section II and then applied to identify the magnitude and frequency and physical dependencies of the non-H_2O contribution to the available data body reported for laboratory and field experiments. The contribution is called EWA (excess water vapor absorption) and it was found that the EWA exhibits in the millimeter wave range a continuum spectrum similar in frequency response to the dielectric loss spectrum of water. The search for liquid water in clear air led to the water-uptake phenomenon of aerosol particles, which grow rapidly in moist air with increasing RH. This problem has been addressed in the infrared (9,20,23) and deserves further study with respect to influences on millimeter waves.

Most of the evidence found in parameterizing EWA data supports a condensation phenomenon driven by relative humidity, RH: (a) the nonlinear pressure dependence (aerosol growth function), (b) the strong negative temperature dependence, (c) hysteresis effects when cycling the RH, (d) the governing variable is relative (RH) and not absolute (ρ) humidity, and (e) the failure of molecular approaches hypothesizing weakly bonded dimers but neither matching the spectral response nor the temperature dependence and number concentration necessary.

From a practical point of view, one is looking for invisible liquid water content in the range W = 0.02 to 0.2 mm when $RH \leq 100\%$, which are normally known to exist under haze, cloud and fog conditions. But clouds and fog imply only larger, optically active (r > 1 um) particle sizes. Should the condensation hypothesis have merit, then EWA can serve as a tracer to the otherwise not directly accessible world of atmospheric sub-micron particles. A systematic EWA study under controlled laboratory conditions of high humidity (RH = 90% to 99.9%) could reveal growth functions for particular aerosol ensembles and elucidate the various stages and time scales that H_2O molecules undergo in moist air until they become barely visible as clusters of > 10^9 molecules.

SYMBOLS AND ACRONYMS

Acronyms

AFGL	Air Force Geophysical Laboratory
CN	condensation nuclei
CCN	cloud condensation nuclei
D1-D4	O_2-MS doublets (Table 1)
EWA	excess water vapor absorption
E18	computer short-form for 10^{18}
EHF	extreme high frequency range (30 to 300 GHz)
HITRAN	high resolution transmission model developed by AFGL
H-bond	molecular hydrogen bond
ID	quantum number identification
IM	imaginary part of
O_2-MS	oxygen microwave spectrum
RE	real part of
W1-W7	atmospheric transmission windows

Symbols

a	coefficient for fitting $\propto \rho$, Tabel 5
a_1-a_5	O_2-MS line coefficients, Eqs. (21) to (23) and Table 1
A	total attenuation, Eq. (6), dB
b	coefficient for fitting data $\propto \rho^2$, Table 5
b_1-b_3	H_2O line coefficients, Eqs. (24) and (25), Table 2
B(t)	second virial coefficient, Eq. (37), m^3
c	speed of light, Eq. (3), km/s
C	continuum magnitude, Eq. (53)
d	molecular spacing, Section III, m
D(v)	dispersion spectrum, Eq. (13), ppm
e	water vapor pressure, Eq. (11), kPa
E	field strength, Eq. (2), V/m
f	relative humidity RH, Eq. (45)
F'	line shape for D(v), Eq. (15), GHz^{-1}
F"	line shape for N"(v), Eq. (16), GHz^{-1}
g(f)	aerosol mass growth factor, Eq. (47)
h	altitude, Eq. (32), km
i	running spectral line index, Tables 1 and 2
I	interference coefficient, Eq. (23)
j	= $\sqrt{-1}$, Eqs. (1) and (3)
k(t)	dimer equilibrium factor, Eq. (39), m^{-3}
ℓ	mean free path length, Section III, um
L	radio path length, Eq. (2), km
m	molecular mass, Eq. (20)
M	molecular number density, Eq. (36), molec/m^3
n	refractive index, Fig. 13
n'	real part of n, Eq. (58)
n"	imaginary part of n, Fig. 13
N	complex refractivity, Eq. (1), ppm
N_o	frequency-independent part of N, Eq. (12), ppm
N'(v)	refraction spectrum, Eq. (27), ppm
N"(v)	absorption spectrum, Eq. (14), ppm
p	dry air pressure, Eq. (12), kPa
δp	fluctuations of p, Eq. (34), kPa
Q	resonator quality factor, Table 3
r	aerosol particle radius, Eq. (35), um
RH	relative humidity, Eq. (45), %
s	ray path length, Eq. (6), km
s_1, s_2	ray path coordinate, Eqs. (6) and (8)
ds	path length increment, Eq. (6), km
S	line strength, Eqs. (21) and (24), kHz
S_A	aerosol surface area, Eq. (46), cm^2
t	300/T, normalized inverse T, Eq. (11)
T	temperature, Eq. (11), K
T_B	brightness temperature, Eq. (10), K
V	visibility, Eq. (52), km
V_v	air volume containing water vapor, Section IV, cm^3
w	total precipitable water vapor, Eq. (33), cm
W	total precipitable liquid water, Eq. (49), mm
x	concentration exponent (ρ), Eq. (53)
y	temperature exponent (t), Eq. (53)
z	frequency exponent (v), Eq. (53)
α	attenuation rate, Eq. (4), dB/km
γ	line width, Eq. (22), GHz
γ_D	Doppler line width, Eq. (20), kHz
Γ	propagation constant, Eq. (3)
ε	deviation from ideal gas behavior, Eq. (38)
η	propagation delay time, Eq. (9), ns
n_{Ad}	time constant for adsorption, Section IV.B., s
n_{De}	time constant for desorption, Section IV.B., s
θ	slant path angle, Section II, degree
λ	optical wavelength, Section III, m
ν	frequency, Eq. (3), GHz
ν_o	line resonance frequency, Eq. (15), GHz
ρ	water vapor concentration, Eq. (36), g/m^3
$\bar{\rho}$	path-averaged value of ρ, Eq. (52), g/m^3
$\delta\rho$	fluctuations of p, Eq. (34), g/m^3
τ	transmittance, Eq. (7)
φ	phase rate, Eq. (5), rad/km
ϕ	total phase delay, Eq. (8), rad
Σ	sum of, Eqs. (13) and (14)

Subscripts

A	aerosol
D	dimer
d	dry
ℓ	absorption line
L	Lorentzian
m	maximum
n	integer, cluster size
o	initial value
s	saturation
v	water vapor
w	liquid water

R   EMA
u   optical wavelength (λ = 0.55 um)

REFERENCES

Atmospheric Attenuation, Refraction, Dispersion, and Emission

1. Van Vleck, J. H., *Phys. Rev. 71*, 425-433 (1947).

2. Birnbaum, G., *J. Chem. Phys. 21*, 57-61 (1953).

3. Zhevakin, S. A., and Naumov, A. P., *Izv. Vysshikh Uchebn, Zavedenii, Radiofiz. 6*, 674-695 (1963) (Russian transl.).

4. Hall, J. T., *Appl. Optics. 6(8)*, 1391-1398 (1967); also in "Proc. Sym. on Sub-MM Waves," pp. 455-465, Polytechn. Inst., Brooklyn, New York (1970).

5. Zhevakin, S. A., and Naumov, A. P., *Radio Engrg. Electronic Phys. 12*, 885-894, 1067-1076 (1967) (Russian trans.).

6. Viktorova, A. A., and Zhevakin, S. A., *Soviet Phys. Doklady, 11*, 1059-1068 (1967) (Russian transl.).

7. Liebe, H. J., *IEEE Trans. AP-17*, 621-627 (1969).

8. Viktorova, A. A., and Zhevakin, S. A., *Sov. Phys.-Kokl. 15(9)*, 836-855 (1971).

9. Hodges, J. A., *Appl. Optics, 11(10)*, 2304-2310 (1972).

10. McClatchey, R. A., Benedict, W. S., Clough, S. A., Burch, D. E., Calfee, R. F., Fox, K., Rothman, L. S., and Garing, J. S., AFCRL Atmospheric Absorption Line Parameters Compilation, AFCRL Environm. Research Paper, No. 434 (1973); revisions in: *Appl. Optics, 15*, 2616 (1976); *17*, 507; *17*, 3517-3518 (1978).

11. Gaut, N. E., and Reifenstein, E. C. III, Environmental Research and Technology, Inc., Tech. Rpt. 75-0-1949 (1975).

12. Roberts, R. E., Selby, J. A., and Biberman, L. M., *Appl. Optics, 15(9)*, 2085-2090 (1976).

13. Lam, K. S., *J.Q.S.R.T. 17*, 351-383 (1977).

14. Derr, V. E., and Calfee, R. F., Spectral Transmission of Water Vapor from 1 to 1200 cm^{-1} at Low Concentration and Low Pressure, NOAA Tech. Memo ERL WPL-24 (July 1977).

15. Liebe, H. J., Gimmestad, G. G., and Hopponen, J., *IEEE AP-25(3)*, 327-335 (1977).

16. McMillan, R. W., Gallagher, J. J., and Cook, A. M., *IEEE MTT-25(6)*, 484-488 (1977).

17. Liebe, H. J., and Gimmestad, G. G., *Radio Science, 13(2)*, 245-251 (1978).

18. Montgomery, G. P., Jr., *Appl. Optics, 17(15)*, 2299-2303 (1978).

19. Liebe, H. J., and Rosich, R. K., Modeling of EHF Propagation in Clear Air, Proc. IEEE Conf. Space Instrum. for Atm. Observation, El Paso, Texas, pp. 5/1-15 (IEEE Catalog No. 79 Ch 138C-5 REG 5) (April 1979); also, AGARD CP 238-II, 45/1-18 (1978).

20. Tam, W. G., and Boily, C., *Infrared Phys. 19*, 151-162 (1979).

21. Suck, S. H., Kassner, J. L., Jr., and Yamaguchi, Y., *Appl. Optics, 18(15)*, 2609-2617 (1979).

22. Carlon, H. R., *Infrared Phys. 19*, 549-557 (1979).

23. Nilsson, B., *Appl. Optics, 18(20)*, 3457-3473 (1979).

24. Burch, D. E., and Clough, S. A., in "Near-Millimeter Wave Technology Base Study, Vol. 1" (S. M. Kulpa and E. A. Brown, eds.), DARPA Report HDL-SR-79-8 (U.S. Army MDRC) (November 1979).

25. Falcone, V. J., Jr., Abreu, L. W., and Shettle, E. P., Atmospheric Attenuation of Millimeter and Submillimeter Waves: Models and Computer Code, U.S. Air Force Geophysics Lab., Tech. Report AFGL-TR-79-0253 (Environm. Research Paper 679) (October 1979).

26. Cutten, D. R., *Infrared Phys. 19*, 663-667 (1979).

27. Pinnick, R. G., Jennings, S. G., Chylek, P., and Auvermann, H. J., *J. Atmos. Sci. 36*, 1577-1586 (1979).

28. Carlon, H. R., and Harden, C. S., *Appl. Optics, 19(11)*, 1776-1786 (1980).

29. Smith, H. J., Dube, D. J., Gardner, M. E., Clough, S. A., Kneizys, F. X., and Rothman, R. S., FASCODE—Fast Atmospheric Signature Code, U.S. Air Force Geophysics Lab., Tech. Report AFGL-TR-78-0081 (January 1978).

30. Delogne, P., Attenuation of Millimetric and Visible Waves by Aerosols, Open Symposium Preprint, A2.1 (May 1980) (URSI-F, Internat. Symp., Lennoxville, Canada).

Comprehensive Treatments

31. Waters, J. R., in "Methods of Experimental Physics, Vol. 12B" (M. L. Meeks, ed.), Chapter 2.3, Academic Press, New York (1976).

32. Kulpa, S. M., and Brown, E. A., "Near-Millimeter Wave Technology Base Study, DARPA Report HDL-SR-79-8 (U.S. Army MDRC), Vol. 1 (November 1979).

33. McCartney, E. J., "Optics of the Atmosphere: Scattering by Molecules and Particles," Wiley, New York (1976).

Selected Properties of Atmospheric Water

34. Yue, G. K., *J. Aerosol Sci. 10*, 75-86 (1979).

35. Hänel, G., in "Advances in Geophysics, Vol. 19," pp. 74-188, Academic Press, New York (1976).

36. Shettle, E. P., and Fenn, R. W., Models for the Aerosols of the Lower Atmosphere and the Effects of Humidity Variations on Their Optical Properties, U.S. Air Force Geophysics Lab., Tech. Report AFGL-TR-0214 (September 1979).

37. Turner, R. E., Gebhardt, F. G., Manning, J. L., Meredith, R. E., Singer, S. M., and Vavra, P. C., Model Development for E-O SAEL: Natural Aerosol, Contrast, Laser Transmission, and Turbulence, U.S. Army ERDC, Atmospheric Sciences Lab. Report ASL-CR-80-0127-1 (January 1980).

38. National Academy of Sciences, Airborne Particles, Report by Subcommittee, Div. Medical Sciences, University Park Press, Baltimore, Maryland (1979).

39. Liou, K. N., and Duff, A. D., *J. Appl. Met. 18*, 99-103 (1979).

40. Guiraud, F. O., Howard, J., and Hogg, D. C., *IEEE Trans. GE-17(4)*, 129-136 (1979); also, Data Report on "Measurements of Precipitable Water Vapor and Cloud Liquid at Fort Sill, 1979, NOAA-Data Report ERL WPL-2 (October 1979).

41. Pruppacher, H. R., and Klett, J. D., "Microphysics of Clouds," Reidel Publishing, Boston, Massachusetts (1978).

42. Barrett, E. W., Parungo, F. P., and Pueschel, R. F., *Meteorol. Resch. 32*, 136-149 (1979).

43. Dyke, T. R., Mack, K. M., and Muenter, J. S., *J. Chem. Phys. 66(2)*, 498-510 (1977).

44. Curtiss, L. A., Fruip, D. J., and Blander, M., *J. Chem. Phys. 71(6)*, 2703-2711 (1979).

45. Ferguson, E. E., Fehsenfeld, F. C., and Albritton, D. L., in "Gas Phase Ion Chemistry, Vol. 1," pp. 45-81, Academic Press, New York (1979).

Laboratory Measurements

46. Becker, E. G., and Autler, S. H., *Phys. Rev. 70(5,6)*, 300-307 (1946).

47. Froome, K. D., *Proc. Phys. Soc. (London), B-68*, 833-835 (1955).

48. Bourdouris, G., *J. Res. NBS, 67D(6)*, 631-684 (1963).

49. Liebe, H. J., Untersuchungen an Gasmischungen, insbesondere Wasserdampf-Luft, Mit einem digitalen Mikrowellen-Refraktometer, Ph.D. Thesis, Techn. University, West Berlin, Electrical Dept. (D83) (1964); also, NTZ Communications J. 19, 79-83 (1966) (in German).

50. Newell, A. C., and Baird, R. C., *J. Appl. Phys. 36*, 79-83 (1965).

51. Rusk, J. R., *J. Chem. Phys. 42(2)*, 493-494 (1965).

52. May, D. R., and Turner, H. E., in "Humidity and Moisture, Vol. 2" (A. Wexler, ed.), pp. 611-615, Reinhold Publishing, New York (1965).

53. Frenkel, L., and Woods, D., *Proc. IEEE, 54(4)*, 498-505 (1966).

54. Burch, D. E., *J. Opt. Soc. Am. 58*, 1383-1394 (1968).

55. Hemmi, C. O., and Straiton, A. W., *Radio Sci. 4(1)*, 9-15 (1969).

56. Mrowinski, D., Refraktion und Absorption in atmosphärischen Gasen in der Umgebung der 22 GHz H$_2$O Linie, Ph.D. Thesis, Techn. University, West Berlin, Germany, Electr. Eng. Dept. (1969); also, Angew. Z., Phys. 29(5), 323-330 (1970) (in German).

57. Liebe, H. J., and Dillon, T. A., *J. Chem. Phys. 50*, 727-732 (1969).

58. Harries, J. E., Burroughs, W. J., and Gebbie, H. A., *J.O.S.R.T. 9*, 799-807 (1969); also, Burroughs, W. J., Jones, R. G., and Gebbie, H. A., *J.O.S.R.T. 9*, 809-824 (1969).

59. Sheppard, A. P., Breeden, K. H., and McSweeney, A., in "Proc. Sym. on Sub-Waves," pp. 445-453, Polytechn. Inst. Brooklyn, New York (1970).

60. Bignell, K. J., *Quant. J. Roy. Met. Soc. 96*, 390-403 (1970).

61. Burch, D., Gryvnak, D., and Pembrook, J., Jr., Continuous Absorption in the 8-4 um Range by Atmospheric Gases, Philco-Ford Report P19 628-69-C-0263 (1971).

62. Straiton, A. W., Fannin, B. M., and Perry, J. W., IEEE
Trans. AP-22(4), 613-616 (1974).

63. Liebe, H. J., Studies of Oxygen and Water Vapor Microwave
Spectra under Simulated Atmospheric Conditions, OT Ppt.
75-66, U.S. Government Printing Office, Washington, D.C.
(June 1975).

64. Llewellyn-Jones, D., Knight, R. J., and Gebbie, H. A.,
J. Phys. E: Sc. Instr. 9, 690-692 (1976).

65. Gimmestad, G. G., An Experimental Study of the Oxygen
Microwave Spectrum, Ph.D. Thesis, Dept. Phys. & Astrophys.,
University of Colorado (1978).

66. Llewellyn-Jones, D. T., Knight, R. J., and Gebbie, H. A.,
Nature, 274(5673), 876-878 (1978).

67. Kemp, A. J., Birch, J. R., and Afsar, M. N., Infrared
Phys. 18, 827-833 (1978).

68. White, K. O., Watkins, W. R., Bruce, C. W., Meredith, R. E.,
and Smith, F. G., Appl. Optics, 17(17), 2711-2720 (1978).

69. Bohlander, R. A., Spectroscopy of Water Vapor, Ph.D.
Thesis, Dept. Physics, Imperial College, London (1979).

70. Peterson, J. C., Thomas, M. E., Nordstrom, R. J., Damon,
E. K., and Long, R. K., Appl. Opt. 18(6), 834-841 (1979).

71. Watkins, W. R., White, K. O., Power, L. R., and Sojka,
B. Z., Appl. Opt. 19(8), 1149-1160 (1979).

72. Jona, M., Physik. Zeitschr. 20, 14-21 (1919) (in German).

Field Measurements

73. Crawford, A. B., and Hogg, D. C., Bell Syst. Tech. J. 35,
907-916 (1956); also, Hogg, D. C., J. Appl. Phys. 30(9),
1417-1419 (1959).

74. Tolbert, C. W., Krause, L. C., and Straiton, A. W.,
J. Geophys. Res. 69(7), 1349-1357 (1964).

75. Chang, S. Y., and Lester, J. D., IEEE Trans. AP-16(5),
588-591 (1968).

76. Malyshenko, Y. I., Rad. Eng. & Electr. Phys. 14(3),
447-450 (1969) (Russian transl.).

77. Whaley, T. W., Characterization of Free Space Propagation
Near the 183 GHz H$_2$O Line, Ph.D. Thesis, U. of Texas,
Electr. Eng. Dept. (1968); also, IEEE Trans. AP-17(5),
682-684 (1969).

78. Wrixon, G. T., Bell Sys. Tech. J. 50(1), 103-114 (1971).

79. Mather, J. C., Werner, M. W., and Richards, P. L.,
Astrophys. J. 170, L59-65 (1971).

80. Thompson, W. I. III, Atmospheric Transmission Handbook,
NASA Tech. Rept. No. DOD-TSC-NASA-71-6, Chapter 9 (1971).

81. Gibbins, C. J., Nature, 243, 397 (1973).

82. Ulaby, F. T., IEEE Trans. AP-21(2), 2666-2669 (1973).

83. Goldsmith, P. F., Plambeck, R. L., and Chiao, R. Y.,
IEEE Trans. MTT22(12), 1115-1116 (1974).

84. Lo, L. I., Fannin, B. M., and Straiton, A. W., IEEE Trans.
AP-23(6), 782-786 (1975).

85. Fogarty, W. G., IEEE Trans. AP-23(3), 441-444 (1975).

86. Emery, R. J., Moffat, P., Bohlander, R., and Gebbie, H. G.,
J. Atm. Terrestr. Phys. 37, 587-594 (1975).

87. Gibbins, C. J., Gordon-Smith, A. C., and Croom, D. L.,
Planet. Space Sci. 23, 61-73 (1975).

88. Gibbins, C. J., Wrench, C. L., and Croom, D. L.,
Atmospheric Emission Measurements between 22 and 150 GHz,
Proc. URSI Comm. F Sym., LaBaule, France (1976).

89. Ryadov, V. Y., and Furashov, N. I., Radio Phys. & Quant.
Electr. 19, 918-922 (1977) (Russian transl.).

90. Moffat, R. H., Bohlander, R. A., Macrae, W. R., and
Gebbie, H. A., Nature, 269, 676-677 (1977).

91. Altshuler, E. E., Gallop, M. A., and Telford, L. E.,
Radio Sci. 13(5), 839-852 (1978).

92. Zabolotniy, V. F., Iskhakov, I. A., Sokolov, A. V., and
Sukhonin, E. V., Infrared Phys. 18, 815-817 (1978).

93. Hills, R. E., Webster, A. S., Alston, D. A., Morse, P. L.,
Zammit, C. C., Martin, D. H., Rice, F. C., and Robson,
E. I., Infrared Phys. 18, 819-825 (1978).

94. Wrixon, G. T., and McMillan, R. W., IEEE Trans. MTT-26(6),
434-439 (1978).

95. Plambeck, R. L., IEEE Trans. AP-26, 737-738 (1978).

96. Robson, E. I., and Rowan-Robinson, M., Infrared Phys. 19,
115-120 (1979).

97. Hogg, D. C., and Guiraud, F. O., Nature, 279(5712),
408-409 (1979).

98. Rice, D. P., and Ade, R. A., Infrared Phys. 19, 575-584
(1979).

99. Ho, K. L., Mavrokoukoulakis, N. D., and Cole, R. S.,
Microwave Opt. Acoust. 3(3), 93-98 (1979).

100. Tanton, G. A., Mitra, S. S., Stettler, J. D., Morgan, R. L.,
Osmundsen, J. F., and Castle, J. G., Near Ground
Attenuation of 0.89 mm Radiation, Proc. 4th Int. Conf.
Infrared & MM-Waves (IEEE Cat. 79 CH 1384-7 MTT), 27
(December 1979).

101. Emery, R. J., and Zavody, A. M., Radio Elect. Eng. 49,
370-380 (1979).

Refractive Index of Water

102. Pottel, R., in "Water--A Comprehensive Treatise, Vol 1:
The Physics and Physical Chemistry of Water" (F. Franks,
ed.), Chapter 7, Plenum Press, New York (1972).

103. Ray, P. S., Appl. Opt. 11(8), 1836-1844 (1972).

104. Afsar, M. N., and Hasted, J. B., J. Opt. Soc. Am. 67(7),
902-904 (1977).

105. Afsar, M. N., and Hasted, J. B., Infrared Phys. 18,
835-841 (1978).

106. Simpson, O. A., Bean, B. L., and Perkowitz, S., Far Infrared
Optical Constants of Liquid Water Measured with an Optically
Pumped Laser, J. Opt. Soc. Am. 70 (1980).

Instrumentation

107. Gerber, H. E., Saturation Hygrometer for the Measurement
of Relative Humidity between 95 and 105%, J. Appl.
Meteorology (1980).

Additional References

108. Crane, R., Attenuation Estimates for Millimeter Wave
Windows near 94, 140, and 220 GHz, ERT Document T-A-502
(May 1980) (available from Environm. Res. and Techn. Inc.
Concord, Massachusetts 01742).

109. Bohlander, R. A., Emery, R. J., Llewellyn-Jones, D. T.,
Gimmestad, G. G., and Gebbie, H. A., in "Proc. Workshop
MM and SubMM Atmospheric Propagation" (O. Essenwanger and
D. Stewart, eds.), pp. 57-66, U.S. Army Missile Command
Tech. Report RR-80-3 (February 1980).

110. Poynter, R. L., and Pickett, H. M., Submillimeter,
Millimeter, and Microwave Spectral Line Catalogue, JPL
(Jet Propulsion Lab., NASA, Pasadena, California 91103)
Publication 80-23 (June 1980).

ABSORPTION OF MILLIMETER TO SUBMILLIMETER WAVES BY ATMOSPHERIC WATER MOLECULES

Masataka Mizushima

Department of Physics
University of Colorado
Boulder, Colorado 80309

Using the values of the rotational molecular parameters (including centrifugal distortion terms) of the $H_2^{16}O$ molecule, which can explain 12 observed transitions below 800 GHz, all rotational energy levels with normalized Boltzmann factors larger than 5×10^{-8} at 300°K are calculated. Probabilities of all possible electric dipole transitions among these states, 2277 lines, are calculated using the eigenfunctions thus obtained, and the permanent electric dipole moment of 1.8546 Debye. Assuming the single and full Lorentzian line forms, we calculated the absorption coefficient for millimeter to submillimeter region. Our result, using the single term Lorentzian line form, agrees quite well with experiment for 1 Torr of water vapor in 760 Torr air at 300°K.

Key words: water vapor, millimeter waves, submillimeter waves, excess absorption, Lorentzian line form, window regions.

Introduction

Burch (1) observed absorption of millimeter to submillimeter waves by moist air, particularly in the "window regions", and found that the experimental values were larger than the values calculated for those resonance lines below 1 THz by a factor of about two. Such excess attenuation was confirmed by both laboratory and field experiments (2) and has been recognized in numerical calculations as an empirical correction term (3)

$$\alpha_{ex} = 4.23 \times 10^{-5} p o (300/T)^{2.1} (\nu/30)^2 \quad \text{dB/km}$$

where p is the air pressure in kPa, o is the water vapor density in g/m³, T is the temperature in °K, and ν is the frequency in GHz.

McClatchy and others (4) gave a list of 1838 H_2O lines below 31 THz, based on a rigid body model of the molecule, and an semi-empirical formula for the line width:

$$\Delta = b_3 (p + 4.80 p_w)(300/T)^{0.6}$$

where p_w is the partial pressure of the water vapor. Liebe (5) summarized the calculated excess absorption due to higher frequency lines as

$$\alpha_{HC} = 1.5 \times 10^{-5} p o (300/T)(\nu/30)^2$$

Crane (6) reviewed the situation presenting more recent experimental data.

Theory

The theory of rotational states of asymmetric top molecules is well established (7,8). For the water molecule $H_2^{16}O$, and its isotope molecules, DeLucia and others (9,10) found sets of values for 11 molecular parameters, including three rotational constants and eight centrifugal distortion constants, by which all transition frequencies below 800 GHz they observed, could be explained. We simply took their values of the molecular parameters, calculated energy levels up to J = 16, and found that all states with normalized Boltzmann factors larger than 5×10^{-8} at 300°K (8×10^{-8} at 313°K) were counted in. The hfs splittings were not calculated, but the statistical weights due to the proton spins were taken into account. The frequencies and intensities of all 2277 electric dipole transitions among these rotational states were calculated using the eigenfunctions obtained above and the accepted value of the dipole moment, 1.8546 Debye.

We then assumed that each line had the Lorentzian form, and added them up to obtain the absorption

coefficient η at frequency ν:

$$\alpha(\nu) = \frac{\nu}{\hbar c \epsilon_0} \sum_{a < b} (n_a - \rho_b) |\langle a | \mu_z | b \rangle|^2 \times$$

$$\left(\frac{\Delta}{(\nu - \nu_{ab})^2 + \Delta^2} - \frac{\Delta}{(\nu + \nu_{ab})^2 + \Delta^2} \right)$$

where ρ_a is the number of molecules in the a-state per unit volume, μ_z is a space component of the electric dipole moment, and ν_{ab} is the transition frequency between the a- and b-states.

The Lorentzian form factor given in the above formula is called the full Lorentzian (abbreviated as F-L). Since the second term, due to the induced emission of photons, may be suppressed by scatterings, it is worthwhile to try the single Lorentzian (abbreviated as S-L) form factor in which the second term is neglected. We tried both F-L and S-L form factors.

We assumed that the transition frequencies are all independent of pressure and the width parameter is

$$\Delta = \frac{2.85}{760} (p + 4.80 p_w)(300/T)^{0.5} \quad \text{GHz}$$

as observed experimentally for some lines. No quantum number dependence was assumed.

Result

Our results for 300°K, p = 760 Torr, and p_w = 1 Torr are shown in Table 1 for some frequencies up to 1 THz, and compared with the model attenuation formula (5) which fits available experimental data. We see that F-L is below experimental values, but S-L result agrees quite well with experiment.

As is known already, the 26 lines below 1 THz contribute only half of the absorption coefficient in that region, out the remaining half, the so-called excess absorption, is simply the accumulated absorptions of the higher frequency transitions in the present theory with the S-L form factor. Figure 1 shows our computer plotting of the water spectrum below 2 THz using the S-L form factor, and it is almost identical to the semi-empirical spectrum, except for the oxygen absorptions which are not considered here.

We also calculated the absorption coefficient at 300°K, p = 760 Torr, and p_w = 10 Torr with the S-L form factor and saw that

$$\log \alpha (10 \text{ Torr}) = \log \alpha (1 \text{ Torr}) + 1.0227$$

holded for 35 GHz through 1 THz, except near resonant regions.

The temperature dependence appears through both Boltzmann factors and the width parameter. Calculation, with the S-L form factor, was made for 273°K, p = 760 Torr, and p_w = 1 Torr, and we found that

$$\log \alpha (273°K) = \log \alpha (300°K) + 0.103$$

holded for the low frequency region up to 150 GHz, and that the additional term went up to 0.108 around 200 GHz.

Including the absorptions by the atmospheric oxygen molecules calculations were made for temperatures up to 1000°K, and we found that the absorption in the 200 GHz region would be quite low.

Acknowledgements

References

1. D. E. Burch, J. Opt. Soc. Am. **58**, 1383 (1968).

2. Reviewed by H. J. Liebe in "Atmospheric Water Vapor" (ed. A Despak et al) Acad. Press, New York, 1980.

3. J. W. Waters in "Methods of Experimental Physics" (ed. M. L. Meeks) Acad. Press, New York, 1976.

4. R. A. McClatchey et al, Appl. Opt. **17**, L3517 (1978).

5. H. J. Liebe, Radio Science **16**, 1183 (1981).

6. R. K. Crane, Proc. IEEE **69**, 196 (1981).

7. S. C. Wang, Phys. Rev. **34**, 243 (1929).

8. For example, P. C. Cross, R. M. Hainer, and G. W. King, J. Chem. Phys. **12**, 210 (1944).

9. F. C. DeLucia, P. Helminger, R. L. Cook, and W. Gordy, Phys. Rev. A **5**, 487 (1972).

10. F. C. DeLucia, P. Helminger, and W. Kirchhoff, J. Phys. Chem. Ref. Data **3**, 211 (1974).

Table 1. Calculated absorption coefficient at 300°K,
1 Torr of $H_2{}^{16}O$ in air of 760 Torr.
$\Delta = (2.85/760)(p + 4.80p_w)$ GHz

| Frequency (GHz)	Calculated S-L (dB/km)	Calculated F-L (dB/km)	Empirical (dB/km)
10	0.0082	0.0007	0.015
20	0.028	0.013	0.032
30	0.028	0.006	0.036
40	0.034	0.006	0.065
80	0.071	0.017	0.12
90	0.082	0.022	0.100
100	0.093	0.028	0.104
130	0.13	0.052	0.145
140	0.15	0.065	0.145
150	0.175	0.083	0.170
160	0.22	0.12	0.215
170	0.30	0.24	0.335
180	1.81	1.71	1.96
190	0.83	0.72	0.83
200	0.35	0.24	0.39
210	0.30	0.18	0.34
220	0.30	0.18	0.35
230	0.31	0.18	0.37
240	0.33	0.20	0.395
250	0.35	0.22	0.43
260	0.38	0.24	0.465
270	0.41	0.27	0.51
280	0.45	0.31	0.55
290	0.50	0.35	0.62
300	0.57	0.42	0.69
400	2.15	1.97	2.38
500	7.11	6.9	7.6
600	14.4	14.2	17.1
700	7.7	7.4	9.4
800	9.8	9.3	11.9
900	8.95	8.7	11.0
1000	82	82	84
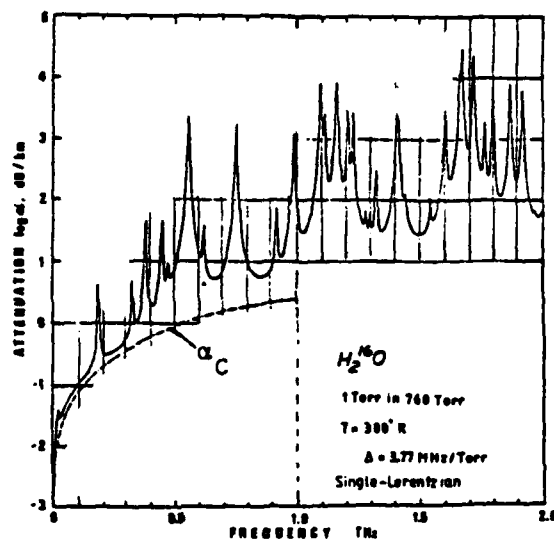
Figure 1. Computer plotting of the calculated absorption
coefficient by water molecules in air.

TRANSPARENCY OF EARTH'S ATMOSPHERE IN THE FREQUENCY REGION BELOW 1 THz

Masataka Mizushima*

Institute for Molecular Science
Myodaiji, Okazaki, 444 Japan

In addition to the water molecule which we considered in a previous paper, the oxygen molecule is taken into account to express theoretically the absorption coefficients of micro-, millimeter-, and submillimeter-waves by air at given temperature and pressure. The theory is applied to each layer of the U S Standard Atmosphere, and the resulting absorption coefficients are integrated for altitude from 0, 2, and 4 km to 80 km to obtain the transparency of earth's atmosphere.

Key words: transparency, absorption coefficient, oxygen molecule, water molecule, U S Standard Atmosphere.

Absorption of Micro-, Millimeter-, and Submillimeter-Waves by the Water Molecule

In a previous paper (1) we calculated all rotational states up to J = 16 of the water molecule, using known rotational and centrifugal distortion constants, and all possible electric dipole transitions among these states, 2277 lines. It was shown that the absorption of micro-, millimeter-, and submillimeter-waves by 1 Torr of water vapor in air of 760 Torr, 300 K could be explained if we assumed that each of these lines had Lorentzian line shape with a common width parameter determined by experiment on some of them. It was seen that the single-Lorentzian line shape gave almost complete agreement with empirical values of the absorption coefficients, while the full-Lorentzian line shape gave calculated values about 1/3 less than the empirical values, which was actually not so bad considering large uncertainties in the empirical values.

In the present calculation we take the full-Lorentzian line shape since it has better theoretical foundation than the single-Lorentzian line shape.

Rotational Transitions of the Oxygen Molecule (X $^3\Sigma_g^-$)

The microwave spectrum of the oxygen molecule, $^{16}O_2$, in its electronic ground state, X $^3\Sigma_g^-$, has been measured carefully (2-4), and the most recent measurement by Endo and Mizushima (5) is shown to be reproduced by the following Hamiltonian

$$H = BN^2 - DN^4 + (2/3)(\lambda(3S_\zeta^2 - S^2) + (1/2)\lambda_D(N^2(3S_\zeta^2 - S^2) + (3S_\zeta^2 - S^2)N^2) + (1/2)\lambda_{DD}(N^4(3S_\zeta^2 - S^2) + (3S_\zeta^2 - S^2)N^4)) + \gamma N \cdot S + \gamma_D N^2 N \cdot S \quad (1)$$

with proper values for the parameters, B, D, λ, λ_D, λ_{DD}, γ, and γ_D.

The resulting eigenstates can be expressed in terms of the eigenstates of N^2, S^2, J^2, and J_z operators, $|NSJM\rangle$,

$$|nJM\rangle = a_J|NJM\rangle + b_J|N+2JM\rangle \quad \text{when} \quad J > N$$
$$|nJM\rangle = a_J|NJM\rangle - b_J|N-2JM\rangle \quad \text{when} \quad J < N$$
$$|nJM\rangle = |NJM\rangle \quad \text{when} \quad J = N \quad (2)$$

where S is not shown explicitly since it is fixed as 1, and a_J and b_J are coefficients determined for each J.

The interaction of the magnetic moment of this molecule with external field B is given (6) by

$$H_{pm} = u_B(g_\zeta S_\zeta B_\zeta + \tfrac{1}{2}g_p(S_+B_- + S_-B_+) - g_N N \cdot B) \quad (3)$$

where u_B is the bohr magneton, ζ is the molecular axis, $S_\pm = S_\zeta \pm iS_\eta$, and

$g_\zeta = 2.002025, \quad g_p = 2.004838, \quad g_N = -0.000126 \quad (4)$

This interaction produces the magnetic dipole transitions between rotational states given by (2). The matrix elements of (3), which give intensities of the transitions, are

$$\langle nnM|H_{pm}|nn-1M\rangle = Bu_B[a_{n-1}(g_p+g_N) + (g_\zeta-g_p)\frac{n-1}{2n-1}]$$
$$+ b_{n-1}(g_\zeta-g_p)\frac{\sqrt{n(n-1)}}{2n-1}]\frac{\sqrt{(n-M)(n+1)}}{n\sqrt{2n+1}}$$

$$\langle nnM|H_{pm}|nn+1M\rangle = Bu_B[a_{n+1}(g_p+g_N) + (g_\zeta-g_p)\frac{n+2}{2n+3}]$$
$$- b_{n+1}(g_\zeta-g_p)\frac{\sqrt{(n+1)(n+2)}}{2n+3}]\frac{\sqrt{[(n+1)^2-M^2]n}}{(n+1)\sqrt{2n+1}}$$

$$\langle nnM|H_{pm}|n-2n-1M\rangle = Bu_B[a_{n-1}(g_\zeta-g_p)+b_{n-1}((g_p+g_N)$$
$$\frac{2n-1}{\sqrt{n(n-1)}}+(g_\zeta-g_p)\sqrt{\frac{n-1}{n}})]\frac{\sqrt{(n-M)(n-1)}}{(2n-1)\sqrt{n(2n+1)}}$$

$$\langle nn-1M|H_{pm}|n-2n-2M\rangle = Bu_B[a_{n-1}(g_\zeta-g_p)-b_{n-1}((g_p+g_N)$$
$$\frac{2n-1}{\sqrt{n(n-1)}}+(g_\zeta-g_p)\sqrt{\frac{n}{n-1}})]\frac{\sqrt{[(n-1)^2-M^2]n(n-2)}}{(2n-1)\sqrt{(n-1)(2n-3)}}$$

$$\langle nn-1M|H_{pm}|n-2n-1M\rangle = Bu_B M(a_{n-1}^2-b_{n-1}^2)(g_\zeta-g_p)$$
$$\frac{1}{(2n-1)\sqrt{n(n-1)}} - a_{n-1}b_{n-1}\frac{2n-1}{n(n-1)}] \quad (5)$$

where each eigenstate is expressed as $|nJM\rangle$. The value of the S quantum number is fixed as 1.

The widths of the microwave lines of the oxygen molecule are measured (7) to be 2.3 MHz/Torr and nearly independent of the quantum numbers. The widths of the 430 and 760 GHz lines are not measured yet, but we simply assume that all oxygen lines have the full-Lorentzian line shape with common width $2.3\sqrt{300/T}$ MHz/Torr. The absorption coefficient for a typical case of 760 Torr, 300 K air with 1 Torr of water vapor is calculated considering the oxygen and water molecules in this way. The result is shown in Fig. 1.
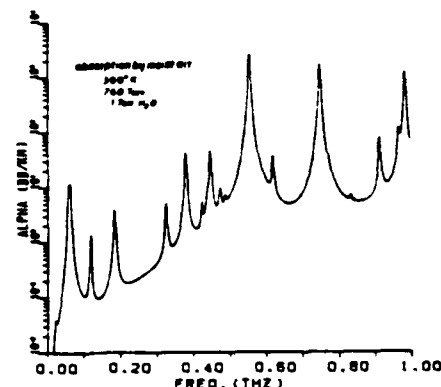

Figure 1. Computer plotting of the absorption coefficient by air of 760 Torr, 300 K with 1 Torr water vapor.

Transparency of the U S Standard Atmosphere

Typical values of temperature and pressure at each altitude of earth's atmosphere are given in the U S Standard Atmosphere. We apply the above explained method of computing the absorption coefficient to each layer of the U.S. Standard Atmosphere and then integrated them over the altitude up to 80 km (top of the mesosphere) to obtain the transparency,

$$\text{transparency} = \exp(- \int_x^{80 km} \alpha \, dh) \quad (6)$$

The lower limit of the integral, x, is chosen to be 0, 2, and 4 km in the computations, results of which are shown in Fig. 2a, 2b, and 2c, respectively.
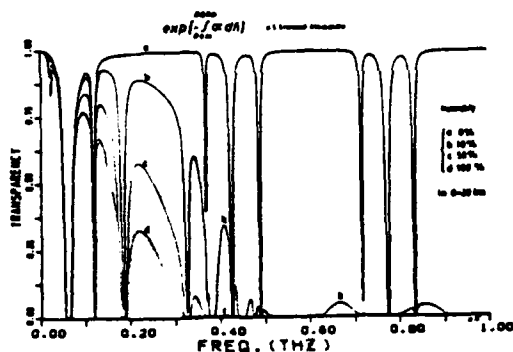
Figure 2a. Transparency of the U S Standard Atmosphere at 0 km altitude in 0 to 1 THz.
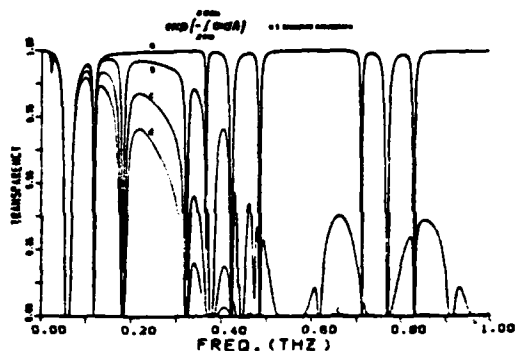

Figure 2b. Transparency of the U S Standard Atmosphere at 2 km altitude in 0 to 1 THz.
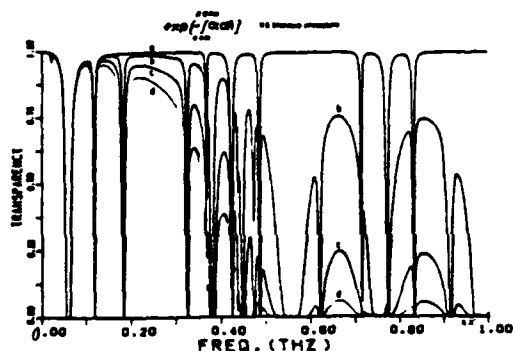

Figure 2c. Transparency of the U S Standard Atmosphere at 4 km altitude in 0 to 1 THz.

It is assumed, in this calculation, that earth's atmosphere contains 20.95% of $^{16}O_2$ at all altitudes. The saturation pressure of water vapor decreases rapidly as the altitude increases as shown in Table I. Since it is so small

Table I. Saturation Vapor Pressure (Torr) as a Function of Altitude in U S Standard Atmosphere.

km	0	1	2	3	4	5	6	7
Torr	12.79	8.33	5.29	3.14	1.91	1.09	0.58	0.29

8	9	10	11-24	25-27	28-29	30
0.15	0.08	0.03	0.02	0.03	0.04	0.05

at the Tropopause(20 km) we assume that water vapor exist only in altitudes below 20 km, and that the humidity stays constant from 0 to 20 km, to simplify computation. The humidity in this sense is taken as 0%, 10%, 50%, and 100% in Figs.2a through 2c.

References

1. M. Mizushima, Int. J. IR. MMW. 3, 379 (1982).

2. R. W. Zimmerer and M. Mizushima, Phys. Rev. 121, 152 (1961).

3. B. G. West and M. Mizushima, Phys. Rev. 143, 31 (1966).

4. T. Amano and E. Hirota, J. Mol. Spectr. 53, 346 (1974).

5. Y. Endo and M. Mizushima, Jpn. J. Appl. Phys. 21, L379 (1982).

6. K. D. Bauers, R. A. Kamper, and C. D. Lustig, Proc. Roy. Soc. (London) A251, 565 (1959).

7. Reviewed in H. J. Liebe, Radio Science 16, 1183 (1981).

THE ATMOSPHERIC WATER VAPOR CONTINUUM
BELOW 300 GHz*

Hans J. Liebe

Institute for Telecommunication Sciences
National Telecommunications and Information Administration
U. S. Department of Commerce
Boulder, Colorado 80303

Absolute attenuation rates due to water vapor and moist
nitrogen have been measured in the laboratory at 138 GHz,
282 and 300 K, pressures up to 1.5 atm, and relative humid-
ities from 80 to 100 percent. The computer-controlled
measuring system is comprised of a millimeter wave reson-
ance spectrometer (0.15 km effective path length) and a
humidity simulator. Several shortcomings of earlier meas-
urement attempts have been rectified. The data are inter-
preted as a water vapor continuum spectrum consisting of
two terms, namely strong self-broadening (H_2O-H_2O) plus
foreign-gas-broadening (H_2O-N_2) contributions. Implica-
tions of the new results for modeling atmospheric EHF
window transparencies and for revising established H_2O line
broadening theory are discussed.

Key Words: Atmospheric radio wave propagation; high-
humidity spectrometer; millimeter wavelength
region; water vapor continuum absorption

Introduction

Millimeter wave propagation through the atmosphere is
affected by meteorological phenomena such as humidity, fog,
clouds, and precipitation. System applications require a
detailed knowledge of atmospheric propagation limitations
and their dependency upon relevant meteorological parame-
ters. The influence of the intervening atmosphere upon
radio waves can be quantified by a propagation model. In
clear air, water vapor and oxygen absorption cause fre-
quency-dependent signal attenuation, propagation delay, ray
bending, and medium noise. Prediction of these propagation
effects is accomplished by a broadband model of the complex
refractivity N (1). To cover frequencies up to 300 GHz, a
reliable expression for N requires more than 200 coeffi-
cients. The refractivity N is formulated in units of parts
per million (ppm) and consists of three components

$$N = N_o + D(f) + jN''(f) \quad ppm$$

where N_o is the frequency independent refractivity, and
$D(f)$ and $N''(f)$ are frequency-dependent dispersion and
absorption terms arising from the molecular spectra of H_2O
and O_2.

The specific rates of the propagation medium are power
attenuation

$$\alpha = 0.1820fN''(f) \quad dB/km \qquad (1)$$

and delay

$$\beta = 3.336[N_o + D(f)] \quad ps/km , \qquad (2)$$

where the frequency f is in units of GHz.

This paper addresses millimeter-wave water vapor at-
tenuation rates. There has been a long-standing discrep-
ancy between theoretical spectroscopic predictions and
experimental data obtained from both laboratory and field
measurements (3,4). Marked differences occur in the window
ranges located around 35, 90, 140, and 220 GHz (2), where
experimental attenuation exceeds the theoretical values.
Since excess factors between 2 and 5 are involved, it has
been speculated that unidentified absorbers related to H_2O

(dimers, clusters, etc.) might be involved. Results for α
from controlled laboratory experiments in the 140 GHz
window are reported which help to clarify the water vapor
excess problem.

Water Vapor Millimeter Wave Spectroscopy

Water in both vapor and liquid states obscures the
millimeter wave transparency of the troposphere. Frequency
dependence and magnitude of H_2O attenuation are both
distinctly different for the same (1 mm) absorber thickness
in water, rain, suspended droplet, moist air, and pure
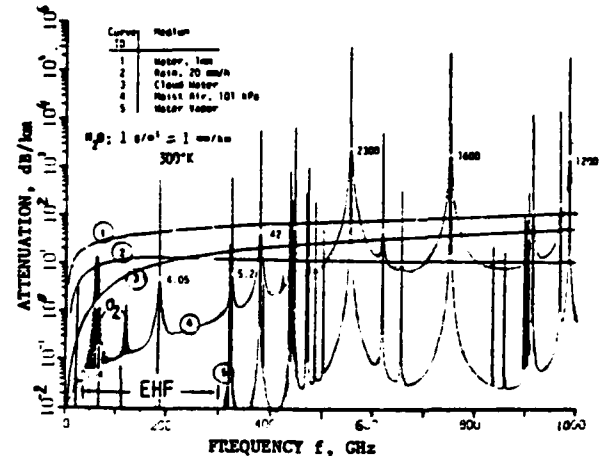water vapor form, as illustrated in Figure 1 (2).

Figure 1. Normalized specific H_2O attenuation over
the frequency range 5 to 1000 GHz for five phase states:
water ①, rain ②, suspended hydrometeors ③, moist
air ④ (numbers shown indicate selected H_2O attenua-
tion peaks), and pure water vapor ⑤.

Water vapor attenuation α_w depends on absolute humidity

$$v = 7.219e\theta \quad g/m^3 \qquad (3)$$

where e is the partial vapor pressure in kPa = 10 mb and
$\theta = 300/T$ is a relative inverse temperature parameter.
Water vapor pressure e is limited by relative humidity

$$RH = 41.51e\theta^{-5}10^{(9.834\theta-10)} \leq 100\% . \qquad (4)$$

The attenuation α_w has its origin in absorption lines of
the molecule H_2O. In principle, α_w can be evaluated from
a line-by-line summation of all line features, each con-
tribution at a given frequency as prescribed by a line
shape function $F(f)$. Seven reported H_2O line data bases
(LB) are indexed in Table I.

Table I. Available data bases for H_2O absorption lines

ID	Frequency cutoff	Number of lines (n)	Remark	Ref.
	THz			
LB1	537	38350	AFGL Tape	5
LB2	126	17201	French version	6
LB3	50	2277	Rotational Spectr. I	7
LB4	3	151	Radio Astronomy	8
LB5	1	30(+α_c)	EHF approximation	1,25
LB6	1.1	17	Russian version	18
LB7	25	555	Rotational Spectr. II	27

The extreme low frequency wings of about 180 stronger (i.e.,
at v_o more than 10^5 times the value of α_w at 100 GHz) lines
below 12 THz make contributions in the EHF range. Six dif-
ferent standard line shape functions $F(f)$ are available to
assess these contributions. Typically, the shape functions
are governed by two spectroscopic parameters: line center
frequency v_o and width γ. An additional parameter v_B was
introduced for covering a wide spectral range, which is
defined by

$$v_B = 2kT/hc = 12510/\theta \quad GHz \qquad (5)$$

(4b, 4h). When these shape functions are normalized to
unity at the center v_o, the functional dependences given
in Table II are obtained.

Table II. Normalized pressure-broadened line shape
functions

Normalization: $\alpha_v = \alpha_o(\nu_o)F(z)$ for a single line,

$a = \gamma/\nu_o$, $b = \nu_o/\nu_B$, $z = f/\nu_o$

ID*	F(z)	6×10^3 (Eq.7)
SL	$a^2z\ [a^2+(1-z)^2]^{-1}$	1.9
FL	$a^2z\ ([a^2+(1-z)^2]^{-1} -[a^2+(1-z)^2]^{-1})$	-0.001
GR	$a^2z^2\ [a^2z^2+(1-z^2)^2/4]^{-1} = (FL)$	-0.001
VW	$a^2z^2([a^2+(1-z)^2]^{-1} +[a^2+(1+z)^2]^{-1})$	637
MGR	(GR)z	8.2
MVW	(VW)[tanh(bz)/tanh b]/z	16.6

*SL = short Lorentzian,   FL = full Lorentzian,
GR = Gross,   VW = Van Vleck-Weisskopf,
MGR = modified GR,   MVW = modified VW (10).

The intensity distribution of a strong H_2O line was
traced with the shape functions listed in Table II and
the example is exhibited in Figure 2. Within the line core,
that is $F(z) \geq 10^{-4}$ or $z = 0.8$ to 1.2, all shapes are alike
and it is inconsequential which one is used. On the other
hand, far-wing intensities depend very much on the chosen
frequency distribution function. For example, the relative
contribution of the line shown in Figure 2 can vary at
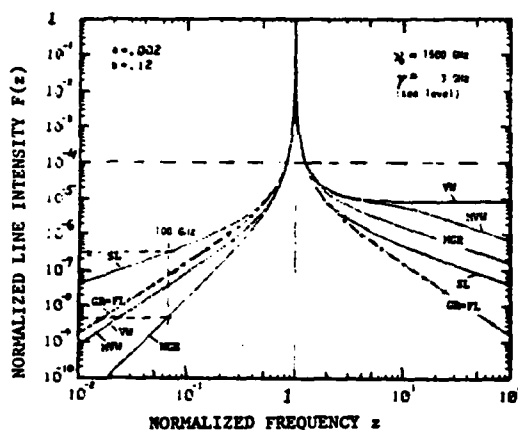100 GHz over a range 1(MGR):75(SL).

Figure 2. Normalized pressure-broadened line shapes
F(z) (see Table II) applied to a single H_2O line.
The line is actually centered at $\nu_o = 1669.907$ GHz
with a peak attenuation rate $\alpha_o = 2.3 \times 10^5$ dB/km
in sea level air ($\theta = 1$, $v = 10$ g/m³).

The EHF (30 to 300 GHz) propagation model developed
by us (1) uses for reasons of computational economy 30
local H_2O lines below 1 THz (LB5, Table I). A theoretical
assessment of EHF attenuation $\alpha_v = \alpha_\ell + \alpha_c$ was accomplished
on the basis of LB3 by subtracting the line contributions
below 1 THz from all 2277. The far-wing contributions
from pressure-broadened lines above 1 THz are then fitted
below 300 GHz to a water vapor continuum absorption

$$\alpha_c = k(p/101)\nu^x\rho^y(f/100)^u \quad dB/km, \quad (6)$$

where p is dry air pressure in kPa. One recognizes ex-
ponents for vapor concentration (x), temperature (y), and
frequency (u) dependences. Applying various shape func-
tions (Table II) to LB3 led to the results summarized in
Table III. As expected, the scale factor k varies over a
wide range. Also, one notices that all three exponents
are influenced by the selected shape function.

Table III. Theoretical EHF water vapor continuum
coefficients (Eq.6)

Line Shape	k	x(v)	y(T)	u(f)
MGR	0.0014	1.00	2.0	2.5
MVW,VW	0.0064	1.01	1.4	2.1
GR,FL	0.012	1.02	1.4	2.0
SL	0.064	1.05	1.2	1.2

The functions were tested for finite integrated
(f = 0 to ∞) line absorption to decide which shape is most
plausible. A limited-range numerical integration resulted
in residuals,

$$\delta = (1/\pi a)\int_{0.001}^{1000} F(z)dz - 1, \quad (7)$$

and it follows (see Table II) that some deviate consider-
ably from the ideal $\delta = 0$. Based on Eq.(7), the shapes VW,
MVW and MGR can not be considered valid intensity descrip-
tors of a pressure-broadened line over a wide frequency
range (22)—and the others are probably overtaxed by
expecting them to predict eight significant orders of
attenuation rate.

Water Vapor Continuum Absorption

The attenuation rate α due to a single line is calcu-
lated with Eq.(1), where the product of strength S and
shape F defines

$$N''(f) = SF(f) \quad ppm \quad . \quad (8)$$

The line properties are formulated in Ref.(1) at $\theta = 1$
(300 K) by a set of spectroscopic coefficients b_1 to b_2.
In the low frequency far wing ($\gamma \ll f \ll \nu_o$), any of the theo-
retical line shapes in Table II is proportional to the
width γ; however, individual continuum shape approximations
$F_c(f \rightarrow 0) =$

$$4f^2\gamma/\nu_o^4 \quad [MGR], \quad 2f\gamma/\nu_o^3 \quad [MVW,VW],$$
$$4f\gamma/\nu_o^3 \quad [GR,FL], \quad \gamma/\nu_o^2 \quad [SL]. \quad (9)$$

predict successively higher contributions (see Fig. 2,
Table III).

In order to formulate the continuum α_c (Eq. 6, Table III)
as a sum of n line terms described by either FL or GR
shapes, the following assumptions have to be made about
strength and width of an "equivalent" line above 1 THz:

$$S = b_1e\theta^{3.5} \exp [b_2(1-\theta)] = b_1e\theta^{1.5} \quad kHz \quad (10)$$

where $b_2 = 2.0$, and

$$\gamma = b_3(m \cdot e + p)\theta \quad GHz \quad . \quad (11)$$

Eqs.(1), (8) to (11) lead to the expression

$$\alpha_c = 0.73f^2e(m \cdot e + p)\theta^{2.5} \times \sum_{i=1}^{m} (b_1b_3/\nu_o^3)_i \quad . \quad (12)$$

The continuum spectrum consists of a self-broadening term
(~ e^2) and a foreign-gas-broadening term (~ ep),

$$\alpha_c = (k_se^2 + k_fep)\theta^y \quad dB/km \quad . \quad (13)$$

Coefficients and temperature exponent are predicted by line
shape theory as follows:

$$k_s = 0.73mf^2 \sum_{i=1}^{m} (b_1b_3/\nu_o^3)_i = mk_f \quad , \quad (14)$$

$$y(e) = 2.5 \quad \text{or} \quad y'(v) = 1.5 \quad . \quad (15)$$

The ratio

$$m = k_s/k_f = 4.80(Air), = 4.39(N_2) \quad (16)$$

is the pressure-broadening efficiency of pure water vapor
with reference to dry air or nitrogen, as determined from
measurements in line cores (15).

There is ample evidence (4a, 10, 12) that in the EHF
range, besides local lines, the low frequency wing of the
complete self-broadened rotational H_2O spectrum is much
stronger than predicted by Eq. (12). A careful review of
H_2O continuum absorption by Burch (10), including all of
his reported data, uncovered increases of the broadening
efficiency in the far wings of lines ranging between m =
20 at 300 GHz and m = 50 at 30 GHz (see later, Table IV).

The laboratory experiment described in the next section was prepared to measure absolute attenuation rates α at three EHF window frequencies (i.e., 92, 138, and 220 GHz) under conditions reaching water vapor saturation. Absorption by neighboring lines is small, so that to first order α ≈ $α_c$. Attenuation data are expected to behave as predicted by Eq.(13). The ongoing experimental studies are aimed at securing accurate coefficients k_a, k_f, and γ, as well as looking for possible anomalies not supported by the pressure-broadened rotational spectrum of the H_2O molecule. The last section of this paper presents first attenuation results obtained at 138 GHz and discusses their implications to EHF propagation modeling.

Millimeter Wave Spectrometer

Controlled experiments that simulate atmospheric conditions provide test cases for studying specific contributions to N in isolation. Assessments of basic physical principles underlying the attenuation rate α are difficult to make from measurements in the actual atmosphere. Reliability, precision, and scale of supporting meteorological data compromise the quality of most field observations. The expected EHF window attenuation is low in a spectroscopic sense (<10 dB/km) and requires long path lengths (>100 m) for a reliable detection. A semi-confocal Fabry-Pérot resonator with a high Q value (437,000 at 138 GHz) offered a good compromise between compactness and detection sensitivity. The computer-controlled measuring system consists of the millimeter wave resonance spectrometer and a humidity simulator. An insulated box contains a high-vacuum stainless steel vessel which houses a temperature-controlled mini-lake (10 cm across) and the radio test path (see Figure 3). Signals at frequencies between 30 and 300 GHz can be employed over equivalent free-space path lengths between 500 and 50 m; temperatures are controlled to better than 1/100 of a degree Celsius; pressure ranges over seven orders of magnitude (10^2 to 10^{-5} kPa); and relative humidity is varied between 0 and 100 percent.

Schematical diagrams of physical (Figure 3) and electronic (Figure 4) arrangements convey an overview of the experiment. Quasi-static diffusion mixing was chosen to generate well defined humidities inside the spectrometer cell. A temperature controlled water reservoir serves as the vapor source. Electropolished stainless steel was used exclusively as construction material. Various hydrophobic coatings were studied as possible means for neutralizing the absorption/desorption cycle on surfaces exposed to water vapor (4d), but were abandoned in favor of slightly heating the mirrors. Four fast-responding (τ < 1s) temperature sensors inside the cell diagnose any disturbance of the gas equilibrium. Data acquisition is computer-controlled.
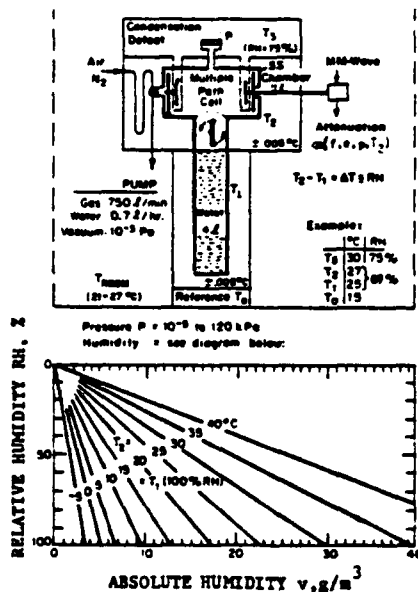

Figure 3. Cross-section of millimeter wave resonance spectrometer and built-in humidity generator. Note three different, extremely stable temperature zones, $T_1(\Theta_1)$ to $T_3(\Theta_3)$. Relative humidity inside the cell is (Eq. 4): log (RH) = 2-9.834 $(\Theta_1 - \Theta_2)$ + 5 $(\log\Theta_1 - \log\Theta_2)$ %. Absolute humidity v is shown in the diagram.
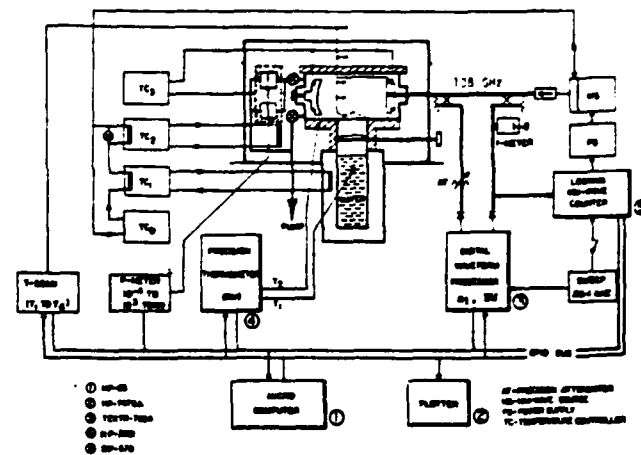

Figure 4. Schematic of high-humidity millimeter wave spectrometer and computer-controlled data acquisition system.

User-friendly software allows the choice of several modes of continuous operation over time scales from one minute to many days. The resonance signal that carries the absorption information is detected with a digital waveform analyzer. The analyzer performs the following tasks under computer control: averaging (1 to 100×), baseline normalization, peak value (P-P) and bandwidth (BW) measurements.

Detection Principles

The dimensionless complex refractivity N is a macroscopic measure of the interaction between gas molecules and mm-waves. Real and imaginary parts are related by the Kramers-Kronig formula. The response curve of a gas-filled resonator is

$$a(f) \propto \{Q^{-1} + Q_M^{-1} + j2[(f/f_R)(1 + N'\times10^{-6})-1]\}^{-1}, \quad (17)$$

where Q is the loaded Q-value, f_R is the resonance frequency of the evacuated resonator, and a Q-value of the gas is defined by

$$Q_M = 91021 \times f_R/\alpha = 10^6/2N'' . \quad (18)$$

Two modes of spectrometer operation follow from Eq.(17) when the evacuated resonator is slowly subjected to a gas pressure P:

Absorption mode. The resonator is swept periodically across its resonance f_R in order to measure α. The shape of the response curve, Eq.(17), appears as a pulse series a(t) when rectified with the detection law ε. The decrease in the maximum amplitude a (P = 0) at f_R to values $a_1(P)$ is sensed by a peak detector. The attenuation rate is obtained from

$$α = 4.343[(a_0/a_1)^{1/\beta} -1]/L_R \quad dB/km , \quad (19)$$

where the effective path length is given by

$$L_R = 4.771 \times 10^{-5} Q/f_R \quad km . \quad (20)$$

From a(t), the peak detector records an absorption pressure profile

$$a_1(P) = a_0/\{[\alpha(P)L_R/4.343] + 1\}^\beta , \quad (21)$$

where the total pressure P = e + p is measured and the expected attenuation rate α is predicted by Eq.(13). A digital waveform processor (see Figure 4) resolves amplitude changes to about 0.1 percent, allowing a detection sensitivity of (16)

$$α_{min} \geq 92 f_R/Q$$

(e.g., F_R = 138 GHz, Q = 437000, $α_{min}$ ≈ 0.05 dB/km). (22)

Refraction mode. To measure N', the shift in resonance frequency by a small amount to f_N is tracked and refraction is given by

$$N' = 10^6 [f_R - f_N(P)]/f_R \quad ppm. \quad (23)$$

Frequency changes of f_R can be compensated with the tuning micrometer, allowing a resolution of N'_{min} ≈ 0.6 ppm.

Specifications for the 138 GHz Test Series

Resonator. Fabry-Pérot reflection-type, semi-confocal arrangement, 10 cm mirror diameter, 20 cm spacing; micrometer tuning: 0.3175 mm/turn with 1.3×10^{-4} mm resolution; loaded Q value at $f_R = 138.2$ GHz: $Q = 437,000$; effective path length (Eq.20): $L_e = 0.151$ km; Fresnel number: 6; response time constant: $Q/\pi f_R = 1.01 \mu s$; coupling coefficient: 0.053; coupling hole: circular, 0.65 mm diameter, 0.075 mm double Mylar vacuum/pressure seal.

Excitation. Linearly frequency-modulated klystron with stabilized center frequency; sweep rate: 50 Hz, sweep width 7 MHz or 19600 μs; reflected signal off-resonance: 150 mV.

Detection. Unbiased Schottky diode ($\delta = 2$) with precision attenuator for dB-calibration; resonance signal peak sensitivity (Eq.22): ± 0.05 dB/km; accuracy: better than ± 10 percent for $\alpha > 1$ dB/km.

Data Run. An example of measuring water vapor attenuation α_w by detecting the resonance peak signal a_1(Pk) with reference to vacuum (a_o) is shown in Figure 5. Relative humidity was increased from RH = 90 to 100 percent over a two-hour period by raising the water temperature from 6.8 to 8.4°C. Condensing water vapor added several tenths of a degree to the cell temperature; however, at 11°C the mirrors remained free of condensation. Some of the data scatter was caused by drift effects of the spectrometer. The calibration of a_1 with ΔT (see Figure 4) determines the dB-scale and is completed by a measurement of the Q value via the bandwidth of the resonance.

Results and Discussion

Experimental Results

Pressure scans of the attenuation rate α_w due to H_2O absorption were made at the frequency $f_1 = 138.2$ GHz. First, pure water vapor pressure e was increased to a constant relative humidity RH, adjusted for values between 80 and 100 percent. Then nitrogen was injected to simulate moist air, although N_2 broadens water vapor lines 1.094 more effectively than dry air (15). The test frequency f_1 falls into an EHF window where little attenuation by local lines is expected (see Eq.27). A summary of reduced and calibrated data is shown in Figure 6. A data fit to Eq.(13) at 300 K amounted to

$$\alpha_w = 0.197e^2 + 0.00750ep \quad dB/km, \qquad (24)$$

resulting in

$$m^x = 26.3 = 5.5m \quad . \qquad (25)$$

The broadening efficiency m^x is determined by pressure pairs e_1 and P_1—points where water vapor attenuation ($\alpha \, e^2$) and moist nitrogen attenuation [$\alpha \, P(e-1)$] are equal, i.e.

$$m^x = (P_1/e_1) - 1$$

Attenuation at points A (2.40 dB/km, e = 3.49 kPa) and B (5.10 dB/km, P = 106.7 kPa) was studied with special care. Point A was stable over a 40-hour period and independent of the water valve position (open/closed), provided a slight mirror heating (1W) was applied. Increasing the mirror heating to 5W (+4°C) did not change the result. Strong anomalies (condensation effects), on the other hand, were observed when the mirror heaters were off. At point B a very long mixing time (several hours) has to be allowed when the water valve is opened against 110 kPa nitrogen. Faster mixing occurs when nitrogen is blended with water vapor already filling the cell.
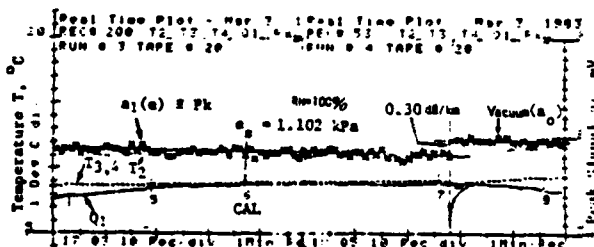

Figure 5. Example of a time series data plot from five instruments, reading temperature: T_2 = mirror, $T_{3,4}$ = cell center and bottom, Q_1 = water; and peak signal Pk (water vapor absorption). The sequence covers a two-hour period during which water vapor saturation was achieved by equalizing the temperature of 8.4°C between cell ($T_{3,4}$) and water (Q_1). CAL = calibration points for a_1 (dB), BW (mm), reference power, and micrometer setting.

Temperature dependence is another diagnostic which can be used to support the theoretical interpretation of continuum attenuation in terms of molecular H_2O line broadening. A series of pure water vapor pressure scans was made at T = 282 K (see Figure 5). Temperature limited the saturation pressure to 1.152 kPa. A preliminary fit of these data yields (compare with Eq.15)

$$y = 3.5 \pm 1 \qquad (26)$$

Pressure dependence indicated by Eq.(13) has been observed in earlier laboratory (10 to 17, 23, 24) and field (4d, 4e) experiments. A selected review of laboratory data is given in Table IV. The following approximate relations can be deduced from this data body:

$$\alpha_w = k_s(e^2 + ep/m^x) \quad \text{(in between lines)};$$
$$k_s \propto f^2 \quad \text{(excluding the 67.7 GHz data)};$$
$$m^x = 1/f^{0.5} \quad \text{(see Ref. 10)};$$
$$y = 5.5 \quad \text{(for the 110 GHz data)}.$$

Absolute data on α_w are difficult to obtain. In spite of existing inconsistencies, our data lend support to the hypothesis that far-wings of self-broadened H_2O lines centered above 1 THz are probably the major source for the EHF continuum (10). Line shape theory needs to be revised to account for the minute ($< 10^{-5}$ the value at line center) contributions in the extreme low frequency wings of pressure-broadened lines located above 1 THz in the rotational H_2O spectrum (4b, 4h, 9, 21, 22).

Table IV. Laboratory results for water vapor attenuation α_w fitted to Eq.(13) yielding the coefficient k_s^x and broadening efficiency m^x.

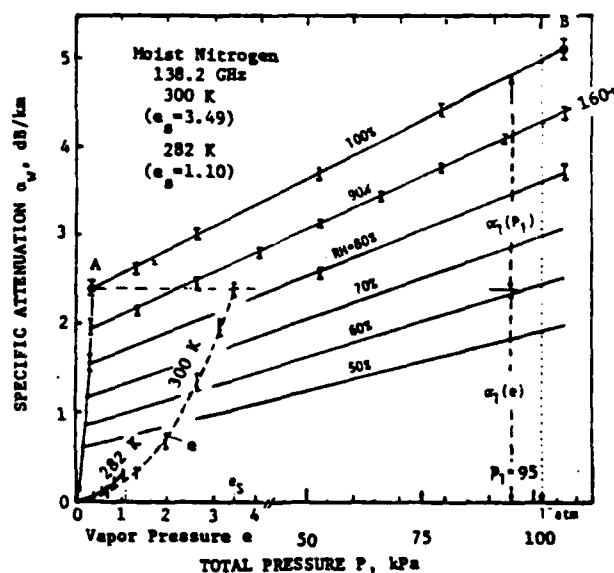| f	k_s^x	m^x	Broadening Agent	T	Ref.
GHz	dB/(km kPa²)			K	
31	0.011	49*	Air	318	11
67.7	0.16	44*	Air	283	24
110	0.12	35*	Air	304	24
110	0.16	35*	Air	292	23
110	0.21	35*	Air	274	24
138	0.197	26.3(29)	N_2(Air)	300	this
138	0.25	–	–	282	paper
213	0.62	24*	N_2	320	4g, 17
345	2.4 ± 1.5	24	N_2	300	19
411	2.9 ± 0.8	18	N_2	300	19
667	4.1 ± 1.1	9.6	N_2	300	19
883	5.2 ± 1.4	9.4 ± 0.9	N_2	300	19

* Our fit to reported raw data

Figure 6. Pressure dependence of specific attenuation α due to water vapor (e) and moist nitrogen (P) measured at 138.2 GHz and relative humidities from RH = 80 to 100 percent.

Water Vapor Continuum and EHF Propagation Modeling

The experimental result at 138.2 GHz for moist nitrogen attenuation (Eq.24) has been incorporated into the EHF propagation model that is based upon LBS (1,25). Reducing the ep-term by 9.4 percent for air-broadening and subtracting line contributions due to LBS,

$$\alpha_i(LBS) = 1.94 \times 10^{-3} \, ep + 0.0093 \, e^2 \quad dB/km, \qquad (27)$$

gives the pressure dependence of continuum attenuation as

$$\alpha_c = \alpha_v - \alpha_i = 4.86 \times 10^{-3} \, ep + 0.188 e^2 \quad dB/km. \quad (28)$$

Adding frequency and temperature dependences to Eq.28 leads to a moist air continuum spectrum for LBS, modeled by

$$N_c'' = (c_1 \, ep\theta^y + c_2 \, e^2 \theta^{y*})f \times 10^{-6} \quad ppm. \qquad (29)$$

The coefficients for Eq.(29) are chosen according to the following scheme:

	c_1	y	c_2	$y*$	Remark
Old	1.30	3.1	0	1	Gaut-Reifenstein
New	1.40	2.5	54.1	3.5	Eqs.28, 15, 26

The "new" continuum spectrum is different from various other empirical forms (summarized in Table V) which have been proposed.

Table VI compares the implications of the old and the new continuum for the case of predicting zenith attenuation A(dB) through a model atmosphere.

Table V. Experimental water vapor continuum coefficients (Eq.6) reported by other workers (2).

k	x(v)	y(T)	u(f)	Local Lines	f, GHz	Ref.
0.023	1.00	2.1	2.50	MVW	50 to 500	10
0.039	1.05	3.0	2.40	GR	20 to 350	18
0.049	1.00	2.1	2.00	VW	15 to 500	(*)
0.061	1.00	2.1	1.22	GR	150 to 410	21

(*) Gaut-Reifenstein model (1).

Summary

Absolute attenuation rates α_v have been measured in the laboratory for pure water vapor and for mixtures of vapor and nitrogen, simulating moist air. Initial studies were performed at 138 GHz, two temperatures (292 and 300 K), partial vapor pressures up to saturation (1.10 and 3.48 kPa), and total pressures up to 160 kPa. Preliminary results were acquired for pressure and temperature dependences of α_v. The data behaved in a fashion similar to that expected from H_2O line-broadening theory (Eq.13). Except for a strong self-broadening component ($\propto e^2$), no additional anomalous behavior was observed—even at saturation pressures (RH = 100%)—contrary to findings by other workers (4,17, etc.).

In our case, we could clearly identify anomalous absorption behavior (e.g., unusually high rates, extreme temperature dependences, hystereses in pressure and temperature cycles) as being instrumental, that is condensation effects on the millimeter wave-active parts of the spectrometer. Considerable effort had to be expended before the instrument produced consistent, reproducible results.

A water vapor continuum N_c'' was formulated for the EHF propagation model (1,25) in order to supplement contributions from 30 H_2O lines below 1 THz. At 138 GHz, the local lines furnish 40 percent to air-broadening but only 5 percent to self-broadening of the water vapor attenuation α_v. Practical implications of the continuum to propagation modeling are not too serious. Up to humidities of $v \leq 10$ g/m³, the widely used empirical Gaut-Reifenstein continuum (1) is roughly confirmed. At higher values, increases over the GR continuum and a nonlinear dependence on absolute humidity are predicted.

Table VI. Comparison of zenith attenuation A(dB) predicted for a synthetic atmosphere (30°N, July) by employing the EHF Propagation Model (1,25) with old (Gaut-Reifenstein) and new (Eq.29) water vapor continuum formulations.

Ray Path Angle: 0.00 Degrees from Zenith

Integrated through Model Atmosphere: p_o = 101.35 kPa, T_o = 301.15 K.

31 Height Levels, h = 0 to 30 km.

Integrated Water Vapor	V = 52.69	70.25 mm.
Electric Path Length	L_e = 2627.2	2739.0 mm.

FREQUENCY (GHz)	ATTENUATION (dB)		ATTENUATION (dB)	
30.00	.59	.61	.72	.83
35.00	.63	.65	.74	.99
40.00	.79	.83	.91	1.11
45.00	1.13	1.18	1.27	1.32
50.00	2.13	2.19	2.29	2.61
55.00	28.16	28.28	28.36	28.77
60.00	148.98	148.94	149.09	149.41
65.00	23.87	23.88	24.16	24.60
70.00	3.19	3.24	3.49	4.03
75.00	2.42	2.49	2.75	3.30
80.00	2.36	2.44	2.72	3.45
85.00	2.48	2.58	2.89	3.71
90.00	2.69	2.79	3.14	4.06
95.00	2.94	3.06	3.44	4.47
100.00	3.23	3.37	3.79	4.94
105.00	3.58	3.74	4.20	5.47
110.00	4.07	4.24	4.75	6.14
115.00	5.47	5.65	6.23	7.75
120.00	11.89	12.09	12.73	14.38
125.00	5.38	5.61	6.31	8.10
130.00	5.51	5.75	6.52	8.46
135.00	5.92	6.18	7.03	9.13
140.00	6.43	6.71	7.66	9.92
145.00	7.03	7.33	8.41	10.83
150.00	7.75	8.07	9.32	11.91
	old	new	old	new

1. H. J. Liebe, Radio Sci., $\underline{16}(6)$, 1183-1199 (1981).

2. H. J. Liebe, IEEE Trans. Ant. Prop., AP-31(1), 127-135 (1983).

3. URSI Commission, URSI Working Party Report, Radio Sci. $\underline{16}(5)$, 825-829 (1981).

4. A. Deepak et al. (Eds.) Atmospheric Water Vapor, 1980 Academic Press, New York. Papers by:
    a) D. E. Burch and D. A. Gryvnak, 77-100;
    b) R. J. Nordstrom and M. E. Thomas, 101-112;
    c) R. A. Gebbie, 122-142;
    d) H. J. Liebe, 143-202;
    e) D. C. Hogg, 219-228;
    f) R. A. Bohlander et al., 241-254;
    g) D. T. Llewellyn-Jones, 255-264;
    h) S. A. Clough et al., 25-46.

5. L. S. Rothman, R. R. Gamache, A. Barbe, A. Goldman, J. R. Gillis, L. R. Brown, R. A. Toth, J.-M. Flaud, and C. Camy-Peyret, Appl. Opt. $\underline{22}(12)$, 2247-2256 (1983).

6. J. M. Flaud, C. Camy-Peyret, and R. A. Toth, Water Vapor Line Parameters from Microwave to Medium Infrared, Pergamon Press, Oxford, England (1981).

7. M. Mizushima, Int. J. Infrar. Millimeter Waves, $\underline{3}(3)$, 379-384 (1982).

8. R. L. Poynter and H. M. Pickett, JPL Publication 80-28, Rev. 1, Jet Propulsion Lab., NASA, Pasadena, CA (1981).

9. M. E. Thomas and R. J. Nordstrom, J. Quant. Spectrosc. Radiat. Trans., $\underline{28}(2)$, 81-112 (1982).

10. D. E. Burch, Ford Aerospace and Communications Corp., Aeronutronic Div., Final Report AFGS-TR-81-0300 (March 1982).

11. G. E. Becker and S. H. Autler, Phys. Rev. $\underline{70}$, 300-307 (1946).

12. L. Frenkel and D. Woods, Proc. IEEE $\underline{54}$, 498-505 (1966).

13. C. Remmi and A. Straiton, Radio Sci. $\underline{4}$, 9-15 (1969).

14. D. Hrowinski, Z. Angew. Phys. $\underline{29}$, 323-330 (1970).

15. R. J. Liebe and T. A. Dillon, J. Chem. Phys. $\underline{50}(2)$, 727-732 (1969).

16. R. J. Liebe, Studies of O_2 and H_2O microwave spectra under simulated atmospheric conditions, OT Report $\underline{75-65}$ (June 1975) (NTIS Accas. No. COM75-10096/AS).

17. D. T. Llewellyn-Jones, R. J. Knight and H. A. Gebbie, Nature $\underline{274}(5674)$, 876-878 (1978).

18. A. Y. Zrazhevskiy, Radio Eng. & Electr. Phys. $\underline{21}(5)$, 31-36 (1976) and $\underline{22}(1)$, 128-129 (1977).

19. K. A. Agambekjan and A. Y. Zrazhevskiy, A study of subms. radiation absorption in pure water vapor and in mixtures with N_2, CO_2 and Ar; priv. comm. (1982).

20. R. J. Hill, R. S. Lawrence and J. T. Priestley, Radio Sci. $\underline{17}(5)$, 1251-1257 (1982).

21. C. C. Zammit and P. A. Ade, Nature $\underline{293}(5833)$, 550-552 (1981); and C. C. Zammit, R. E. Hill and R. W. Baker, Int. J. Infrar. Millimeter Waves $\underline{3}(2)$, 189-203 (1982).

22. G. Birnbaum, J.Q.Spectr. Rad. Transf. $\underline{21}$, 597-607 (1979).

23. D. T. Llewellyn-Jones and R. J. Knight, IEE Conf. Publ. $\underline{195}$, 81-83 (1981).

24. R. J. Knight and D. T. Llewellyn-Jones, Measurements of water vapour absorption in the RAL untuned cavity, Rutherford Appleton Lab. Res. Note $\underline{RL-82-051}$ (July 1982).

25. H. J. Liebe, An atmospheric millimeter wave propagation model, NTIA Report $\underline{83-137}$ (December 1983).

26. H. J. Liebe and D. H. Layton, Proc. URSI Com. F 1983 Symp., Louvain-La-Neuve, Belgium (ESA $\underline{SP-194}$, 477-486).

27. J. K. Messer, F. C. DeLucia, and P. Helminger, Int. J. Infrar. Millimeter Waves $\underline{6}(4)$, 505-539 (1983).

END

FILMED

4-84

DTIC